



KATHOLIEKE UNIVERSITEIT LEUVEN
FACULTEIT TOEGEPASTE WETENSCHAPPEN
DEPARTEMENT BURGERLIJKE BOUWKUNDE
LABORATORIUM voor HYDRAULICA
de Croylaan 2, B-3001 Leuven (Heverlee)

MODELLING FLOW IN COMPOUND CHANNELS



Promoter:
Prof. Dr. ir. J. Berlamont

Proefschrift voorgedragen tot
het behalen van het doctoraat
in de toegepaste wetenschappen

door

M. A. ELZEIR

October 1996

VLIZ (vzw)

VLAAMS INSTITUUT VOOR DE ZEE

FLANDERS MARINE INSTITUTE

Oostende - Belgium



KATHOLIEKE UNIVERSITEIT LEUVEN
FACULTEIT TOEGEPASTE WETENSCHAPPEN
DEPARTEMENT BURGERLIJKE BOUWKUNDE
LABORATORIUM voor HYDRAULICA
de Croylaan 2, B-3001 Leuven (Heverlee)

66446

MODELLING FLOW IN COMPOUND CHANNELS

Jury:

Prof. E. Aernoudt, Voorzitter
Prof. J. Berlamont, Promoter
Prof. G. De Roeck
Prof. J. Monbaliu
Prof. E. Smets
Dr. K. Shiono (Univ. Of Loughborough, U.K.)
Prof. E. Van den Bulck

Proefschrift voorgedragen tot
het behalen van het doctoraat
in de toegepaste wetenschappen

door

M. A. ELZEIR

81433

© Copyright by Katholieke Universiteit Leuven

Zonder voorafgaandelijke toestemming van en de auteur, en de promotor is overnemen, kopiëren, gebruiken of realiseren van deze uitgave of gedeelten ervan verboden.

Voor aanvragen tot of informatie i.v.m. het overnemen en/of gebruik en/of realisatie van gedeelten van dit werk, wendt U tot de K.U. Leuven, Dept. Bouwkunde, de Croylaan, 2, 3001 Leuven, België.

Voorafgaandelijke toestemming is eveneens vereist voor het aanwenden van de in dit proefschrift vermelde (originele) methoden, schakelingen en programma's voor industrieel of commercieel nut.

D/1996/7515/40

ISBN 90-5682-054-0

Acknowledgements

My deepest gratitude and thanks are to my promoter Prof. J. Berlamont for his continuous guidance and encouragement. Within my Ph.D. study, he introduced me first of all to current modelling in shallow coastal waters and then to turbulence modelling within the framework of the E.C. Large Installation Plan (LIP2) research project.

I am very grateful to my reading committee members- Prof. G. De Roeck and Prof. J. Monbaliu for their valuable comments and suggestions and to Prof. E. Smets, Dr. K. Shiono and Prof. E. Van den Bulck for accepting to be my jury members.

When my research career is considered, Prof. J. Monbaliu deserves all my respect and gratitude. He gave me insight into how to formulate my research work and how to tackle different problems for both my Master and Ph.D. thesis.

The experimental work of my thesis is a part of the LIP2 Project, which was carried out at Delft Hydraulics in the Netherlands. The Project was a great opportunity to collect data for calibrating the turbulence model that I developed. It was impossible to achieve such a bulk of work without the help of Dr. K. Shiono. The useful discussions with him both in Delft Hydraulics during the experiment, and via E-mail after the experiment were extremely useful for me. The scientific material he offered me was indispensable for fulfilling my research.

I would like to thank very much the friends and colleagues at the Hydraulic Laboratory and the Universiteit Reken Centrum, who greatly supported my work.

The scholarship offered by ABOS and the financial support provided by the Laboratory during the last six months of my research are gratefully acknowledged. I acknowledge, also, the long study leave permission offered by my university, El-Minia University.

I want to thank especially my parents, and family, and all my Muslim brothers in Leuven, for their support during my long stay in Leuven.

Last, but above all, praise be due to Our Lord, Almighty Allah, for everything He bestowed upon me. Without His blessings, I would not have been able to perform any of my achievements.

“وآخر دعوانا أن الحمد لله رب العالمين”

Leuven, October, 1996

Mohamed Elzeir

Abstract

Turbulent flows in conduits of non-circular cross-sections are often encountered in engineering practices. Examples are open channels. The flow in such conduits is accompanied by secondary motions in the plane perpendicular to the stream-wise direction; and this secondary motion can be caused by two different mechanisms. First, secondary motion caused by centrifugal forces in curved passages. Such (pressure induced) secondary velocities are quite large (say 20-30% of the bulk stream-wise velocity) and occur equally in laminar and turbulent flows. Second, secondary flow produced by turbulence in non-circular straight conduits. Although the secondary velocity of this kind is only 2-3% of the stream-wise bulk velocity, it can have important consequences on both the flow hydrodynamics and scalar transport. For these reasons, it is important to understand and be able to predict secondary flow phenomena in developing flow situations and in the asymptotic developed state.

Within the framework of the E.C. LIP2 project, an experiment was performed in the tidal flume of Delft Hydraulics, the Netherlands. The experiment was conducted to study mixing mechanisms and momentum exchange (in compound channels) between fast main-channel flow and slow flood-plain flow. Although the experiment was performed for both homogeneous and stratified flows, the homogeneous case only is analysed. Despite the limited area accessible by the measuring instruments, which caused loss of important information near (free and solid) surfaces, the following conclusions could be extracted from the experiment. At the upstream measuring section, the splitter plate effect disappears but the turbulence is not yet fully developed. The secondary flow at the downstream measuring section and its effect on the longitudinal velocity component indicates a fully developed flow. However, the position of the fully developed section is still open for research. Although the point measurement at a single cross section along the flume provides useful information regarding the turbulence, it is not sufficient. It is believed that the study of turbulence along the flume and consequently recognising the coherent structures is important to fully understand the (not fully random but "partly" organised) turbulence phenomena.

The flow is numerically modelled using a finite difference 3D scheme. The model is explicit using the ULTIMATE QUICKEST scheme to discretise the advection term. The scheme is modified so that three grid points are used (instead of four) for interpolation. The ULTIMATE QUICKEST suffers from reverting to the diffusive first order upwind when the monotonicity condition is violated. Patankar and Spalding algorithm is used to determine the pressure field. The Algebraic Stress Model (ASM) is found to be a reasonable compromise combining the economy of the simple eddy viscosity model and the accuracy of the stress transport models. Haque's ASM is found to be of limited applicability because it suffers from first, solving a set of simultaneous equations at each grid point; second, the ill-conditioned problem; third, neglecting the stress transport terms. On the other hand, Naot's ASM is found to be a reasonable alternative taking into account surface proximity and overcoming the disadvantages of Haque's model. The results obtained from the numerical model are in reasonable agreement with the experimental ones.

The model is compared with the large-scale POM model. It is concluded that the assumptions underlying large scale models are so different from those underlying small-scale models that they cannot replace one another, even with any degree of approximation.

TABLE OF CONTENTS

Acknowledgements	i
Abstract	iii
Table of contents	v
List of Figures	ix
List of Tables	x
List of Symbols	xi
Chapter 1: INTRODUCTION	1
1.1 Flow in Compound Channels	1
1.1.1 Challenge to environmental engineers	1
1.1.2 Laboratory studies and mathematical models	2
1.2 Objectives and Scope of the Study	3
1.3 Structure of the Research	4
Chapter 2 PHYSICAL MODEL	5
2.1 Introduction	5
2.2 Experimental Setup	6
2.3 Measurements	10
2.3.1 Instruments	10
2.3.2 EMS	10
2.3.3 Turbulence Measurement	15
2.4 Data Analysis	20
2.4.1 Introduction	20
2.4.2 Mean velocity and secondary circulation	21
2.4.3 Kinetic energy and velocity fluctuations	24
2.4.4 Reynolds stresses	30

2.5	Conclusion	31
Chapter 3	NUMERICAL MODELLING	35
3.1	Introduction	35
3.2	The Governing Equations	36
3.3	Advection Term	43
3.3.1	Introduction	43
3.3.2	ULTIMATE QUICKEST	45
3.3.3	Evaluation of the ULTIMATE QUICKEST	49
3.4	Pressure Term	51
3.4.1	Introduction	51
3.4.2	The pressure correction method	53
3.5	Boundary Conditions	58
3.5.1	Introduction	58
3.5.2	Radiation Boundary Condition	59
3.5.3	Boundary Conditions for Poisson Equation	61
3.6	Conclusion	62
Chapter 4	TURBULENCE CLOSURE	63
4.1	Introduction	63
4.2	Reynolds Stress Equations	64
4.3	Turbulence Models	66
4.4	Two-Equation Models	68
4.5	Algebraic Stress Model	72
4.5.1	Introduction	72
4.5.2	Haque's model	73
4.5.3	Naot's model	74
4.6	Numerical Model	77
4.6.1	Discretization and Solution Algorithm	77
4.6.2	Boundary Conditions	80
4.7	Numerical Results	84

4.8	Model Comparison	86
4.9	Program Structure	88
4.10	Conclusion	90
Chapter 5	CONCLUSIONS AND RECOMMENDATIONS	93
5.1	Summary	93
5.2	Conclusions	94
5.2.1	The experiment	94
5.2.2	The numerical model	94
5.2.3	The turbulence closure	96
5.2.4	Model comparison	97
5.2.5	New contributions by the current research	97
5.3	Recommendations	98
References		101
Appendix A: TENSOR NOTATION		107
Appendix B: SPLITTING METHOD FOR THE ASM		111
Curriculum Vitae		115
List of Relevant Publications		116

List of Figures

Figure 2.2.1	Schematic drawing for the experimental setup	7
Figure 2.3.1	EMS measuring locations	11
Figure 2.3.2	Longitudinal velocity component U (m/s) measured at the inlet by EMS	14
Figure 2.3.3	Measuring area in the cross section	19
Figure 2.3.4	Effect of the alignment error on the measured velocity vectors .	19
Figure 2.4.1	Secondary circulation	22
Figure 2.4.2	Isovels for U (m/s)	23
Figure 2.4.3	Depth averaged longitudinal velocity, U versus lateral distance, y	25
Figure 2.4.4	Isolines for u' (cm/s)	26
Figure 2.4.5	Isolines for v' (cm/s)	27
Figure 2.4.6	Isolines for w' (cm/s)	28
Figure 2.4.7	Isolines for k (cm^2/s^2)	29
Figure 2.4.8	Contours for $v'^2-w'^2$ (cm^2/s^2)	31
Figure 2.4.9	Isolines for $\overline{u'v'}$ (cm^2/s^2)	32
Figure 2.4.10	Isolines for $\overline{u'w'}$ (cm^2/s^2)	33
Figure 3.3.1	Advection through the right face of control volume CV_1	45
Figure 3.3.2	Measured velocity distribution at the upstream boundary and the difference between the upstream (measured) velocity and the downstream (calculated) one	51
Figure 3.3.3	Velocity re-distribution at the upstream open boundary	51
Figure 3.4.1	Staggered grid in 3D	56
Figure 4.5.1	Sketch explaining mean distance from a point to a surface	77

Figure 4.6.1	Distribution of the variables on the finite difference mesh	77
Figure 4.7.1	Secondary circulation (m/s)	83
Figure 4.7.2	Isolines of U (m/s)	85
Photo 2.2.1	Delft Tidal Flume	7
Photo 2.2.2	Cylinder shaped overflow weir	9
Photo 2.2.3	Upstream splitter plate	9
Photo 2.2.4	Downstream splitter plate	9
Photo 2.3.1	VILDA/HEAD system	17
Photo 2.3.2	HILDA/HEAD system	17
Photo 2.3.3	Position of the conductivity head with respect to HILDA	17

List of Tables

Table 2.2.1	Flow conditions for different runs	10
Table 2.3.1	Instruments used in LIP2 experiment	12
Table 4.4.1	k- ϵ model constants reported in the literature	72

List of Symbols

Roman symbols:

C_{ij}	convective transport of turbulence (m^2/s^2)
C_L	ratio between physical wave velocity and numerical wave velocity in Sommerfeld equation
CURV	curvature term in the interpolation formula of the advective term
c	Courant number
c_r	the advection velocity in the Sommerfeld radiation condition.
$c_{\epsilon 1}, c_{\epsilon 2}$	constants for the k- ϵ model.
c_μ	constant for the eddy viscosity model
c_1, c_2	constants of Haque's model
c_3, c_4, α, β	constants of Naot's model
D	diffusion (tensor) of the turbulence kinetic energy (m^2/s^3)
DEL	measure of the rate of change of the variable ϕ in the interpolation formula of the advective term.
E	roughness parameter (=9 for hydraulically smooth walls)
f_1, f_2	functions for the distance from surfaces in Naot's model
g	acceleration due to gravity ($= 9.81 \text{ m/s}^2$)
H	total water depth (m)
H	length scale of vertical distance (m)
h_s, y_s	root mean squared reciprocal distances from solid wall and open surface, respectively, in Naot's model.
k	turbulence kinetic energy (m^2/s^2).

\hat{L}	characteristic length scale of turbulence.
L	length scale of horizontal distance (m).
l	dissipation length
m	true mass flow rate in boundary layer flow (kg/s)
N	total number of readings at a certain point in the turbulence experiment.
P	mean (dynamic) pressure (N/m^2)
P_o	a reference pressure (N/m^2)
\bar{P}	space-averaged pressure over a cross section (N/m^2).
P	scale for the pressure divided by density (m^2/s^2).
p	pressure (N/m^2)
$p_o(z)$	the hydrostatic pressure (N/m^2)
p_d	the dynamic part of the pressure (N/m^2)
p'	fluctuation part of the dynamic pressure (N/m^2)
s_{ij}	components of the strain-rate tensor.
t	time (s)
t_{ij}	components of the viscous stress tensor divided by ρ_o (m^2/s^2)
U, V, W	Cartesian components of the mean velocity vector in x, y, z , respectively (m/s)
U_i	components of the mean velocity (m/s)
U_{res}	resultant velocity parallel to the wall (m/s).
U	shear velocity = $\sqrt{\frac{\tau_o}{\rho}}$ (m/s)
u_i	the components of the instantaneous velocity vector (m/s)

u_i^*	Components of the velocity fluctuation (m/s)
u, v, w	Cartesian components of the velocity vector in x, y, z, respectively (m/s)
u', v', w'	Cartesian components of the fluctuating part of the velocity vector (m/s)
$\overline{u_i u_j}$	Components of the Reynolds' stress tensor (m^2/s^2)
\hat{V}	characteristic velocity scale of turbulence.
V	velocity scale of horizontal velocity components (m/s)
W	velocity scale of vertical velocity component (m/s).
x_i	the coordinate axes
x, y, z	Cartesian coordinates, with x positive eastward, y positive northward and z positive upward.
y^+	non-dimensional wall distance $= \frac{y^+ U_*}{\nu}$
y'	distance from the solid wall (m)

Greek symbols:

Γ	artificial numerical diffusion coefficient (m^2/s).
Δ	difference between two successive values (size of the step).
δ_{ij}	the Kronecker delta.
ϵ	dissipation (tensor) of the turbulence kinetic energy (m^2/s^3)
θ	misalignment angle for the measuring instruments.
κ	von Kármán's constant ($=0.41 \pm 0.015$)
μ	constant applied in the radiation OBC to account for the value of C_L .
ν	the kinematic viscosity (m^2/s)

ν_t	turbulence eddy viscosity (m^2/s).
Π_{ij}	pressure-strain correlation in the Reynolds stress equation (m^2/s^3)
ρ	the fluid density (kg/m^3)
ρ_0	a reference density (kg/m^3)
ρ^*	the difference between the density and the reference density (kg/m^3)
σ_k	Prandtl number for turbulence kinetic energy
σ_ϵ	Prandtl number for dissipation of turbulence kinetic energy
τ_{ij}	the components of the viscous stress tensor (N/m^2)
τ_0	wall shear stress (N/m^2).
Φ	production (tensor) of the turbulence kinetic energy (m^2/s^3)
ϕ	dummy name representing dependent variables

Subscripts and superscripts:

*	(a superscript) indicating transitional value.
B	boundary value
D,C,U	Downstream, Centre and Upstream points with respect to a velocity vector.
i,j,k	indices indicating spatial dimensions of the discretized variables.
l,r	left and right faces of a control volume
m	measured values
max	maximum value
n	index for time level
num	numerical
p	cross-section position
R	rotated values

REF	reference value
x,y,z	Cartesian coordinates indices.

Abbreviations:

ADV	ADVection term
ASM	Algebraic Stress Model.
CV	Control Volume.
DIF	DIFfusive terms including the turbulence closure terms.
MAC	Marker And Cell
$N(u_i)=0$	symbolic expression of the momentum equation in the i^{th} direction.
OBC	Open Boundary Condition.
PLDS	Power Law Differencing Scheme.
QUICK	Quadratic Upstream Interpolation for Convective Kinematics.
QUICKEST	Quadratic Upstream Interpolation for Convective Kinematics with Estimated Streaming Term.
SOR	Successive Over-Relaxation method.
TDMA	Tri-Diagonal Matrix Algorithm.
ULTIMATE	Universal Limiter for Transient Interpolation Modelling of Advective Transport Equations.

Chapter 1

INTRODUCTION

1.1 Flow in Compound Channels

1.1.1 Challenge to environmental engineers

The discharge of pollutants into water courses is becoming an increasing threat to our water resources. The pollutants can be thermally or chemically polluted water from power stations, industrial plants and households. The threat to the environment is faced in the form of ecological impact on marine life, health hazard to the users of the water courses and damage to the recreational areas usually settled around the water courses. The understanding and control of the transport and diffusion of pollutants are real challenges to hydraulic engineers.

Civil engineering projects such as harbors, traffic tunnels, pipelines and storm surge barriers often require the dredging of trenches or channels in the alluvial bed of a river or estuary. The siltation of the dredged trenches and the fluid forces acting on the submerged structures are another type of challenge to hydraulic engineers. A third challenge to hydraulic engineers is control of rivers in times of flood.

To find a practical solution for any of the above-mentioned problems, it is necessary to understand the mechanisms which govern both water motion and pollutant transport. In general, the mean motion in rivers is three dimensional, where the pollutants are convected by the mean fluid motion and diffused by turbulence. Particularly complicated flow patterns arise when the boundaries are irregular. Irregular boundaries are encountered in many practical situations, e.g. a river channel with flood plains, a canal

with side berms and a main flow estuarine channel with side storage zones. Under these circumstances, the flow-cross-section is compound, consisting of a main channel with fast flow and (a) flood plain(s) with relatively slow flow. The hydraulic characteristics of compound channels are significantly different from those of rectangular channels due to interaction between the flow in the main channel and the relatively slow flow on the flood plains. For example, the discharge capacity of a compound channel is lower than the combined capacities of the individual separate channels and the typical bed shear stress on the flood plain is higher than expected for the flood plain considered on its own (Thomas and Williams, 1995b). Actually, the primary flow field is considerably modified by the lateral and vertical momentum transfer between regions of different depths (Knight and Demetriou, 1983).

1.1.2 Laboratory studies and mathematical models

For a better understanding of the structure of (turbulent) flow in compound channels, it is necessary to undertake detailed measurements. Because of the difficulty in obtaining sufficiently accurate and comprehensive field measurements of velocity and shear stress in compound channels under unsteady flow conditions, considerable reliance must still be placed on well focused laboratory investigations under steady flow conditions to provide the information concerning the details of the flow structures and lateral momentum transfer. Attention must be paid to the fact that physical models are very expensive, especially when a large number of influence parameters have to be studied. Sometimes, it is impossible to construct a physical model for certain prototypes, e.g. the continental shelf. Therefore, an urgent need for economic mathematical prediction models is emphasized. A mathematical model must be capable of describing correctly both the mean velocity field and the turbulent diffusion characteristics. Unfortunately, building a general mathematical model is very difficult because of the many phenomena involved. Fortunately, a general model is not necessary in most circumstances, for rarely are all of the phenomena simultaneously of importance and in many cases the flow

situations can be idealized to make them more accessible to a mathematical description. The immediate problem is therefore to develop mathematical models of various complexity for suitably idealized river and discharge situations and to investigate how complex a model is required for any particular situation (Rastogi and Rodi, 1978). For example, many turbulence models are available (e.g. $k-\epsilon$ model, the algebraic stress model, the Reynolds stress model and the large eddy simulation) each of which has its own assumptions and hence its own limitations and field of application. Passing through calibration and validation procedures, the mathematical model needs reliable data and results to compare with. The laboratory experimental results provide such reliable information with bounty while field data suffer from both uncertainty and scarcity.

1.2 Objectives and Scope of the Study

Vertical and lateral exchange of momentum and secondary circulations in a compound channel are of primary importance because of their direct impact on the flow field and consequently on transport and diffusion of pollutants. Laboratory experiments are essential in understanding the flow patterns. Mathematical models, on the other hand, are vital tools in predicting the flow field. The mathematical model is validated and calibrated using reliable laboratory data.

The objectives of this study have been set as,

- 1 The flow field and the turbulence characteristics in a compound channel will be analyzed. The limitations, difficulties and uncertainties associated with the experiments will be discussed.
- 2 A numerical model will be developed. The objectives of building the model are
 - 2-1 to study the performance of different turbulence closure models. Special attention will be paid to the standard $k-\epsilon$ model and the algebraic stress model. While the $k-\epsilon$ model cannot predict the secondary circulation in compound channels, the algebraic stress model predicts it with a reasonable accuracy. The reasons for the different behaviour will

be discussed.

2-2 to study the scope of validity of a numerical model. Two mathematical models are compared: a large scale model and a small scale model. It will be shown that if the model limitation, assumptions and scope of application are exceeded the results (if any) are physically erroneous and cannot be accepted with any degree of approximation.

1.3 Structure of the Research

The current research consists mainly of an experimental part and a numerical part. The experimental part has been conducted within the framework of the E.C. Large Installation Plan (LIP2) in the tidal flume of Delft Hydraulics. In Chapter 2, the experiment is explained. The experiment is meant to study the vertical and lateral exchange of momentum and secondary circulation in the shear layer region of a compound channel. The data is analyzed and compared with previous work. The limitations of the experiment and the possible source of inaccuracies are discussed.

In Chapter 3, the Reynolds-averaged Navier-Stokes equations are discussed. Discretization of the advection and pressure terms is explained. The model is applied to the LIP2 data and the results are analyzed.

Chapter 4 is devoted to the turbulence closure problem. The closure problem is shown to be endless if exact transport equations are to be solved. Therefore, it is necessary to model higher order correlations. The $k-\epsilon$ model is the most popular model. It is amended by the Algebraic Stress Model (ASM) to be able to predict secondary circulation in compound channels. The numerical solution of the ASM is explained. A comparison between the small scale model, which has been developed in this study and a large scale model is carried out in the last section of the chapter. Conclusions of the thesis and recommendations for further work can be found in Chapter 5.

Chapter 2

PHYSICAL MODEL

2.1 Introduction

Environmental hydraulic situations are characterized by complex flow geometries and multiple forcing functions and boundary conditions that interact non-linearly. Moreover, field data collection is very expensive and cannot provide reasonable spatial and temporal resolution. It is carried out under a very large variability of different parameters and factors. The laboratory experiments provide a suitable alternative. In contrast to environmental hydraulic situations, the conditions (both geometry and forcing conditions) under which laboratory data are collected, are, necessarily, simplified. Such simplified conditions can be controlled so that the results are expected to be reliable and of high quality. Another important advantage of laboratory models is the possibility of collecting data with very dense spatial and temporal resolution; a resolution which spans and samples most of the variability in the laboratory flow and transport field. The above mentioned advantages of laboratory models help in understanding the physical phenomena and calibrating and validating mathematical models (ASCE Committee, 1988).

Turbulent flows in conduits of non-circular cross-section are often encountered in engineering practices. Examples are open channels (canals and rivers). The flow in such conduits is accompanied by secondary motions in the plane perpendicular to the stream-wise direction, and this secondary motion can be caused by two different mechanisms (Demuren and Rodi, 1984): first, secondary motion of Prandtl's first kind is produced by centrifugal forces in curved passages. Such

(pressure-induced) secondary velocities are quite large (say 20-30% of the bulk stream-wise velocity) and occur equally in laminar and turbulent flows. Second, secondary flow of Prandtl's second kind is produced by turbulence in non-circular straight conduits. Although the secondary velocity of this kind is only 2-3% of the stream-wise bulk velocity, it can have important consequences on both the flow hydrodynamics and scalar transport. For these reasons, it is important to understand and be able to predict secondary flow phenomena in developing flow situations and in the asymptotic developed state (Demuren and Rodi, 1984).

Within the framework of the European Large Installation Plan (LIP), a program for executing experiments in the Delft tidal flume of Delft Hydraulics has been performed. The main objectives of this second LIP program (so-called LIP2) were to study the vertical and lateral exchange of momentum and secondary circulations in the shear layer region for a compound channel. The experiments have been executed for homogeneous and stable stratified flow conditions (Shiono et al, 1994). However, the current study is concerned only with the homogeneous case. Although the general setup depicted in Section 2 is designed to suit the stratified experiments, it is used (without change) for the homogeneous experiments. In Section 3, the measuring instruments and the related measurement precautions and difficulties are explained. The data analysis is given in Section 4.

2.2 Experimental Setup

The delft tidal flume of Delft Hydraulics may be considered as a schematized estuary. It is not only "tidal" but it can also be used for uni-directional flow with one or two layers. The setup adopted in the current study is suitable for uni-directional two-layer flow. The two major sections of the facility are a basin with a surface area of 120 m² representing a sea, and a flume with a width of 1 m, a depth of 1 m, and a length of 130 m, representing a river (Fig. 2.2.1 and Photo 2.2.1). The water level

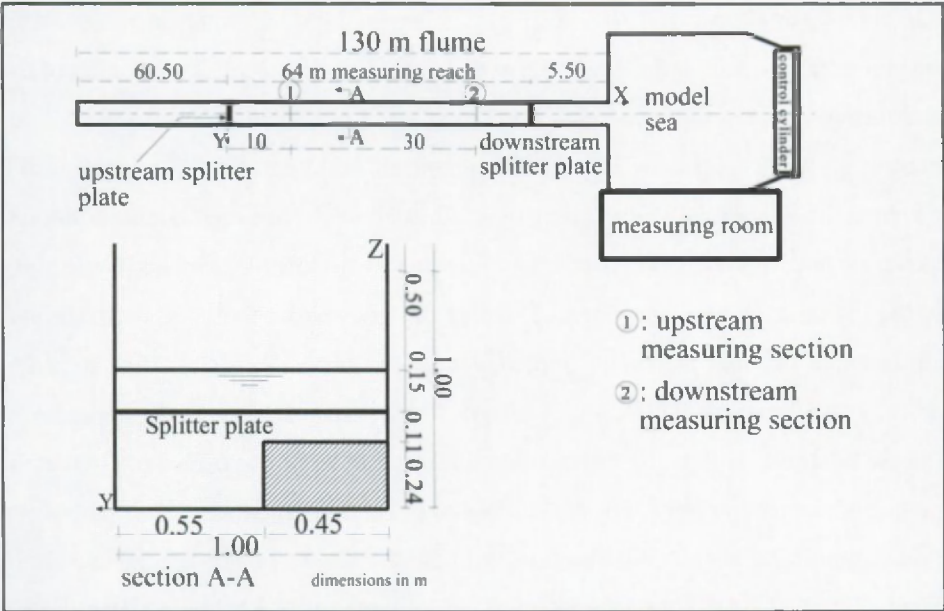


Figure 2.2.1 Schematic drawing for the experimental setup

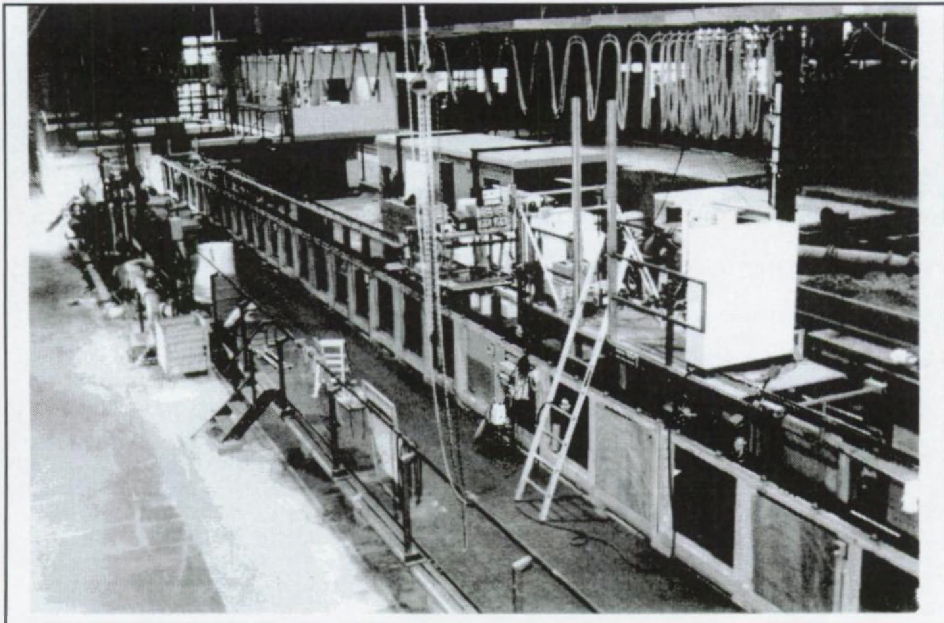


Photo 2.2.1 Delft Tidal Flume

which may vary between 0.10 and 0.90 m, is adjusted through rotation of a cylinder shaped overflow weir at the downstream end of the sea (Photo 2.2.2). The inlet of the measuring section is equipped with a 3 m long and 2 mm thick stainless steel splitter plate (Fig. 2.2.1 and Photo 2.2.3). Through elastic bending of this plate, the initial height at the inlet of the lower layer can be adjusted while still maintaining a smooth curvature and thus outflow. After a dust filter, a low turbulence level and uniformity of the lower layer flow are achieved by three meshes with increasing permeability. Upstream of the inlet section the upper layer passes dust filters. Only a fine screen to fix the end of the splitter plate removes some turbulence at the inlet of the upper layer. In case of stratified flow, the water of both layers can be re-used. This re-circulation saves both water and brine. For the purpose of circulation, the lower layer part of the flow is removed, at the outlet section, with another splitter plate also adjustable in height (Photo 2.2.4). Although the splitter plates are useful only for stratified flows, they are maintained for homogeneous experiments, producing the upstream velocity distribution depicted in Section 2.3.2. The water is recirculated through a system of reservoirs and pumps (Delft Hydraulics, 1986).

The measuring sections are located between the splitter plates which are 64 m apart. The cross section is shaped using sand-lime bricks (43.5x30x12 cm) covered by plywood 2.5 cm thick. The plywood is fixed to the bricks by screws. The resulting cross section is asymmetric (Fig. 2.2.1) with a main channel 0.50 m deep and 0.55 m wide at the right side (observed in downstream direction) and a 0.45-m-wide shallower channel with bottom level 0.24 m above that of the main channel on the left side. This cross section starts at the inlet and goes on under the downstream splitter plate up to the outlet. The thickness of the lower layer (determined by the upstream splitter plate position) is 0.35 m while the upper layer is 0.15 m thick.

For the sake of completeness, a summary of the four conducted runs is given in table 2.2.1 although the current study deals only with the homogeneous run.



Photo 2.2.2 Cylinder shaped overflow weir

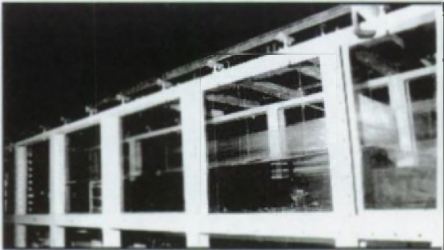


Photo 2.2.3 Upstream splitter plate

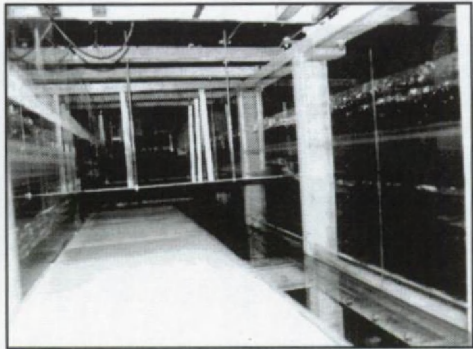


Photo 2.2.4 Downstream splitter plate

Table 2.2.1: Flow conditions for different runs

run no.	Discharge (l/s)		velocity difference (m/s)	density difference (kg/m ³)
	upper layer	lower layer		
H1	60	90	0.00	0.000
I1	60	90	0.00	15.000
I2	68	82	0.10	15.000
I3	60	90	0.00	7.500

2.3 Measurements

2.3.1 Instruments

The instruments used are listed in table 2.3.1. The following items can be recognized in the table. Five groups of instruments are used; namely, the discharge, the water level, the velocity, the temperature and the conductivity. The last two groups (temperature and conductivity) are used to determine the water density in the stratified runs. Therefore, they will not be elaborated on in the current study. Table 2.3.1 contains the position and function of each instrument.

The data collected from all the instruments are saved in ASCII files with a sampling rate of 5 Hz. This rate is not sufficient for turbulence measurements. Therefore, the ILDA and conductivity Heads (turbulence measuring instruments) data are saved in binary files with a frequency of 200 Hz.

2.3.2 EMS

The EMS, an ellipsoid of 11 mm height and 33 mm diameter, has a measuring volume of the order of the size of the probe. It is used to measure the velocity at the

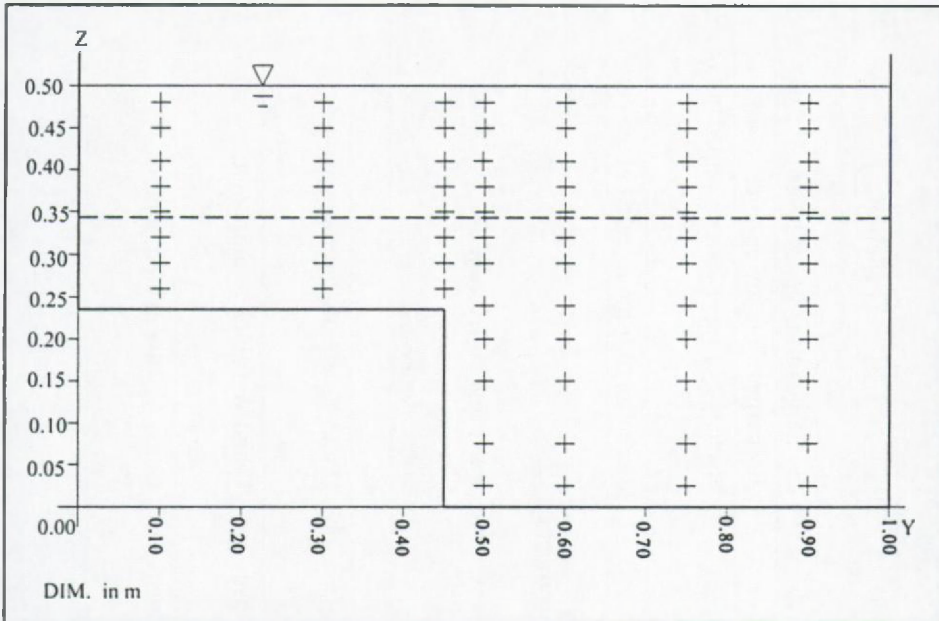


Figure 2.3.1 EMS measuring locations

upstream section of the flume (just downstream of the upstream splitter plate). The measuring points are shown in Fig. 2.3.1. The measuring time at each location is 60 seconds with 5 Hz frequency (i.e. about 300 readings are collected at each location). The isolines of the longitudinal velocity component are shown in Fig. 2.3.2. Part b of the figure shows the isovels after applying an alignment correction to the measured values shown in part a. The alignment correction angle is $2^{\circ}10'40''$. The alignment correction procedure is similar to that explained in section 2.3.3. The effect of the splitter plate is made clear in Fig. 2.3.2 where the velocity does not have a logarithmic distribution. Instead, the velocity contours have a depression around the splitter plate and peaks both above and below it. Also, from the figure, it can be seen that the correction angle is too small to affect the general distribution of the velocity field. The longitudinal velocity component measured by the EMS is used as a boundary condition for the numerical model (as described in chapter 3).

Table 2.3.1 Instruments used in LIP2 experiment

Instrument	Position	Function
I) DISCHARGE (l/s)		
DEBIET_1	upstream end of the flume	discharge of the upper layer
DEBIET_2	upstream end of the flume	discharge of the lower layer
DEBIET_3	fresh water pump	discharge of fresh water pumped out of the system
DEBIET_4	brine pump	discharge of brine injected in the system
II) WATER LEVEL		
WAVO_1	45.5 m downstream of the upstream splitter plate	water level difference
WAVO_2	7.5 m downstream of the upstream splitter plate	
III)VELOCITY (m/s)		
HILDA: Horizontal Immersible Laser Doppler Anemometer	10\40 m downstream of the upstream splitter plate	U and V velocity components
VILDA: Vertical Immersible Laser Doppler Anemometer	10\40 m downstream of the upstream splitter plate	U and W velocity components
EMS: Electro-Magnetic Flow-meter	just downstream of the upstream splitter plate	U and V velocity components

Table 2.3.1 Instruments used in LIP2 experiment (cont.)

IV) TEMPERATURE (degree Celsius)		
TEMP_1	upstream end of the flume	temperature of the upper layer
TEMP_2	upstream end of the flume	temperature of the lower layer
TEMP_3	40 m downstream of the upstream splitter plate	temperature at the downstream measuring section
TEMP_4	10 m downstream of the upstream splitter plate	temperature at the upstream measuring section
V) CONDUCTIVITY (mS)		
VAZO_1	upstream end of the flume	conductivity of the upper layer
VAZO_2	upstream end of the flume	conductivity of the lower layer
VAZO_3	40 m downstream of the upstream splitter plate	temperature at the downstream measuring section
VAZO_4	10 m downstream of the upstream splitter plate	temperature at the upstream measuring section
Pr.v. Head_1	connected to HILDA	conductivity at the same position as HILDA
Pr.v. Head_2	connected to VILDA	conductivity at the same position as VILDA

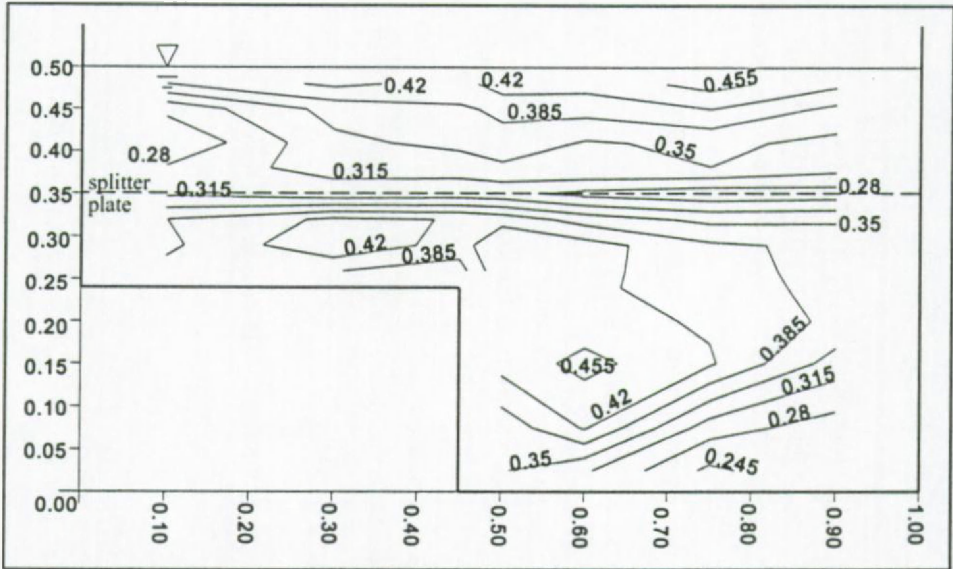
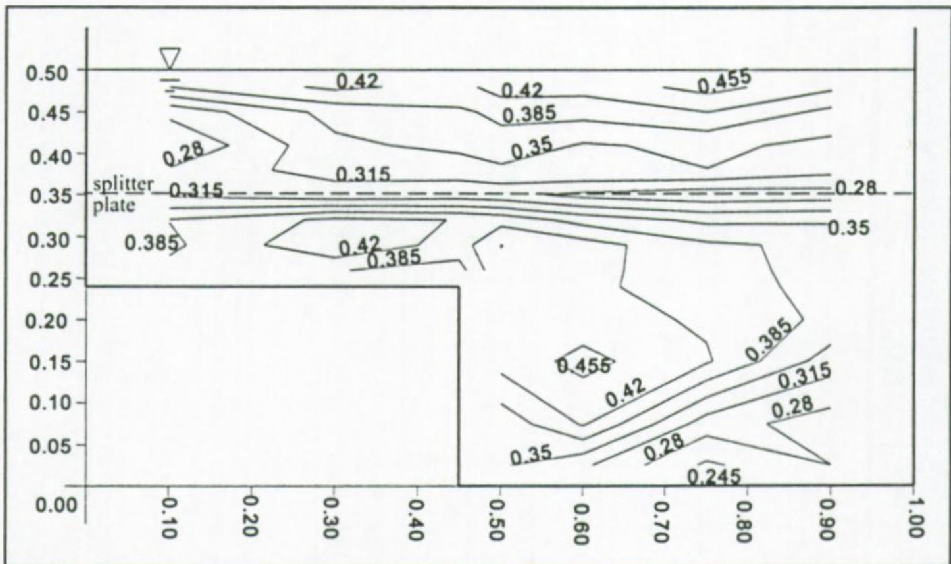
a) Isolines of U before correctionb) Isolines of U after correction

Figure 2.3.2 Longitudinal velocity component U (m/s) measured at the inlet by EMS

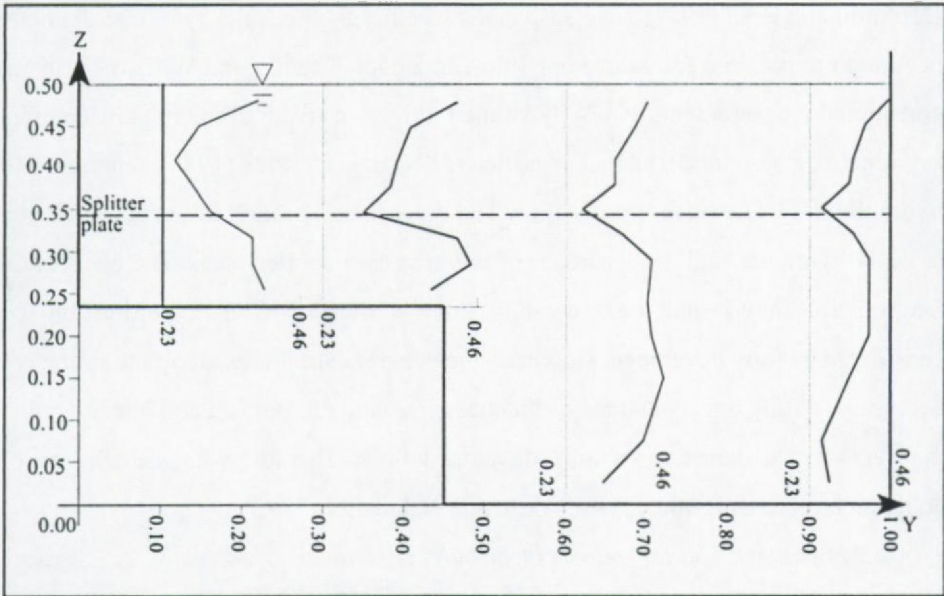


Figure 2.3.2(Cont.) c) Vertical profiles of U after correction

2.3.3 Turbulence Measurement

The fluctuating quantities are the three velocity components (u , v and w in x , y and z directions respectively) for the homogeneous run; for the stratified runs, the density which is determined as a function of conductivity and temperature is also a fluctuating quantity. While the temperature fluctuations are so small that 5 Hz sampling rate is adequate, the conductivity is as fluctuating as the velocity components. Therefore, at each point in the cross section, both velocity components and conductivity are measured simultaneously.

The turbulence measurements are performed at two sections; namely, 10 m and 40 m downstream of the upstream splitter plate. They are referred to hereafter as upstream section and downstream section respectively. It is expected that at 10 m the flow is not yet fully developed while at 40 m the flow is fully developed. The distance necessary to obtain a fully developed flow is still a matter of dispute. For example,

Demuren and Rodi (1984) were suspicious whether 84 times the hydraulic diameter is enough to obtain a fully developed flow in a duct. Thomas and Williams (1995a) considered measurements at 174 hydraulic radii downstream of the inlet place of an asymmetric compound channel insufficient. Nezu and Rodi (1986) reported 240 hydraulic radii as a sufficient distance. The downstream section of the current study is ~204 hydraulic radii downstream of the upstream splitter plate. The analysis in Section 2.4 shows that the secondary flow at the downstream section can be considered as fully developed. However, the coherent structures along the flume are necessary to fully understand the turbulence onset and mechanism and hence predict the necessary distance for a fully developed flow. The following description of coherent structures is quoted from Nezu and Nakagawa (1993):

"A well correlated spatial, parcel of turbulence, known as an 'eddy' or 'vortex', appears to have a life cycle including birth, development, interaction and breakdown. Such evolutionary relations cannot be described by means of conventional probabilistic tools...In the strict sense, coherent structures of turbulence are identified with motions of fluid parcels that have a life cycle, i.e., 'organized motion' or 'ordered motion'."

The data are collected at both upstream and downstream sections simultaneously using two measuring sets:

- The VILDA/HEAD system (Photo 2.3.1) measures the longitudinal and vertical velocity components and conductivity simultaneously at one location.
- The HILDA/HEAD system (Photo 2.3.2) measures the longitudinal and lateral velocity components and conductivity simultaneously at one location.

The ILDA's have short optical paths (avoiding change in refractive indices between layers and at the surface), and a small measuring volume (1.8 mm length and 0.1 mm maximum diameter). Hence, the flow disturbance is minimum. A very important precaution is that the laser system must warm up for some 24 hours before

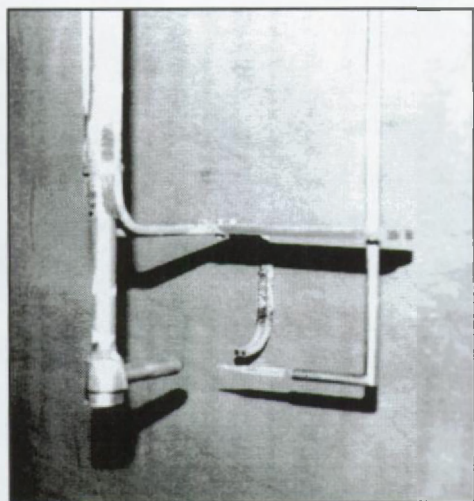


Photo 2.3.1 VILDA/HEAD system

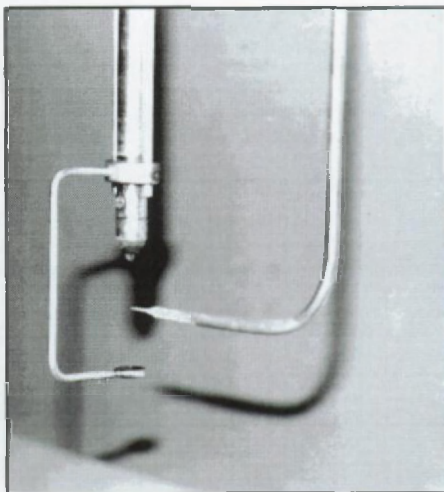


Photo 2.3.2 HILDA/HEAD system

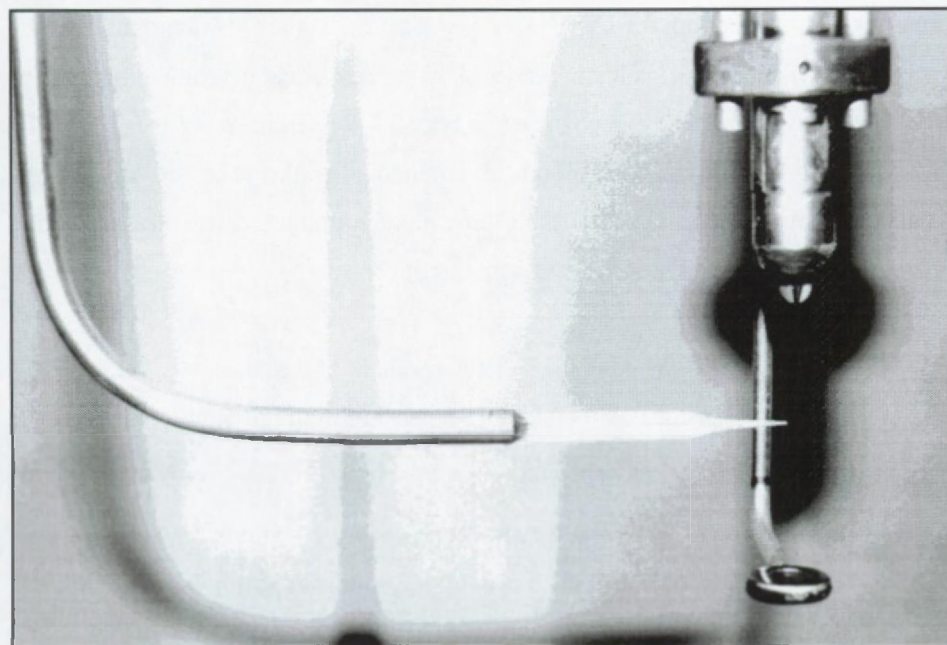


Photo 2.3.3 Position of the conductivity head with respect to HILDA

conducting measurements and it should not be switched off up to the end of the measurement campaign (nearly ten days) to avoid signal noise. The conductivity head is located 1 mm downstream of the measuring volume of the ILDA's (Photo 2.3.3) so that it has no influence on the velocity measurements.

One of the most important drawbacks of the ILDA's used in the current study is the limitations on the measuring volume. Fig. 2.3.3 shows the measuring area with the measuring locations. The hatched area represents parts that cannot be accessed by the ILDA/HEAD system because of either ILDA limitation or assembly frame limitations. For example, HILDA can measure up to 20 mm from the side wall, 40 mm from the bottom and 70 mm below the water surface. VILDA, on the other hand, can measure up to 60 mm from the side wall, 20 mm from the bottom and 10 mm below the water surface. On the other hand, the carrying frame hinders the measurements in nearly half of the cross section. Although it may be argued that this limitation is not important while studying the shear layer at the salient corner, it was found that the analysis of the shear layer is badly hindered by the frame and instrument limitations (the limitation effect can be recognized in Sec. 2.4 while analysing the data). The measurements are taken at 39 points distributed over the accessed area of the measuring cross section. The sampling time at each point is 5 minutes producing nearly 60 000 readings for each measured variable.

To satisfy the mass conservation, the resultant of the secondary velocities (V and W) in the measuring volume should vanish i.e. the total flow coming in the measuring volume should leave it. The vector \bar{V} (Fig. 2.3.4) is projected on two axes systems: the measuring system and the rotated one with a common origin and an angle of rotation θ . Knowing that the angle θ is the angle required to bring W_R down to zero, one can deduce the following relations, using the geometry of Fig. 2.3.4:

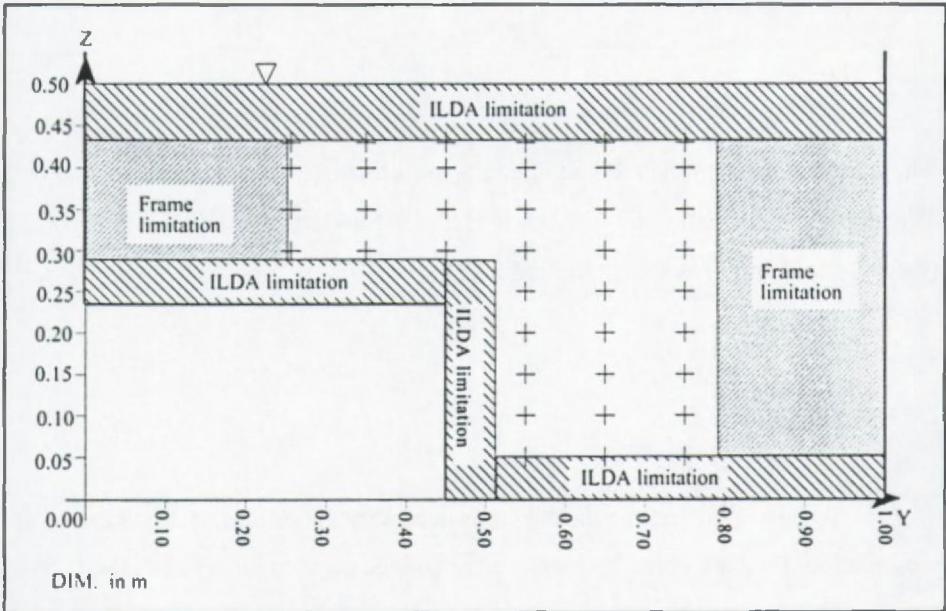


Figure 2.3.3 Measuring area in the cross section

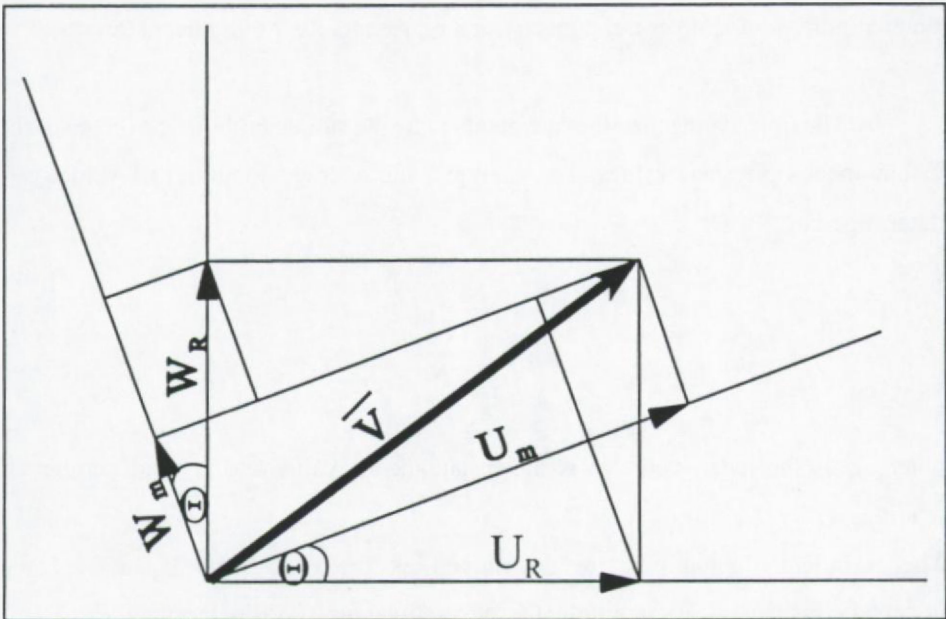


Figure 2.3.4 Effect of the alignment error on the measured velocity vectors

$$\tan \theta = \frac{W_m}{U_m}, U_R = U_m \cos \theta + W_m \sin \theta.$$

where m stands for measured and R stands for rotated.

The alignment correction for VILDA is $-1^{\circ}21'54''$ and that for HILDA is $-1^{\circ}18'22''$ (the axes convention is shown in Fig. 2.2.1).

2.4 Data Analysis

2.4.1 Introduction

To be able to analyse the data, it is necessary to perform data processing and presentation. Data are normally measured in voltage (in both binary and ASCII files). Using calibration equations, the voltage data are converted into physical units (the readings of each instrument are converted by a unique equation). The physical instantaneous values are precessed as follows to obtain time averaged values, fluctuations and double correlations (which represents Reynolds shear stresses).

The time averaged values are obtained by the simple arithmetic average of the instantaneous physical values. For example, the average longitudinal velocity is determined as

$$U = \frac{\sum_{i=1}^N u_i}{N}$$

where U is the mean value, u is the instantaneous value and N total number of readings.

The turbulent fluctuations are determined as the root mean squares of the instantaneous values. For example, the fluctuating part of u is determined as

$$u' = \sqrt{\frac{\sum_{i=1}^N (u_i - U)^2}{N}}$$

where u' is the fluctuating part of the velocity.

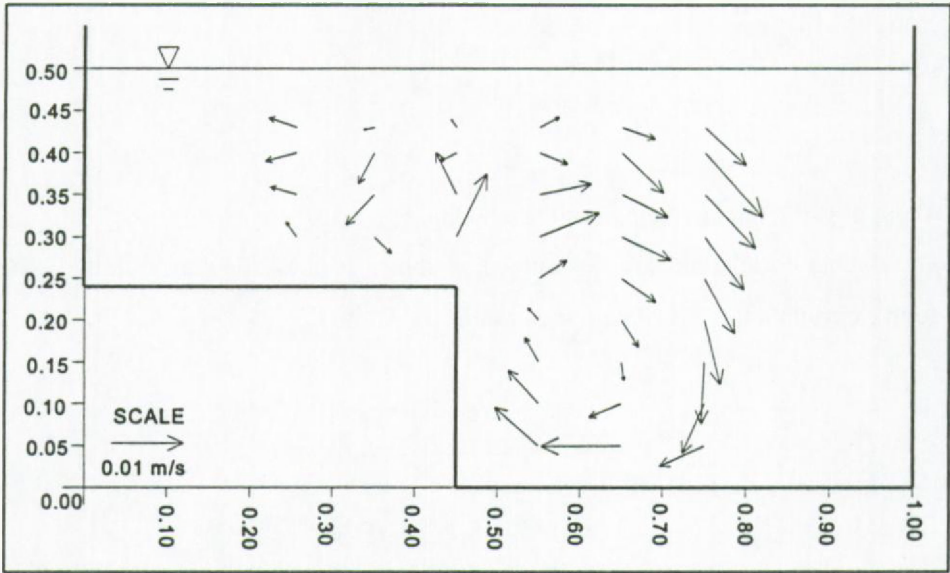
The double correlations are determined as shown in the following example. The double correlation $\overline{u'v'}$ is determined as

$$\overline{u'v'} = \frac{\sum_{i=1}^N (u_i - U)(v_i - V)}{N}$$

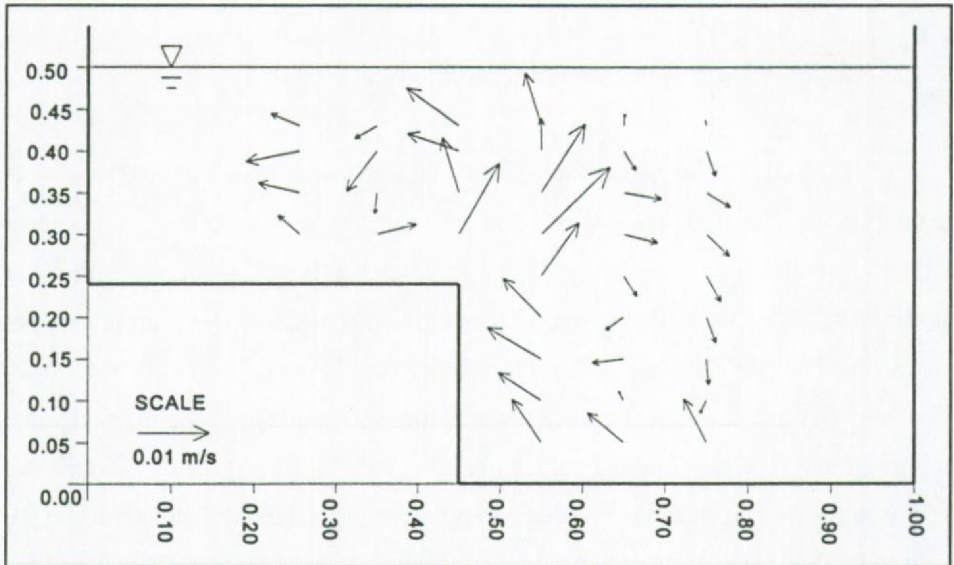
The data processing and presentation are performed for all test cases listed in table 2.2.1 (see Shiono et al, 1994). However, the homogeneous test case H1 only is analysed in this section.

2.4.2 Mean velocity and secondary circulation

Both circulation patterns at the upstream and downstream sections (Fig. 2.4.1) show two vortices; flood-plain vortex and main-channel vortex. At the salient corner (the end of the flood-plain bed near the main channel), the vortices are inclined towards the main channel. However, detailed analysis is hindered by the area being not measured. The effect of the secondary circulation is to move slow moving water from the flood plain at the salient corner towards the water surface in the main channel causing the typical longitudinal velocity contour bulging (Fig. 2.4.2). On both sides of the bulge, the isovels bulge towards the walls (i.e. the bed of the flood plain and the side wall of the main channel) due to high momentum transport by the secondary flow. At the upstream section (Fig. 2.4.2 a), the splitter plate effect noticed in Fig. 2.3.2 disappears but the typical fully developed bulging pattern noticed at the downstream

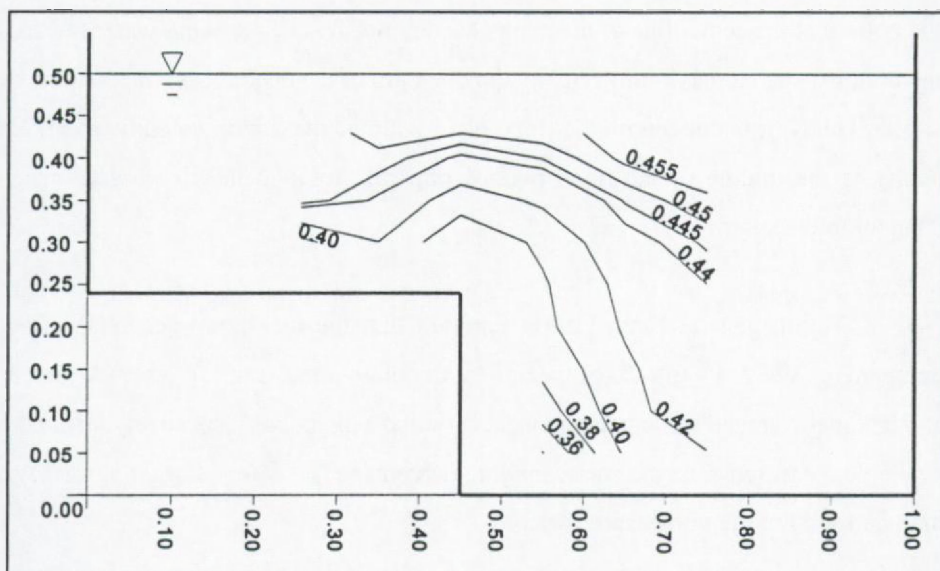


a) Upstream section

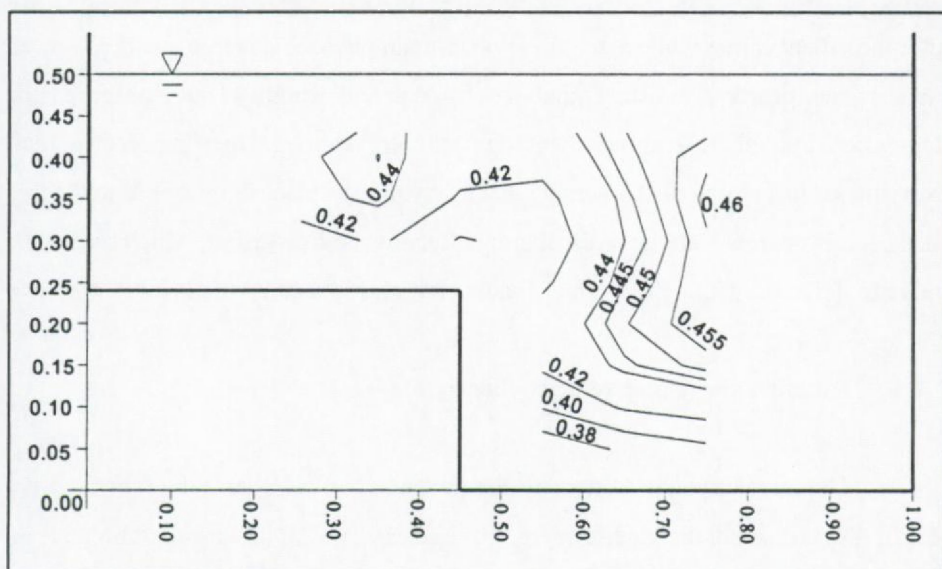


b) Downstream section

Figure 2.4.1 Secondary circulation



a) Upstream section



b) Downstream section

Figure 2.4.2 Isovels for U (m/s)

section (Fig. 2.4.2 b) is not pronounced yet. The secondary flow movement towards the bottom at the center line of the main channel transfers fast moving water towards the bottom causing maximum velocity dip one third of the depth below the surface. A similar behavior is noticed on the flood plain with the maximum velocity occurring nearly at the middle of the flood plain depth and closer to the flood-plain-main-channel intersection.

Tominaga and Nezu (1991) reported that the maximum secondary flow component $(V^2+W^2)^{1/2}$ was 4% of the maximum longitudinal one (U), where V and W are the time-averaged velocity components in y and z directions respectively. From the available measurements, the corresponding percentage is 2.8%. A Larger percentage may be found in the unmeasured area.

The depth-mean velocity (Fig. 2.4.3) has a peak on the flood plain just before the salient corner, in agreement with the observation of Rhodes and Knight (1994). However, the depression of the depth-mean velocity occurs in the main channel just after the salient corner while at the flood-plain-main-channel interface, the depth-mean velocity has nearly a constant gradient. Rhodes and Knight (1994) observed the depression immediately above the salient corner. Although they performed their experiments in a closed duct assuming that the symmetry plane corresponds to the free surface, it is obvious that the redistributing effect by the free surface which causes the bulge to deflect towards the main channel is not reproduced by the symmetry plane.

2.4.3 Kinetic energy and velocity fluctuations

The three turbulence intensity components show a bulge at the salient corner (Fig. 2.4.4,5,6). Also, the kinetic energy ($k=\frac{1}{2}(u'^2+v'^2+w'^2)$) has a similar bulge (Fig. 2.4.7). The bulging indicates that the turbulence increases in the wall region as well as the free shear layer region. Such a turbulence behavior is consistent along the flume

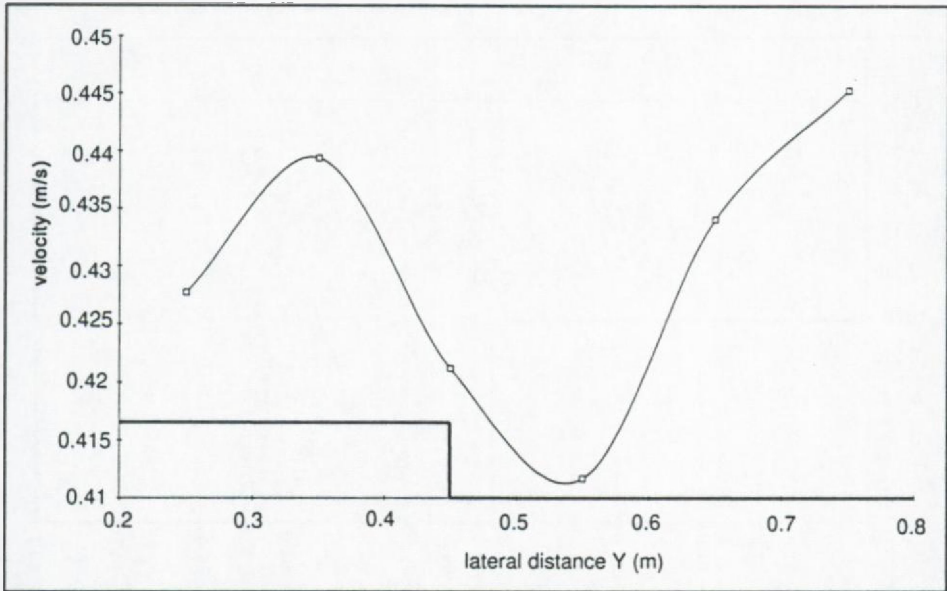
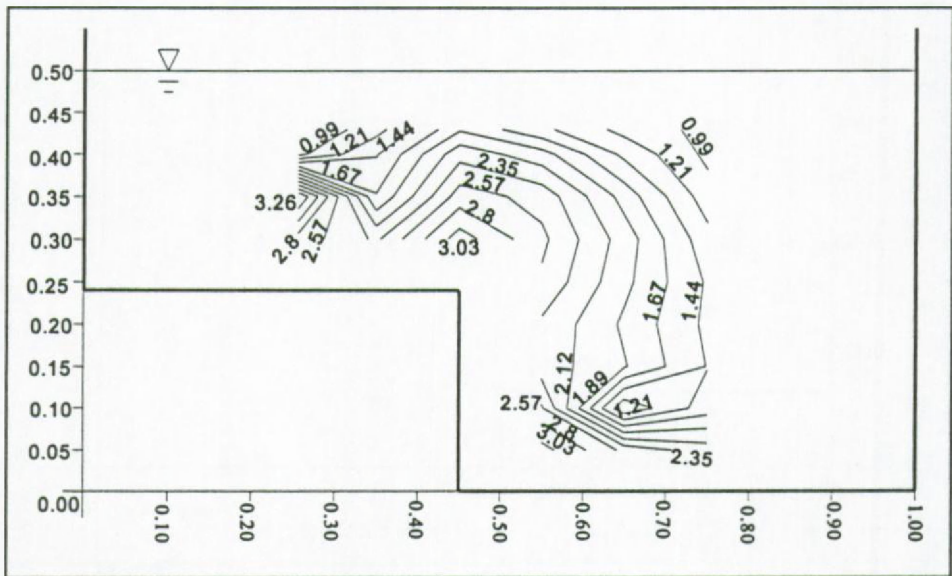
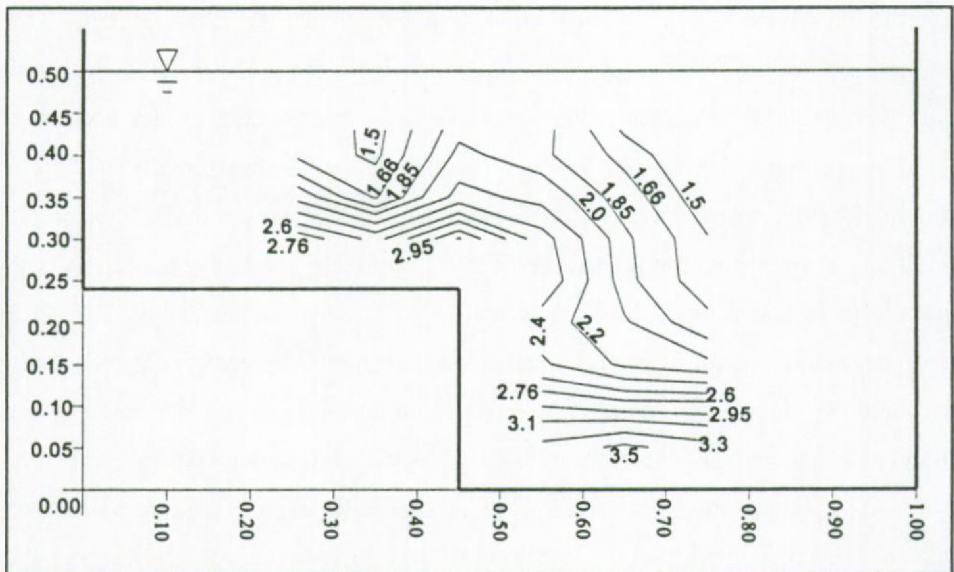


Figure 2.4.3 Depth-averaged longitudinal velocity, U versus lateral distance, y

since it is noticed in both measuring sections (compare parts a and b of the above mentioned figures). The fluctuation of u is always larger than the other two components in the shear layer. At the salient corner, both v and w fluctuations are nearly equal. v -fluctuations have steeper vertical gradient and milder horizontal gradient, compared with w . Thus, v -fluctuations bulge horizontally while w -fluctuations bulge vertically. This is in agreement with the explanation of Thomas and Williams (1995a) that the fluctuation of a velocity component is enhanced by wall parallel to it and damped by wall normal to it. The depression in Fig. 2.4.5 b is considered as a measuring error noticed also in the anomalous vectors at $(y=65, z=10 \text{ cm})$ and $(y=75, z=5 \text{ cm})$ in Fig. 2.4.1 b. The turbulence drops to a minimum on the flood plain at a horizontal distance of 0.4 flood plain depth from the salient corner then starts to increase again. Unfortunately, the turbulence behavior in the side wall region of the flood plain could not be determined. The corresponding depression near the main channel side wall is much less pronounced. From such distribution of turbulence intensity, it can be concluded that the shear layer extends laterally in the main channel

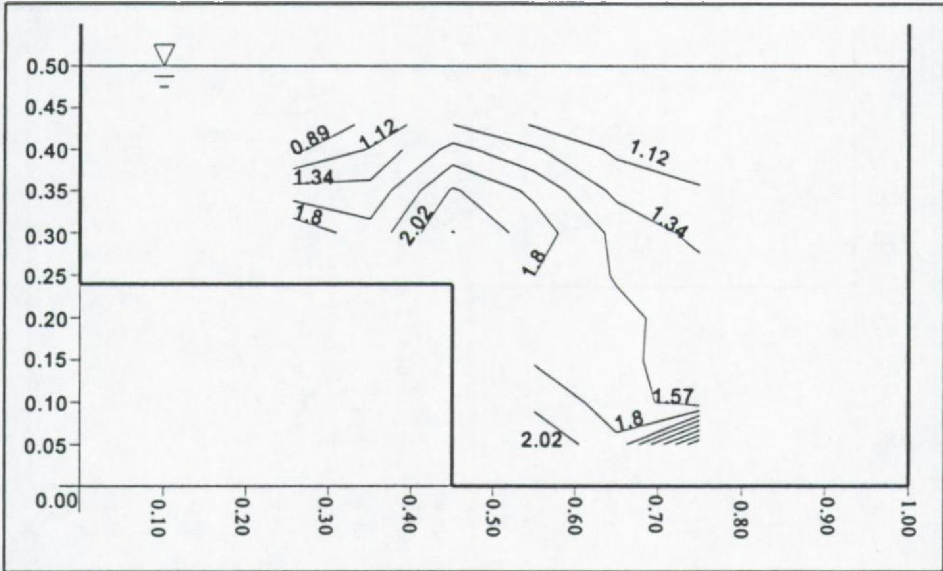


a) Upstream section

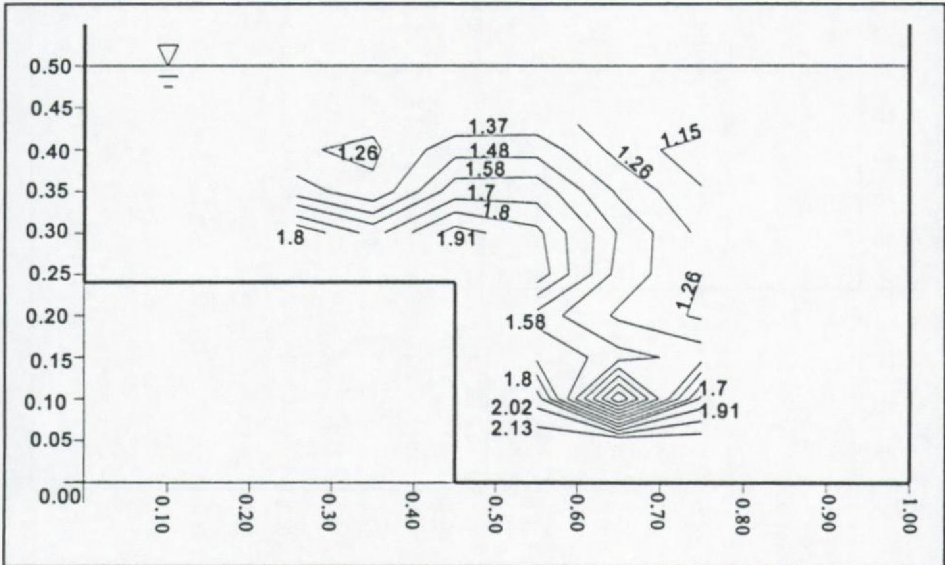


b) Downstream section

Figure 2.4.4 Isolines for u' (cm/s)

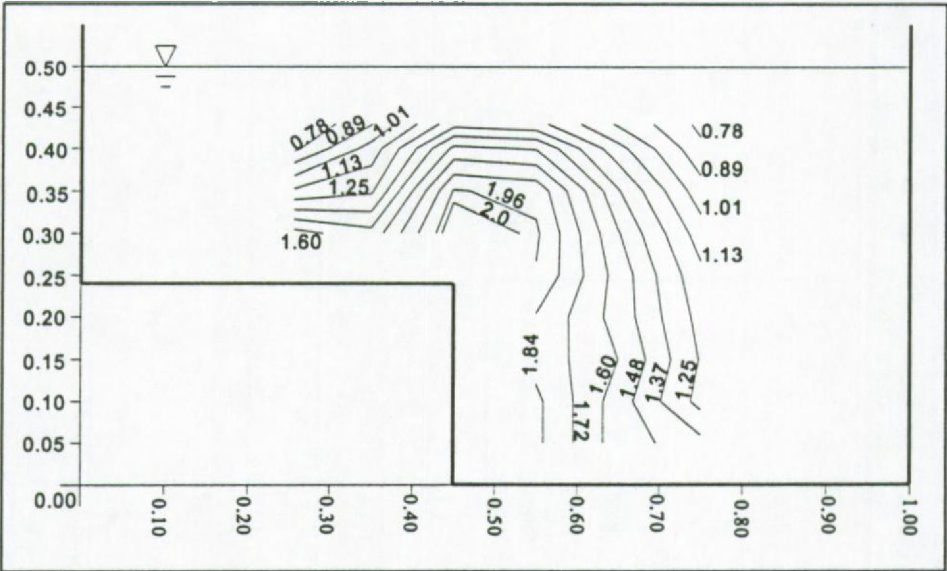


a) Upstream section

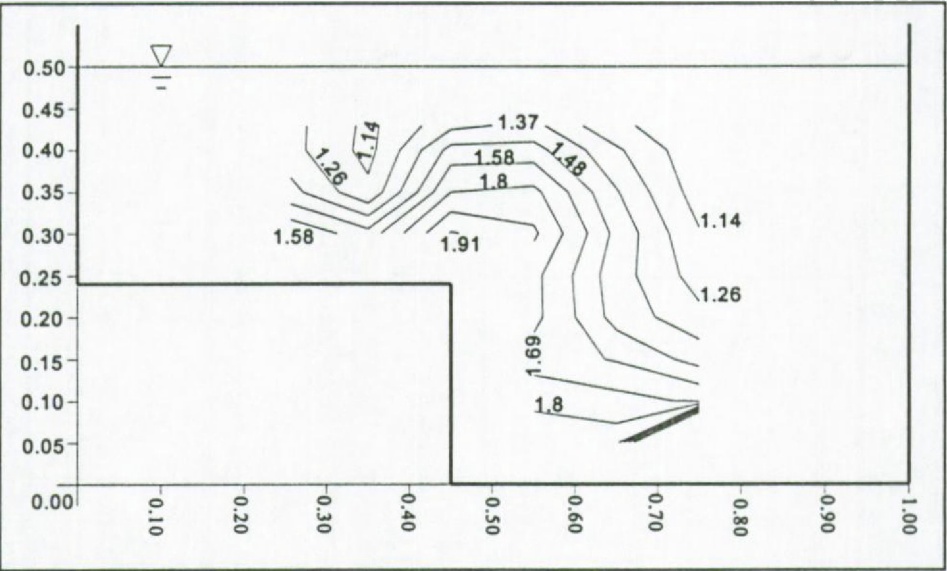


b) Downstream section

Figure 2.4.5 Isolines for v' (cm/s)

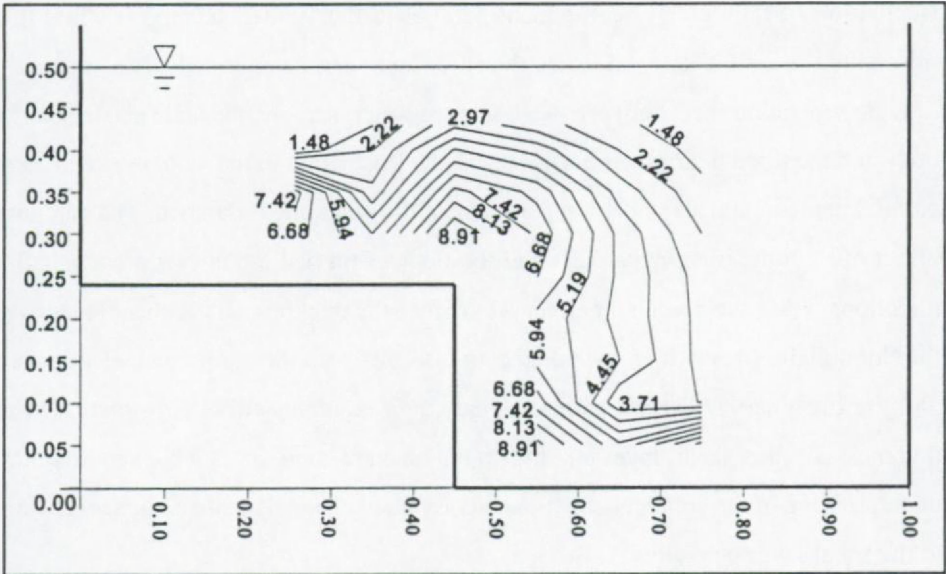


a) Upstream section

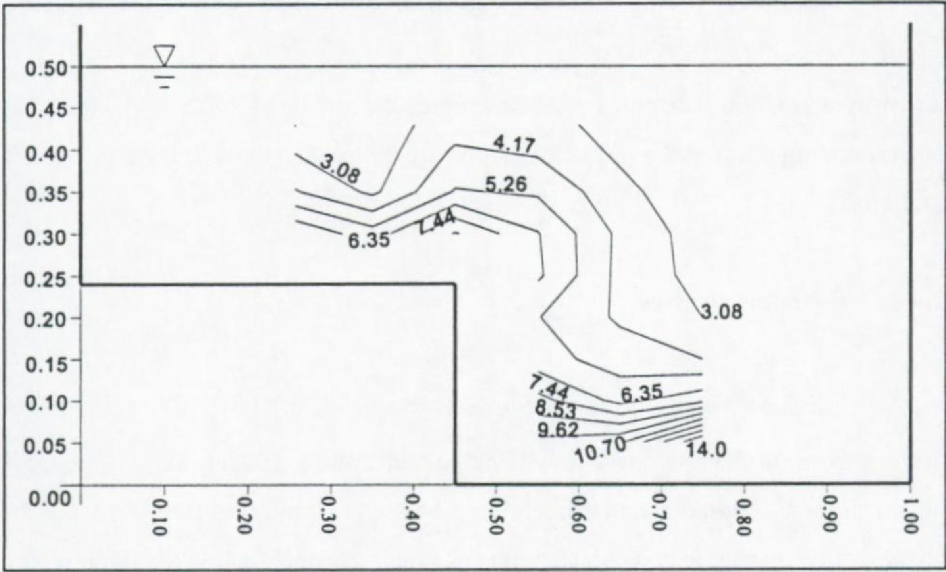


b) Downstream section

Figure 2.4.6 Isolines for w' (cm/s)



a) Upstream section



b) Downstream section

Figure 2.4.7 Isolines for k (cm^2/s^2)

while it is limited on the flood plain. A possible interpretation is that near the wall the fluctuation of the velocity component parallel to the Wall is enhanced while that normal to the wall is damped. Also, the shear layer can be regarded as an imaginary moving separation sheet between two bodies of water, namely, the main channel water body and the flood plain water body. Hence, the fluctuation of the velocity component parallel to the imaginary sheet is enhanced and the other one is damped. The damping effect of both the imaginary sheet and the flood plain bed are in two perpendicular directions. Thus, their resultant effect is to reduce the thickness of the shear layer over the flood plain. Meanwhile, the enhancing effect of both the main-channel side wall and the imaginary sheet are parallel. Thus, their resultant effect is to increase the thickness of the shear layer on the main channel side. It is believed that the understanding of the coherent structure in compound channels will add better analysis to the shear layer behavior.

The ratios $\frac{v'}{u'}$ and $\frac{w'}{u'}$ are ~ 0.6 near walls (side wall and bed) at the

downstream section. The ratios increase towards the middle of the main channel. The corresponding ratios at the upstream section are larger than those at the downstream section.

2.4.4 Reynolds stresses

Fig. 2.4.8 shows the contour lines of the difference $(v'^2 - w'^2)$ which is the driving force for the secondary flow (Cokljat and Younis, 1995a). The difference is high near the bed of the main channel. It can be seen that the zero isoline divides the cross section into three parts: deep part of the main channel (below the flood plain), shallow (upper) part of the main channel and the flood plain. Comparing Fig. 2.4.8 with both Figs. 2.4.9 and 2.4.10, it can be seen that at the zero isolines, the Reynolds

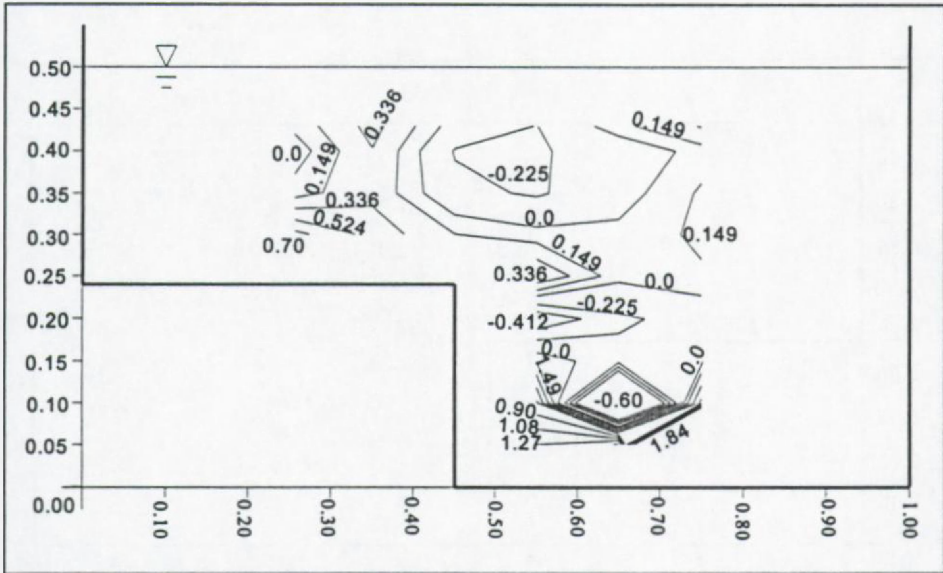


Figure 2.4.8 Contours for $v'^2-w'^2$ (cm^2/s^2)

shear stress is maximum. v and w used in this analysis are not measured simultaneously at the same location causing inaccuracy in the obtained results.

The Reynolds shear stresses $-\overline{u'v'}$ and $-\overline{u'w'}$ (Fig. 2.4.9 and 2.4.10) exhibit two peaks: one is along a vertical in the shear layer and the other is along a horizontal plane dividing the main channel at the flood plain bed level.

2.5 Conclusion

Within the framework of LIP2, the tidal flume of Delft Hydraulics is used to study the vertical and lateral exchange of momentum and secondary circulation in the shear layer region of a compound channel. The discussion provided in this chapter deals with the homogeneous flow run of LIP2. The compound channel structure and the measuring instruments are explained. The limited area, accessible by the ILDA/HEAD systems, caused loss of important information near the (free and solid)

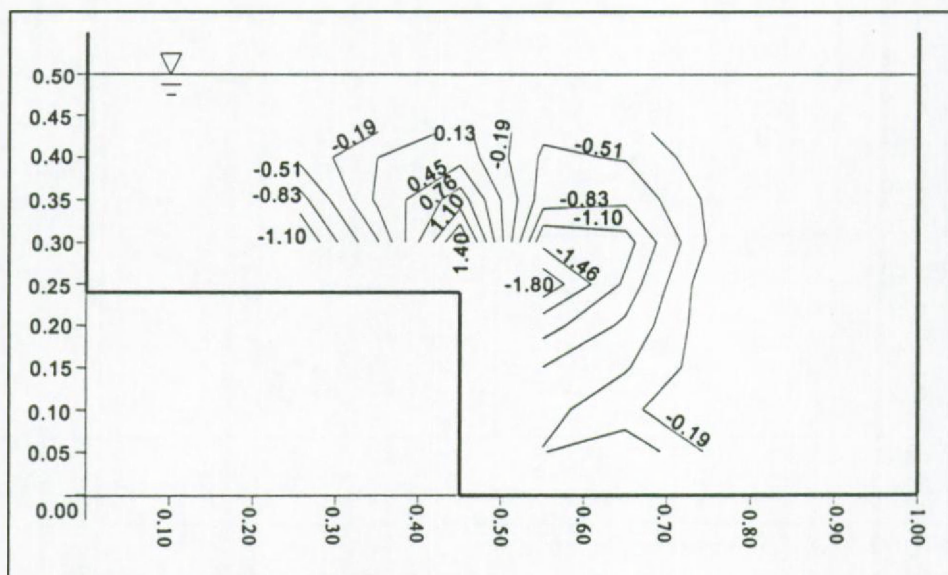


Figure 2.4.9 Isolines for $\overline{u'v'}$ (cm^2/s^2)

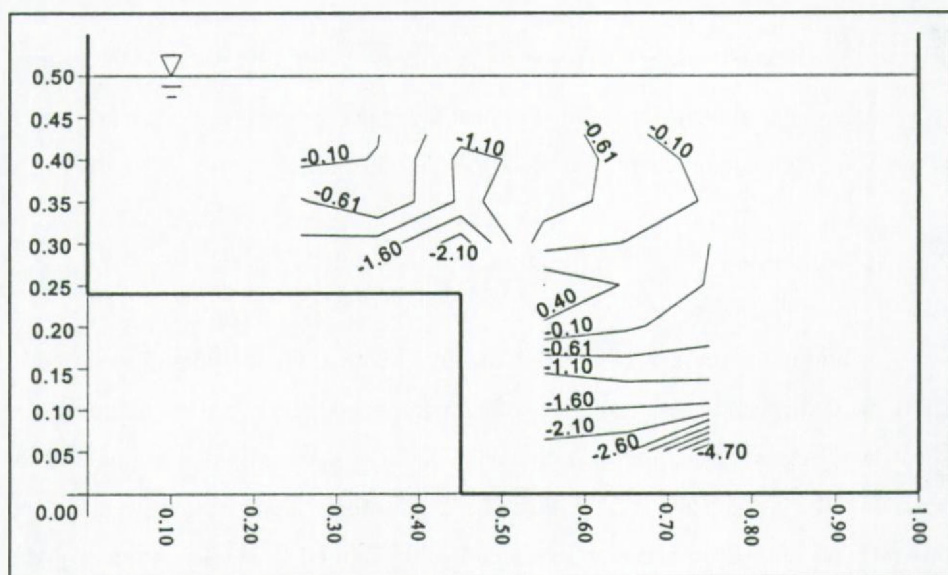


Figure 2.4.10 Isolines for $\overline{u'w'}$ (cm^2/s^2)

surfaces. The misalignment of the instruments is corrected so that the mass conservation is maintained in the cross section.

At the upstream section, the splitter plate effect disappears but the turbulence is not yet fully developed. The secondary flow at the downstream section and its effect on the longitudinal velocity component indicates a fully developed flow. However, the position of the fully developed section is still open for research. Although the point measurement at a single cross section along the flume provides useful information regarding the turbulence, it is not sufficient. It is believed that the study of turbulence along the flume and consequently recognizing the coherent structures is important to fully understand the (not fully random but "partly" organized) turbulence phenomena (Yalin, 1992).

The study of the turbulence kinetic energy, the turbulence intensity and the Reynolds stresses give a picture of the flow pattern in the cross section and the driving forces. The cross section is divided by two shear layers into three parts: deep main channel, shallow main channel and flood plain.

It is noticed that the shear layer extends laterally in the main channel but has a small thickness over the flood plain. A new interpretation is introduced.

Chapter 3

NUMERICAL MODELLING

3.1 Introduction

Physical models are powerful tools to investigate and understand the different phenomena controlling the flow. Although this fact holds true, as has been emphasized in Chapter 2, physical models have their own limitations and difficulties. Some examples are scaling and distortion, cost, inflexibility, being not transportable, and not adaptable (Falconer and Cahyono, 1993). The attention is, then, directed, with the assistance of the physical understanding of the phenomena, to expressing the physics in mathematical form. This new trend is promoted by the great advancement in numerical methods, programming techniques, and computer hardware (Song, 1995). However, scientists and engineers should be cautious in dealing with numerical techniques. When interpreting the output of the solution from the numerical models, the engineer should be able to judge how far the results represent reality. Given a physical problem, one first needs a mathematical model whose solution in some sense approximates the solution of the physical problem. Next, a numerical model of the mathematical problem is needed. The solution to the numerical model only approximates the mathematical model solution. The final step is to solve the numerical model. Again, because of the solution method and the finite word length of digital computers, the computer solution only approximates the solution to the numerical model (Hageman and Young, 1981).

In the subsequent sections, the following mathematical issues will be discussed: The differential equations representing the hydrodynamic behaviour of open

channel flow are stated in section (3.2); together with the necessary assumptions underlying the governing equations. Section (3.3) explains the difficulties associated with discretizing the advection term and the proposed remedies. Section (3.4) deals with the pressure term when treated in a full 3D model. Section (3.5) is devoted to the difficult problem of treating the boundaries. The remaining part of the governing equations is the Reynolds turbulent stress term. The numerical treatment of the turbulence is elaborated on in chapter 4.

3.2 The Governing Equations

For a fluid, Newton's law (mass times acceleration equals the sum of forces) is better stated per unit volume, with density replacing mass. This produces the momentum equations (Cushman-Roisin, 1994)

$$\rho \left(\frac{\partial u_i}{\partial t} + \frac{\partial u_i u_j}{\partial x_j} \right) = - \frac{\partial p}{\partial x_i} + \rho g_i + \frac{\partial \tau_{ij}}{\partial x_j}$$

where tensor notation is used to define repeated variables (see Appendix A); and,

t time (s).

i, j indices indicating spatial dimensions.

x_i, x_j the coordinate axes. Here, x_1, x_2, x_3 correspond to the Cartesian coordinates x, y, z , respectively, with x positive eastward (main flow direction), y positive northward (lateral direction) and z positive upward.

u_i, u_j tensor notation of the components of the instantaneous velocity vector. In a Cartesian system, they take the values u_1, u_2, u_3 (or u, v, w) which are the components in x, y , and z directions respectively (m/s).

p : the pressure (N/m^2).

g_i : acceleration due to gravity ($= 9.81 \text{ m/s}^2$ in the vertical direction).

ρ : the fluid density (kg/m^3).

τ_{ij} : the components of the viscous stress tensor (N/m^2).

The mass conservation is expressed in the form of the continuity equation,

$$\frac{\partial \rho}{\partial t} + \frac{\partial}{\partial x_i}(\rho u_i) = 0$$

The Boussinesq approximation consists of neglecting any variation of the density except in the gravitational term (Currie, 1993). The density can, generally, be expressed as,

$$\rho = \rho_0 + \rho'(x, y, z, t)$$

where ρ_0 is a reference density and ρ' is the fluctuating part of the density. Applying the Boussinesq approximation, the continuity equation becomes

$$\frac{\partial u_i}{\partial x_i} = 0 \quad (3.2.1a)$$

which states that the conservation of mass has become conservation of volume.

The pressure,

$$p = p_0(z) + p_d(x, y, z, t)$$

and

$$p_0(z) = P_0 - \rho g z$$

where $p_0(z)$ is the hydrostatic pressure which is a function of z only, P_0 is a reference pressure (e.g. the atmospheric pressure) and p_d is the dynamic part of the pressure. $p_0(z)$ has no derivatives with respect to x and y .

The momentum equations are then reduced to

$$\frac{\partial u_i}{\partial t} + \frac{\partial u_i u_j}{\partial x_j} = \frac{1}{\rho_0} \left(-\frac{\partial p_d}{\partial x_i} + \rho g_i + \frac{\partial \tau_{ij}}{\partial x_j} \right) \quad (3.2.1b)$$

or, using the Cartesian notation and combining the local and advective accelerations in a total derivative (the so-called the inertial term),

$$x: \frac{du}{dt} = \frac{1}{\rho_0} \left(-\frac{\partial p_d}{\partial x} + \frac{\partial \tau_{xx}}{\partial x} + \frac{\partial \tau_{xy}}{\partial y} + \frac{\partial \tau_{xz}}{\partial z} \right)$$

$$y: \frac{dv}{dt} = \frac{1}{\rho_0} \left(-\frac{\partial p_d}{\partial y} + \frac{\partial \tau_{xy}}{\partial x} + \frac{\partial \tau_{yy}}{\partial y} + \frac{\partial \tau_{yz}}{\partial z} \right)$$

$$z: \frac{dw}{dt} = \frac{1}{\rho_0} \left(-\frac{\partial p_d}{\partial z} - \rho g + \frac{\partial \tau_{xz}}{\partial x} + \frac{\partial \tau_{yz}}{\partial y} + \frac{\partial \tau_{zz}}{\partial z} \right)$$

Equations (3.2.1) are one particular form of the well-known Navier-Stokes equations.

Most of the engineering flows consist of randomly fluctuating flow properties. The Reynolds' statistical approach is the best way to express the fluctuating turbulent nature of the flow. All the quantities are expressed as the sum of mean and fluctuating

parts i.e.

$$u_i = U_i + u_i'$$

and

$$p_d = P + p'$$

The momentum and continuity equations are then integrated over a time interval which is very long relative to the maximum period of the turbulent fluctuations but very short relative to the time scale characteristic for the mean flow variations that are not regarded as belonging to turbulence. The time averaging yields the Reynolds averaged Navier-Stokes equations of motion in conservation form (Wilcox, 1993)

$$\frac{\partial U_i}{\partial x_i} = 0 \quad (3.2.2a)$$

$$\frac{\partial U_i}{\partial t} + \frac{\partial U_i U_j}{\partial x_j} = -\frac{1}{\rho_0} \frac{\partial P}{\partial x_i} - \frac{\rho'}{\rho_0} g_i + \frac{\partial}{\partial x_j} (t_{ij} - \overline{u_i u_j'}) \quad (3.2.2b)$$

where t_{ij} is the viscous stress tensor divided by ρ_0 defined by

$$t_{ij} = \frac{\tau_{ij}}{\rho_0} = 2\nu s_{ij}$$

where ν is the kinematic viscosity and s_{ij} is the strain-rate tensor,

$$s_{ij} = \frac{1}{2} \left(\frac{\partial U_i}{\partial x_j} + \frac{\partial U_j}{\partial x_i} \right)$$

U_i is the mean velocity, P is the mean (dynamic) pressure, u_i' is the fluctuation of the velocity; p' is the fluctuation of the pressure, and $\overline{u_i u_j}$ is the Reynolds' stress.

It can be easily noticed that the Reynolds' averaged Navier-Stokes equations (3.2.2) are identical to the instantaneous Navier-Stokes equations (3.2.1) with the mean velocity and pressure replacing the instantaneous ones. The only difference between the time-averaged and the instantaneous equations is the appearance of the correlations $\overline{u_i u_j}$ in the time averaged momentum equations. This correlation term will be the subject of Chapter 4.

When hydraulic applications are concerned, the momentum equation in the vertical z -direction is usually reduced to an hydrostatic pressure equation. In the following, it will be shown that the hydrostatic pressure assumption is not valid as a mathematical representation of the flume experiment explained in chapter 2. Hence, the mathematical model, developed in the current study, consists of the continuity equation and three full momentum equations besides the turbulence closure model.

The hydrostatic pressure assumption is only valid when there is a strong geometric disparity of the flow i.e. the horizontal dimensions are much larger than the vertical ones as is the case in shallow coastal areas (Cushman-Roisin, 1994). The relative importance of different terms is expressed in terms of their orders of magnitude. The orders of magnitude of different terms in the governing equations can be studied as follows. The horizontal velocity can be scaled by the velocity scale V and

the vertical one by W . The horizontal distances can be scaled by the length scale L and the vertical one by H . The pressure divided by density can be scaled by P . The focus will be on the advection and pressure terms. The same conclusion will be obtained if other terms are included. The terms of the continuity equation

$$\frac{\partial U}{\partial x} + \frac{\partial V}{\partial y} + \frac{\partial W}{\partial z} = 0$$

can be scaled as

$$\left[\frac{V}{L} \right] \quad \left[\frac{V}{L} \right] \quad \left[\frac{W}{H} \right]$$

Thus

$$\frac{V}{L} \sim \frac{W}{H} \quad (3.2.3)$$

The momentum equation in the x- and y-directions have the same scaling. Consider the x-momentum equation

$$\frac{\partial UU}{\partial x} + \frac{\partial UV}{\partial y} + \frac{\partial UW}{\partial z} = -\frac{1}{\rho} \frac{\partial P}{\partial x}$$

Its terms can be scaled as

$$\left[\frac{V^2}{L} \right] \quad \left[\frac{V^2}{L} \right] \quad \left[\frac{VW}{H} \right] \quad \left[\frac{P}{L} \right]$$

Substituting from Equation (3.2.3), one gets the following two forms

$$\frac{P}{L} \sim \frac{V^2}{L}$$

$$\frac{P}{L} \sim \frac{VW}{H}$$
(3.2.4)

The terms of the z-momentum equation

$$\frac{\partial UW}{\partial x} + \frac{\partial VW}{\partial y} + \frac{\partial WW}{\partial z} = -\frac{1}{\rho} \frac{\partial P}{\partial z}$$

can be scaled as

$$\left[\frac{VW}{L} \right] \quad \left[\frac{VW}{L} \right] \quad \left[\frac{W^2}{H} \right] \quad \left[\frac{P}{H} \right]$$

substituting from Equations (3.2.3) and (3.2.4), the scaling will be

$$\left[\frac{W^2}{H} \right] \quad \left[\frac{W^2}{H} \right] \quad \left[\frac{W^2}{H} \right] \quad \left[\frac{W^2}{H^3} L^2 \right]$$

Multiplying by H^3 and dividing by W^2

$$[H^2] \quad [H^2] \quad [H^2] \quad [L^2]$$
(3.2.5)

From Equation (3.2.5), it is clear that the pressure term is scaled by L^2 while the advective terms are scaled by H^2 in the vertical momentum equation. If there is a geometric disparity of the flow, then $L \gg H$ and the pressure term dominates over the advection term, which justifies the hydrostatic pressure assumption. However, in the flume experiment H can be taken as the flow depth (0.5 m) and L can be taken as the flume width (1.0 m) which are comparable. Therefore, the hydrostatic pressure assumption contains an intolerable approximation to the flume experiment and the

need to full vertical momentum equation cannot be disposed of.

3.3 Advection Term

3.3.1 Introduction

The final target of the current study is to simulate and analyse the secondary circulations. Secondary circulations are mainly driven by the turbulence (not advection). Although one would expect to pay all attention to the turbulence model, the infamous advection term must be given prime importance in discretizing the governing equations. Actually, it seems to make no sense to use sophisticated (and expensive) multiple equation turbulence models with advection schemes which omit the turbulent transport terms from the momentum and scalar transport equations (and from the turbulent transport equations themselves), replacing them by the artificial numerical diffusion inherent in the truncation error of the modelled convection terms (Leonard and Mokhtari, 1990).

Guinot (1995) stated that there are two major difficulties associated with the numerical (finite differences or finite elements) solution of the advection equation. First, numerical schemes may produce spurious diffusion and/or dispersion. The former leads to artificial damping of the computed solution; the latter results in oscillations "wiggles" in the vicinity of moving fronts. Second, boundary conditions should be expressed in a way that is consistent with the numerical scheme used. Moreover, Leonard (1988) concluded that no single scheme seems to be totally successful under all circumstances. The problems of the currently available schemes can be categorised as follows. The standard second-order central differencing of the convection terms suffers from the well-known odd-even decoupling and requires the addition of some higher-order artificial dissipation terms to create the required damping of high frequency errors (Hirsch, 1991). This lack of inherent numerical convective stability is common to all centrally distributed finite difference methods

irrespective of the order of the method (Leonard, 1980). The upstream-weighted methods are inherently stable giving oscillation-free solutions. Unfortunately, the first-order upwind scheme achieves its stability through the effective introduction of an artificial diffusion term which is equivalent to a central difference technique to which an artificial numerical diffusion coefficient (or viscosity) of the form

$$\Gamma_{\text{num}} = \frac{u \Delta x}{2}$$

has been added. The artificial diffusion corrupts or dominates the modelled physical diffusion under high-convection conditions giving highly inaccurate results (Leonard, 1980, Sweby, 1984, Leonard and Mokhtari, 1990, Falconer and Cahyono, 1993). In second-order upwind schemes, the leading truncation error term involves a spacial third derivative which under some conditions may introduce weak oscillations (Leonard, 1988, Sweby, 1984). Total Variation Diminishing (TVD) schemes and other schemes like Hybrid and Power Law Differencing Schemes (PLDS) revert to first-order upwinding (Leonard and Mokhtari, 1990, Leonard, 1991). The third-order upwinding (QUICK and QUICKEST) algorithm is seen to be promising because of its increased accuracy over the diffusive first-order method and oscillatory second-order method, its enhanced stability over the oscillatory fourth-order method and its computational simplicity in comparison with the more accurate but highly complex fifth-order method. However, with sharp change of gradients, third-order upwinding produces some leading overshoots and trailing undershoots. Leonard (1991), in his effort to "inject some self-confidence (as opposed to self-satisfaction) into computational fluid dynamics", introduced the universal limiter. The ULTIMATE QUICKEST scheme is then expected to give better results (Leonard, 1991, Cahyono, 1992). Cahyono, 1992 has conducted a comprehensive study of the advection term.

The ULTIMATE QUICKEST scheme will be explained in the following sub-section. A comment on the method will be given in sub-section 3.3.3.

3.3.2 ULTIMATE QUICKEST

The ULTIMATE QUICKEST scheme consists of two parts: QUICKEST stands for Quadratic Upstream Interpolation for Convective Kinematics with Estimated Streaming Term, and the monotonicity maintaining part, ULTIMATE which stands for Universal Limiter for Transient Interpolation Modelling of Advective Transport Equations. Although the QUICKEST scheme, when applied to multi-dimensional problems involves transverse curvature terms, the one-dimensional QUICKEST formulation can be safely applied neglecting the (practically small) transverse curvature terms (Leonard, 1988). Moreover, the limiting step is locally one-dimensional in the normal direction for each face of the control volume. Thus, the one-dimensional formulation of the ULTIMATE QUICKEST is applied to the current 3D model. Each face of the control volume is treated separately.

The ULTIMATE QUICKEST scheme (Leonard, 1991) can be summarized as follows.

Consider the advection equation

$$\frac{\partial \phi}{\partial t} + \frac{\partial u \phi}{\partial x} = 0$$

for the quantity ϕ in the x -direction with velocity u , and consider the usual notation of n for time indexing and i for distance indexing.

The target is to evaluate

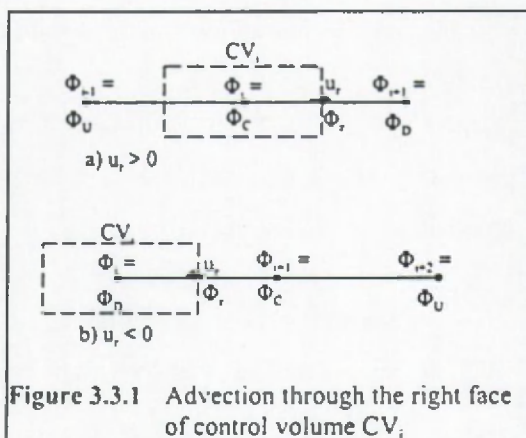


Figure 3.3.1 Advection through the right face of control volume CV_i

the face value ϕ_f as a function of the neighbouring grid-point values i.e. two straddling the face value (ϕ_D and ϕ_C) and one upstream value (ϕ_U) (depending on the direction of u), Fig. (3.3.1). There are two terms which control the evaluation of ϕ_f and its limiters. First, the direction of u ; second, the monotonicity, its existence and direction.

The monotonicity exists if

$$\phi_U > \phi_C > \phi_D$$

$$\text{or } \phi_U < \phi_C < \phi_D$$

The Monotonicity condition can be better formulated as,

$$|\text{CURV}| < |\text{DEL}| \quad (3.3.1)$$

where

$$\text{CURV} = \phi_D - 2\phi_C + \phi_U$$

$$\text{DEL} = \phi_D - \phi_U$$

A total of four groups of constraints can be constructed which incorporate all possible combinations of monotonicity and flow direction; namely,

$$\text{group 1: } u_f > 0, \text{ DEL} > 0$$

$$\text{group 2: } u_f > 0, \text{ DEL} < 0$$

$$\text{group 3: } u_f < 0, \text{ DEL} > 0$$

$$\text{group 4: } u_f < 0, \text{ DEL} < 0$$

Leonard (1991) explained (briefly) the method. A detailed study over group 1 will be given here. The other groups can be easily derived.

- 1) Evaluate the face value using the QUICKEST scheme

$$\phi_{\text{REF}} = \frac{1}{2}(\phi_D^n + \phi_C^n) - \frac{|c|}{2}(\phi_D^n - \phi_C^n) - \frac{1}{6}(1 - c^2) \text{CURV}$$

where $c = \frac{u \Delta t}{\Delta x}$ is the Courant number. It is, in the current case, positive.

- 2) Examine monotonicity,

if $|\text{CURV}| \geq |\text{DEL}|$ the variable is non-monotonic and the first-order upwinding is good enough

$$\phi_r = \phi_C$$

Otherwise, apply the monotonicity limiters as follows.

- 3) If $\text{DEL} > 0$ then $\phi_{i-1}^n < \phi_i^n < \phi_{i+1}^n < \phi_{i+2}^n$.

The face value should satisfy the following conditions, regardless of the flow direction.

$$\phi_i^n \leq \phi_r \leq \phi_{i+1}^n \quad (3.3.2)$$

A general discretization of the advection equation is

$$\phi_i^{n+1} = \phi_i^n + c_l \phi_l - c_r \phi_r \quad (3.3.3)$$

where subscript l denotes the left face of control volume CV_i .

Now, require, conservatively, for monotonicity maintenance

$$\phi_i^{n+1} \geq \phi_{i-1}^n$$

substituting for ϕ_i^{n+1} from formula (3.3.3),

$$\phi_i^n + c_l \phi_l - c_r \phi_r \geq \phi_{i-1}^n$$

rearranging

$$c_r \phi_r \leq \phi_i^n - \phi_{i-1}^n + c_l \phi_l \quad (3.3.4)$$

but from condition (3.3.2) applied to CV_{i-1}

$$\phi_{i-1}^n \leq \phi_l \leq \phi_i^n$$

Then, the worst case for ϕ_l is (when ϕ_l attains its smallest possible value)

$$c_r \phi_r \leq c_l \phi_{i-1}^n + \phi_i^n - \phi_{i-1}^n$$

or, in terms of D, C, U,

$$c_r \phi_r \leq c_l \phi_U + \phi_C - \phi_U \quad (3.3.5)$$

One further condition is

$$\phi_i^{n+1} \leq \phi_{i+1}^n$$

Following the same derivation steps,

$$\phi_i^n + c_l \phi_l - c_r \phi_r \leq \phi_{i+1}^n$$

$$c_r \phi_r \geq \phi_i^n - \phi_{i+1}^n + c_l \phi_l$$

The worst case for ϕ_r is (when ϕ_l attains the largest possible value)

$$c_r \phi_r \geq c_l \phi_i^n + \phi_i^n - \phi_{i+1}^n \quad (3.3.6)$$

or, in terms of D, C, U,

$$c_r \phi_r \geq c_l \phi_C + \phi_C - \phi_D \quad (3.3.7)$$

The face value is determined in step 1 above. Conditions (3.3.2,5,7) are the monotonicity limiters for the right-face value of control volume CV_i when $u_i > 0$ and $DEL > 0$. It is assumed, in the derivation, that c_l has the same sign (and direction) as c_r . If c_l has a different sign, it may not be appropriate to require persistence of monotonicity.

In the original paper of Leonard (1991), condition (3.3.6) was established viewing ϕ_r as the left-face value of CV_{i+1} and using a worst-case estimate for the far right-face value. Leonard's approach uses an extra grid point ($i+2$) to establish the constraints. The current approach provides the same result with less stencils (grid points).

3.3.3 Evaluation of the ULTIMATE QUICKEST

The problem of discretizing the advection term does not appear in the large scale applications. For example, the POM model developed by the University of Princeton uses a standard second-order central differencing scheme. The model attains worldwide acceptance when applied to large scale applications. When the same

(second-order central differencing) scheme is applied to the LIP2 experiment, the resulting solution suffers from the typical strong oscillations manifesting central difference schemes. To damp the oscillations, artificial diffusion must be introduced. Introducing artificial diffusion is not suitable for the existing study so long as turbulence is concerned. Hence a more accurate (interpolation) scheme is needed. The ULTIMATE QUICKEST, recommended by many researchers (see Cahyono, 1992), is applied to the LIP2 experiment.

The momentum equation

$$\frac{\partial U}{\partial t} + \frac{\partial UU}{\partial x} = 0$$

produced fairly good results, with faithful transport of the upstream imposed velocity towards the downstream. When the vertical velocity component is included

$$\begin{aligned} \frac{\partial U}{\partial t} + \frac{\partial UU}{\partial x} + \frac{\partial UW}{\partial z} &= 0 \\ \frac{\partial U}{\partial x} + \frac{\partial W}{\partial z} &= 0 \end{aligned} \tag{3.3.8}$$

the horizontal velocity is diffused at the point where the vertical gradient of the U-component of the velocity is changed (Fig. 3.3.2). The velocity distribution at the upstream open boundary, as measured by the EMS (see Chapter 2), has a point of changing gradient which is created by the splitter plate. As a matter of numerical test, the velocity distribution at the upstream open boundary is rearranged as shown in Fig. (3.3.3). The results obtained by Equations (3.3.8) are again faithful transport of U in the horizontal direction with zero vertical component. The diffusion starts at the point where the monotonicity condition (3.3.1) fails i.e. when the face value is determined

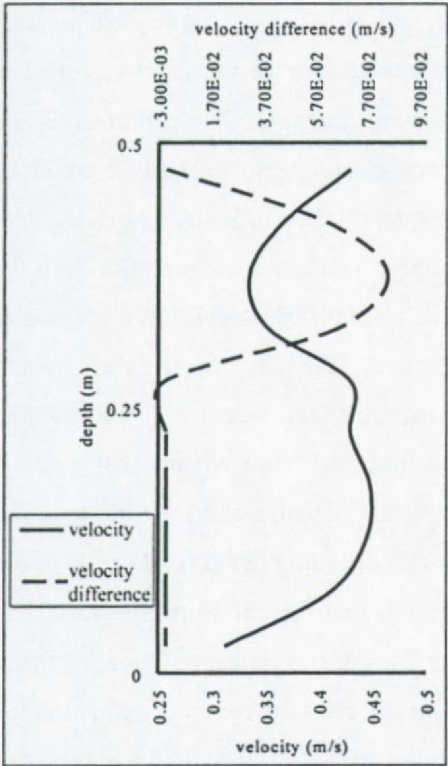


Figure 3.3.2 Measured velocity distribution at the upstream open boundary (solid line) and the difference between the upstream (measured) velocity and the downstream (calculated) one (dashed line).

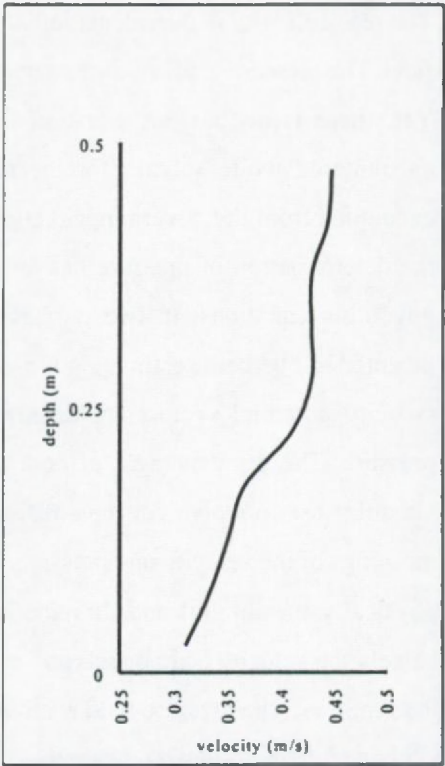


Figure 3.3.3 Velocity re-distribution at the upstream open boundary.

by first-order upwinding. Thus, the current scheme shares with other schemes the weakness of reverting to first-order upwinding with the consequent inherent artificial diffusion. Research in this field continues (Falconer and Cahyono, 1993).

3.4 Pressure Term

3.4.1 Introduction

The velocity components are governed by the continuity equation and the momentum equations which are particular cases of the general transport equations.

The real difficulty in the calculation of the velocity field lies in the unknown pressure field. The pressure gradient forms a part of the source terms for a momentum equation. Yet, there is no obvious equation for obtaining pressure. This difficulty is not encountered while solving for the turbulence closure term because it could be decoupled from the governing equations (Chapter 4). The difficulty associated with the determination of pressure has led to methods that eliminate pressure from the governing equations. In two dimensions, the stream-function/vorticity method is invented to overcome estimating the pressure. In three dimensions, the vorticity and velocity potential vectors are determined instead of the velocity vector and the pressure. The disadvantages of both methods outweigh their advantages; e.g., the variables used involve concepts that are harder to visualize and interpret than the meanings of the velocity and pressure. Therefore, the current study makes use of the physically meaningful and illuminating methods that use the primitive variables, namely the velocity components and pressure. The general concept of these methods is as follows. The pressure field is indirectly specified via the continuity equation (as explained in the following paragraphs). When the correct pressure field is substituted into the momentum equation, the resulting velocity field satisfies the continuity equation (Patankar, 1980).

The methods using the primitive variables are broadly classified as methods applied to unsteady flow and methods applied to steady flow. The unsteady methods are applicable to steady flow by marching in time until the solution no longer changes (Fletcher, 1991). The time steps are, thus, iterations with the unsteady term in the equations providing a kind of under-relaxation (Patankar, 1980).

Examples of the steady methods are the artificial compressibility method and the SIMPLE algorithm. The principle of the artificial compressibility method is to consider the solution of the steady equations as the limit when $t \rightarrow \infty$ of the solution of unsteady equations obtained by associating the unsteady momentum equation with a

perturbed divergence equation (Peyret and Taylor, 1983). The perturbed divergence equation contains the (so-called) pseudo-speed-of-sound coefficient to whose value the method is very sensitive. Unfortunately, the coefficient has to be optimized empirically (Hirsch, 1991).

The SIMPLE algorithm was originally introduced by Patankar and Spalding (1972). The method is applicable to boundary layer flow. Patankar and Spalding (1972) call a flow a boundary layer, a) if there exists a predominant direction of flow (i.e. there is no reverse flow in that direction) b) if the diffusion of momentum, heat, mass, etc. is negligible in that direction c) if the downstream pressure field has little influence on the upstream flow condition. The advantages of the method are the saving on computer time and storage. However, the proposed solution introduces errors which are not introduced by a fully iterative procedure.

The unsteady methods are usually pressure correction methods. The Marker-and-Cell (MAC) method is the prototype of such methods. They consist of a basic iterative procedure between the velocity and the pressure fields. Starting with an approximation of the pressure, the momentum equation can be solved to determine the velocity field. The obtained velocity field does not satisfy the divergence-free continuity equation and has therefore to be corrected. Since this correction has no impact on the pressure field, a related pressure correction is defined, obtained by showing that the corrected velocity satisfies the continuity equation. This leads to a Poisson equation for the pressure correction (Hirsch, 1991). This is the method used in the current study. The details of the method will be given in the following subsection.

3.4.2 The pressure correction method

The method consists of the following steps (see, for example, Peyret and

Taylor, 1983, Fletcher, 1991, Hirsch, 1991).

The momentum equation (3.2.2b), expressed as (for homogeneous flow, $\rho' = 0.0$)

$$\frac{\partial U_i}{\partial t} + ADV = \frac{-1}{\rho_0} \frac{\partial P}{\partial x_i} + DIF$$

where $ADV = \frac{\partial U_i U_j}{\partial x_j}$ and $DIF = \frac{\partial}{\partial x_i} (t_{ij} + u_i' u_j')$

can be split into two parts,

$$\frac{U_i^* - U_i^n}{\Delta t} = -(ADV - DIF)^n$$

or

$$U_i^* = U_i^n - \Delta t (ADV - DIF)^n \quad (3.4.1)$$

where the superscript * is used to indicate a temporary (transitional) variable introduced to help in partitioning the equation.

and

$$\frac{U_i^{n+1} - U_i^*}{\Delta t} = \left(\frac{-1}{\rho_0} \frac{\partial P}{\partial x_i} \right)^{n+1}$$

or

$$U_i^{n+1} = U_i^* - \frac{\Delta t}{\rho_0} \left(\frac{\partial P}{\partial x_i} \right)^{n+1} \quad (3.4.2)$$

The continuity equation is

$$\left(\frac{\partial U_i}{\partial x_i} \right)^{n+1} = 0 \quad (3.4.3)$$

substituting from (3.4.2) into (3.4.3), one gets the following (elliptic) Poisson equation for the pressure.

$$\frac{\partial U_i^*}{\partial x_i} - \frac{\Delta t}{\rho_0} \left(\frac{\partial^2 P}{\partial x_i^2} \right)^{n+1} \quad (3.4.4)$$

The solution sequence is as follows.

1. Solve equation (3.4.1) for U_i^* .
2. Solve equation (3.4.4) for the pressure field, P .
3. Solve equation (3.4.2) for the velocity field U .

The momentum equations (steps 1 and 3) are explained in detail in Section 3.3 and in Chapter 4. Step 2 will be studied in detail in the following paragraphs.

1. Boundary Conditions: Because the pressure is determined by the Poisson equation (3.4.4) which is elliptic, the boundary conditions applied to the (parabolic) momentum equations cannot be extended to the pressure equation. A detailed discussion of the boundary conditions is deferred to subsection 3.5.3.

2. *Discretization Grid:* A staggered grid is used.

In the staggered grid, the pressure is defined at the center of each cell and the velocity components are defined at the cell faces (Fig. 3.4.1). The use of the staggered grid permits coupling of the U , V , W and P solutions at adjacent grid points. This in turn prevents the appearance of oscillatory solutions, particularly for P , that can occur if centered differences are used to discretise all derivatives on a non-staggered grid. The oscillatory solution is a

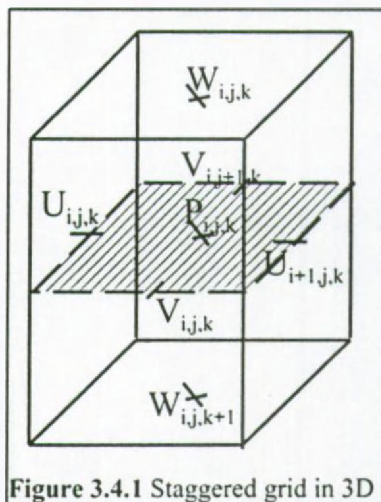


Figure 3.4.1 Staggered grid in 3D

manifestation of two separate pressure solutions associated with alternate grid points, which the use of centered differences on a non-staggered grid permits. The use of staggered grids has some disadvantages. Generally, boundary conditions are more difficult to impose consistently with a staggered grid, since at least one dependent variable (e.g. U) will not be defined on a particular boundary.

3. *Relative Nature of the Pressure:* The absolute value of the pressure is not relevant at all; only differences in pressure are meaningful and these are not altered by an arbitrary constant added to the pressure field. Moreover, since, in properly specified problems, the given boundary velocities must satisfy overall mass conservation, the continuity equation for the last control volume does not convey any information that is not already contained in the continuity equations for all other control volumes. Thus, even if one control volume equation is discarded and the value of the pressure is prescribed there the resulting velocity field would satisfy the continuity for all control volumes. One more thing to notice is that, in many problems, the value of the absolute pressure is much larger than the local differences in pressure (Patankar, 1980).

The above-mentioned observations lead to the following practice. After

obtaining the pressure field (Eq. 3.4.4), the minimum pressure value is set to zero and the pressure values in the rest of the computational domain are accordingly adjusted. This way, the pressure field does not acquire a large absolute value. Moreover, the next time step (i.e. next iterative solution of Eq. (3.4.4)) does not start with a cold start (zero pressure field); rather, it starts from the previous pressure estimates, which is expected to be a good first guess because the numerical method marches with small increments of the dependent variables.

4. Solution of the Poisson Equation: A direct solution of Poisson equation is prohibitively expensive in terms of computer time and storage, at least with the existing computer facilities. One should then resort to iterative methods. The iterative methods are applied either by point-by-point approach or line-by-line approach. The former approach is explicit. In each step, the pressure is determined at one grid point as a function of the pressure values at the neighboring points; typical methods of this type are Jacobi method, Gauss-Seidel method and Successive Over-Relaxation (SOR) method (see, for example, Patankar, 1980, Peyret and Taylor, 1983, Smith, 1985, Fletcher, 1991, Hirsch, 1991). The latter approach results in a Tri-Diagonal Matrix which can be solved by any of the well-known Tri-Diagonal Matrix Algorithms (TDMA). Patankar (1980) pointed out that while a solution cannot be obtained by the TDMA unless a pressure value is set at one end of each line, the point-by-point solution can be obtained without setting any value. Hence, the convergence of the point-by-point method is faster because the solution converges to a certain level obtained by iteration rather than approaching a level controlled by defining a value at a particular grid point. In more than one dimension, the line-by-line approach converges to a solution with a fixed error of convergence. The error of convergence is attributed to the value needed at the end of each line which can be seen as over-specification of the boundary conditions or decoupling of the sweeps in different directions. However, the iterative solution of the algebraic equations need not be taken to complete convergence because the values at any intermediate stage are just

tentative. Peyret and Taylor (1983) mentioned 12 as a good number of iterations at each time step, whereas Patankar and Spalding (1972) recommended 3 executions of the double sweeps. In the current numerical experiment, it is found that the convergence error after 12 iterations is ~30% different from that after 3 iterations. Hence, it can be concluded that 12 iterations are appropriate provided that the convergence error is reduced as the number of iterations increases. The convergence error is determined as the difference between the pressure values obtained at the same grid point in two consecutive iterations.

3.5 Boundary Conditions

3.5.1 Introduction

The boundaries of the computational domain are actually nothing but a mathematical trick to isolate the area of interest from the infinite surrounding physical environment. Hence, it can be easily expected that no physical law that prescribes the boundaries can be established. However, to give the problem an engineering solution, boundaries are divided into solid boundaries and open boundaries. Solid boundaries are real physical boundaries. They do not constitute a problem, except perhaps in cases of movable boundaries e.g. those used in modeling flooding and drying (Lorenzetti and Wang, 1986). No-normal-flow condition, no-slip condition or slip condition can be applied at solid boundaries. The no-slip condition is the one adopted in the current study. On the other hand, the open boundaries have an obscure physical interpretation, i.e. the lack of knowledge of the numerical behavior of the environment in the region outside the computational domain and the interaction between that environment and the computational domain. Thus, some kind of extrapolation of knowledge obtained in the interior of the domain must be used. The extrapolation is ad-hoc to the problem under consideration. An Open Boundary Condition (OBC) could probably be tailored to fit the desired behavior. The specification of the OBC depends on, among others, the character of the equations to be solved i.e. hyperbolic, parabolic or elliptic

(Orlanski, 1976). In subsection 3.5.2, the OBC for the momentum equation will be explained. In subsection 3.5.3, it will be seen that OBCs of subsection 3.5.2 are not suitable for the elliptic Poisson equation and the suitable OBC will be introduced.

3.5.2 Radiation Boundary Condition

Unfortunately, there is no numerical treatment of open boundaries which is generally applicable. Consequently, it has been suggested that approximate ad hoc OBCs may be the most reasonable approach to the problem at this time. For flow problems dominated by advection and/or wave motion, the OBC should be transparent i.e. it should allow propagating waves which are generated within the computational domain to pass through with minimum reflection and/or distortion. Once a reflected wave has been generated, it will remain in the interior domain either until bottom friction damps it out or until it encounters another open boundary where some of the wave energy may be transmitted through the boundary and some may be reflected (Chapman, 1985). Moreover, the OBC must be used to input some external forcing representing the interaction of the modeled region with the exterior environment (Lorenzetti and Wang, 1986 and Orlanski, 1976).

The (zero) gradient BC, clamped (constant value) BC and sponge layer BC (Chapman, 1985) are perfectly reflecting boundary conditions; a criterion which is not suitable for the existing flow conditions. The sponge layer BC has one more disadvantage. It wastes a significant number of grid points close to the boundary (Orlanski, 1976 and Chapman, 1985).

The Sommerfeld radiation condition is stated as (Chapman, 1985)

$$\frac{\partial \phi}{\partial t} + c_r \frac{\partial \phi}{\partial x} = 0 \quad (3.5.1)$$

The prescription of the phase speed (or advection velocity) c_r determines the type of the boundary. For the (zero) gradient BC $c_r = \infty$ and for constant value BC $c_r = 0$. Chapman (1985) surveyed other methods, e.g. when c_r has a fixed value (the gravity wave speed) or when an extra friction-like term is added to the right hand side of Equation (3.5.1). All these methods reflect some part of the generated waves. Instead of fixing the value of c_r , the BC introduced by Orlanski (1976) calculates a propagation velocity from the neighboring grid points. If the propagation direction is outward from the domain, a boundary value is extrapolated from the interior values close to the boundary. Otherwise, the boundary value is either specified or unchanged (Røed and Smedstad, 1984). In practice, large values of c_r may occur when derivatives in Equation (3.5.1) are very small. This source of error is controlled by requiring

$$0 \leq |c_r| \leq \frac{\Delta x}{\Delta t}$$

Chapman (1985) stated the Orlanski BC as follows. Considering that

$$c_r = \frac{-\partial \phi / \partial t}{\partial \phi / \partial x}$$

evaluate

$$C_L = c_r \frac{\Delta t}{\Delta x} = \frac{\phi_{B-1}^{n-2} - \phi_{B-1}^n}{\phi_{B-1}^n + \phi_{B-1}^{n-2} - 2\phi_{B-2}^{n-1}}$$

set

$$\mu = \begin{cases} 1 & \text{if } C_L \geq 1 \\ C_L & \text{if } 0 < C_L < 1 \\ 0 & \text{if } C_L \leq 0 \end{cases}$$

calculate

$$\phi_B^{n+1} = \frac{\phi_B^{n-1}(1-\mu) + 2\mu\phi_B^n}{1+\mu}$$

where the subscript B represents the boundary grid point and the superscript n represents the time level.

Israeli and Orszag (1981) interpreted the radiation BC as requiring that the amplitude of waves entering from infinity be zero while no condition be placed on outgoing waves propagating to infinity.

3.5.3 Boundary Conditions for Poisson Equation

Peyret and Taylor (1983) stressed that the open boundaries pass through the points where the velocity component is normal to the boundary and that the pressure is not defined on the boundary. Fletcher (1991) reported that in some applications it is useful to specify velocity components at inflow and pressure and zero gradient of the streamwise velocity component at outflow.

In the current study, the following boundary conditions are adapted.

1. *At upstream*, the U-component is specified (as measured by the EMS, see section 2.3.2) and Orlanski BC is used as an extrapolation technique for V and W which is needed in the QUICKEST scheme. This technique replaces the boundary conditions suggested by Leonard (1980).
2. *At downstream*, the velocity components are determined by Orlanski BC.
3. *At the surface*, the rigid lid assumption is imposed. The surface slope is assumed to be zero. This approximation introduces a certain error into the calculation which is, however, negligible when the variation of the surface elevation is small compared with the water depth. The effects of the surface slope are still accounted for in the

momentum equation by the pressure term (Rastogi and Rodi, 1978)

3.6 Conclusion

The Navier-Stokes equations are considered. It is shown that the full 3D form is necessary to simulate the LIP2 experiment. The Boussinesq assumption and the Reynolds' averaging are the only simplifications done for the Navier-Stokes equations.

A full 3D finite-difference model is built to find a numerical solution to the governing equations. The advection term is discretized using the ULTIMATE QUICKEST scheme. The scheme has been modified to reduce the number of grid points being involved in the solution (Eq. 3.3.6). Although the scheme performs reasonably well in most of the cases, it shares with other schemes the weakness of reverting to first-order upwinding with the consequent artificial diffusion.

After determining the three velocity components using the three momentum equations, the pressure is determined using a MAC-type method. The Poisson equation, thus formed, is solved using an iterative technique. It is shown that the line-by-line method is not suitable. Hence the point-by-point method is adopted. As a further development, the relative nature of the pressure is exploited to avoid large absolute values of the pressure field. At each time step, the pressure, as evaluated from the previous time step, is used as a first guess for the solution of the Poisson equation.

The Orlanski BC is used as both OBC at the downstream and extrapolation method at the upstream to replace the extrapolation suggested by Leonard (1980).

The model, with the above-mentioned features, is ready to insert the turbulence terms and thus investigate the calculated secondary circulations.

Chapter 4

TURBULENCE CLOSURE

4.1 Introduction

The Reynolds-averaged Navier-Stokes equations (3.2.2) cannot be solved for the mean values of velocity and pressure unless the turbulence correlations $\overline{u_i u_j}$ are determined (the closure problem). Exact transport equations can be derived for $\overline{u_i u_j}$ (Sec. 4.2); but these equations contain correlations of the next higher order. Therefore, closure of the equations cannot be obtained by resorting to equations for correlations of higher and higher order; instead, a turbulence model must be introduced which approximates the correlations of a certain order in terms of lower order correlations and/or mean-flow quantities (Rodi, 1980).

Modeling of higher order correlations $\overline{u_i u_j}$ ranges from a simple constant eddy viscosity model to as highly sophisticated models as the Direct Numerical Simulations (Markatos, 1986). In section 4.3, a short review of the available closure models will be given. The section will include some criteria according to which a closure model is chosen.

The k- ϵ model will be discussed in Section 4.4. The importance of the k- ϵ model is two-fold. First, it is the most popular turbulence closure model, so far. Second, The Algebraic Stress Model (ASM), to be used in the current study, is an extension to the k- ϵ model. The ASM will be explained in Section 4.5.

In Section 4.6, the numerical solution method for the turbulence closure

model will be explained. The section includes both the discretization and the everlasting problem of boundary conditions.

Section 4.7 is devoted to the simulation results and their analysis. Section 4.8 contains algorithmic comparison between the current model and the large-scale model, POM. Section 4.9 highlights the main features of the program, developed in this research to code the mathematical model described in both chapters 3 and 4. Finally, Section 4.10 will conclude the chapter.

To highlight the size of the closure problem, it is interesting to quote the following paragraph from the ASCE Committee (1988):

"A typical team working on the development of a turbulence model-based code may consist of two or more senior researchers, two or more junior researchers and often graduate students. A balance in the experience of the senior researchers is desirable, with at least one having a good grasp of the physics of turbulence and another one with a strong background in computational fluid mechanics. The duration of a code development project may be from two to four years"

4.2 Reynolds Stress Equations

The exact transport equations for the Reynolds stresses may be derived by taking the moments of the Navier-Stokes equations i.e. averaging (over time) the set of nine equations arising from a multiplication of each of the three Navier-Stokes equations (3.2.1b) by the three turbulent velocity fluctuations, u_i^* (Leschziner, 1990 and Wilcox, 1993). Taking the moment can be expressed as

$$\overline{u_i^* N(u_j)} + \overline{u_j^* N(u_i)} = 0$$

where $N(u_j)=0$ is a symbolic expression of the Navier-Stokes equation for the j^{th} velocity component.

Using tensor notation (Appendix A), the full Reynolds stress equation becomes, (Rodi, 1980 and Wilcox, 1993)

$$\text{rate of change} + C_{ij} = D_{ij} + \Phi_{ij} + \Pi_{ij} + \epsilon_{ij} \quad (4.2.1)$$

where

$$\text{rate of change} = \frac{\partial \overline{u_i u_j}}{\partial t} \quad (4.2.2a)$$

$$C_{ij}: \text{convective transport} = U_k \frac{\partial \overline{u_i u_j}}{\partial x_k} \quad (4.2.2b)$$

$$D_{ij}: \text{diffusive transport} = -\frac{\partial}{\partial x_k} \left(\overline{u_k u_i u_j} + \nu \frac{\partial \overline{u_i u_j}}{\partial x_k} \right) - \frac{1}{\rho_0} \left(\frac{\partial \overline{u_j p}}{\partial x_i} + \frac{\partial \overline{u_i p}}{\partial x_j} \right) \quad (4.2.2c)$$

$$\Phi_{ij}: \text{stress production} = -\overline{u_i u_k} \frac{\partial U_j}{\partial x_k} - \overline{u_j u_k} \frac{\partial U_i}{\partial x_k} \quad (4.2.2d)$$

$$\Pi_{ij}: \text{pressure strain correlation} = \frac{p}{\rho_0} \left(\frac{\partial \overline{u_i}}{\partial x_j} + \frac{\partial \overline{u_j}}{\partial x_i} \right) \quad (4.2.2e)$$

$$\epsilon_{ij}: \text{viscous dissipation} = -2 \nu \overline{\frac{\partial u_i}{\partial x_k} \frac{\partial u_j}{\partial x_k}} \quad (4.2.2f)$$

The above equation states that the rate of change of the Reynolds stress is balanced by the advection transport due to the mean motion, the diffusive transport by both turbulent fluctuation (of both velocity and pressure) and viscosity, the turbulence production by mean-flow-turbulent-stress interaction, pressure-strain redistributing effects and the dissipation by the viscous action into heat. The rate of change, convection and production are exact and need no modeling. On the other hand, diffusion, pressure-strain and dissipation terms contain higher correlations which can be determined by taking higher moments of Navier-Stokes equations. Unfortunately, new unknown correlations are generated at each level. However, such operations are strictly mathematical in nature, and introduce no additional physical principles. The function of turbulence modeling is to devise approximations for the unknown correlations in terms of flow properties that are known so that a sufficient number of equations is obtained. In making such approximation, the system is closed (Wilcox, 1993).

4.3 Turbulence Models

To model the unknown correlations, hypothesis must be introduced for their behavior which are based on empirical information; hence turbulence models always contain empirical constants and functions. Further, turbulence models do not describe the details of the turbulent fluctuations but only the average effects of these terms on the mean quantities (ASCE Committee, 1988).

Markatos (1986) divided turbulence models into five groups:

- 1- Analytical turbulence theories.
- 2- Sub-grid scale closure models.
- 3- Direct Numerical Simulation.
- 4- Turbulence transport models.
- 5- Two-fluid models of turbulence.

Modeling of most practically relevant turbulent flows will continue to be based on the solution of the turbulence transport models (Leschziner, 1995). Although Younis and his co-workers (e.g. Basara and Younis, 1995, Cokljat and Younis, 1995a,b) directly solved the Reynolds stress transport equations after modeling the higher order correlations, they admit that these models are still so complex and computationally expensive that they are impractical for every day engineering use. The available alternative (from among the turbulence transport models) is the models which apply the eddy viscosity concept. Lakshminarayana (1986) divided these models into:

- 1- Eddy viscosity models which include the zero- one- and two-equation models.
- 2- Pseudo-eddy viscosity models which include the modified two-equation models and the Algebraic Stress Models (ASM).

The level of turbulence model necessary to obtain accurate predictions of the mean flow quantities depends on the relative importance of the turbulent transport terms. In certain flows or flow regions, the inertial terms (= rate of change+advective terms) of the momentum equations are balanced mainly by the pressure gradient and/or buoyancy terms even if the flow is turbulent. In such cases, for example in predominantly horizontal flows in large shallow water bodies, the turbulence simulation is not important because it is ineffective and an effective eddy viscosity term is sufficient (see Sec. 4.8). In most flows, however, the turbulent transport terms are of significance, and in some situations, they are the only terms to balance the inertial terms so that their proper simulation is essential for the prediction of the flow

(Rodi, 1980, ASCE Committee, 1988).

The current study is concerned mainly with simulating secondary flow in compound channels. The turbulence driven secondary motion can be obtained only with a turbulence model which adequately describes the partitioning of the normal stresses. Therefore, the eddy viscosity models are incapable of predicting the required phenomenon (see e.g. Rodi, 1980, Naot and Rodi, 1982, Markatos, 1986, ASCE Committee, 1988). The full transport models, on the other hand, provide the necessary prediction with the desired accuracy but are still computationally expensive. Therefore, the current study does not use them. The pseudo-eddy viscosity models are the remaining alternative, from which the ASM is chosen for application.

4.4 Two-Equation Models

Boussinesq approximation for turbulent flows is based on the analogy between the molecular and turbulent motion. Thus, in analogy with the molecular viscous stress, the Reynolds turbulent stresses are modeled according to (Markatos, 1986, Wilcox, 1993)

$$-\overline{u_i u_j} = \nu_t \left(\frac{\partial U_i}{\partial x_j} + \frac{\partial U_j}{\partial x_i} \right) - \frac{2}{3} k \delta_{ij}$$

where δ_{ij} is the Kronecker delta (Appendix A), ν_t is referred to as the turbulence eddy viscosity which, in contrast with the molecular viscosity, is not a fluid property but depends on the local state of turbulence. The symbol k denotes the kinetic energy of the turbulent motion expressed as

$$k = \frac{1}{2} \overline{u_i u_i}$$

This, being a measure of the normal turbulence stresses, is also the turbulence equivalent of the static pressure of the molecular motion.

Prandtl's mixing length hypothesis is based on the analogy between turbulent motion and kinetic theory of gases. Thus, v_t can be determined, to a good approximation, by writing

$$v_t \propto \hat{V} \hat{L}$$

where \hat{L} is a length scale characteristic of the large turbulence eddies and \hat{V} is a velocity scale characteristic of the fluctuating velocities (of the large eddies) (Rodi, 1980, Markatos, 1986, Wilcox, 1993).

The two-equation models determine the length and velocity scales (\hat{L} and \hat{V}) via transport equations; k is used as the dependent variable for the \hat{V} -equation. A combination of k and \hat{L} , having the form $k^m \hat{L}^n$ is chosen as the dependent variable for the \hat{L} -equation. From among the two-equation models, the standard k - ϵ model will be applied. In that model, the dissipation rate of the turbulent kinetic energy (ϵ) defined as (Markatos, 1986)

$$\epsilon \propto \frac{k^{\frac{3}{2}}}{\hat{L}}$$

is the dependent variable for the \hat{L} -equation.

The exact equation for k , derived by taking the trace of the terms in Eq. 4.2.1 (see Appendix A), reads

$$\frac{dk}{dt} = \text{production}(\Phi) + \text{Diffusion}(D) - \text{Dissipation}(\epsilon)$$

In this equation, the convection term is exact; the production term, which is exact in the Reynolds stress models, should be modeled. It is modeled as (Haque, 1994)

$$\Phi = v_i \left(\frac{\partial U_i}{\partial x_j} + \frac{\partial U_j}{\partial x_i} \right) \frac{\partial U_i}{\partial x_j}$$

The diffusion term is modeled as (Wilcox, 1993)

$$D = \frac{\partial}{\partial x_i} \left(\frac{v_i}{\sigma_k} \frac{\partial k}{\partial x_i} \right)$$

where σ_k is the Prandtl number for energy.

Recalling that ϵ is defined by Eq. 4.2.2f, the exact equation for ϵ is derived by taking the following moment of the Navier-Stokes equation (Wilcox, 1993)

$$\overline{2\nu \frac{\partial u_i}{\partial x_j} \frac{\partial}{\partial x_j} [N(u_i)]} = 0$$

where $N(u_i)=0$ is a symbolic expression of the Navier-Stokes equation for the i^{th} velocity component.

This exact equation is far more complicated than its k -counterpart. Its modeled form is obtained either by tuning it into a tractable form by model

assumptions or by conceiving a heuristic model. Both methods produce similar models; in fact all equations possess a common form (Rodi, 1980, Wilcox, 1993).

Compiling the above-mentioned modeling assumptions, the standard k - ϵ model takes the form (see e.g. Rodi, 1980, Wilcox, 1993, Haque, 1994)

$$v_t = c_\mu \frac{k^2}{\epsilon} \quad (4.4.1)$$

$$\frac{\partial k}{\partial t} + U_i \frac{\partial k}{\partial x_i} = \frac{\partial}{\partial x_i} \left(\frac{v_t}{\sigma_k} \frac{\partial k}{\partial x_i} \right) + \Phi - \epsilon \quad (4.4.2)$$

$$\frac{\partial \epsilon}{\partial t} + U_i \frac{\partial \epsilon}{\partial x_i} = \frac{\partial}{\partial x_i} \left(\frac{v_t}{\sigma_\epsilon} \frac{\partial \epsilon}{\partial x_i} \right) + c_{\epsilon 1} \frac{\epsilon}{k} \Phi - c_{\epsilon 2} \frac{\epsilon^2}{k} \quad (4.4.3)$$

The closure constants (c_μ , $c_{\epsilon 1}$, $c_{\epsilon 2}$, σ_k , σ_ϵ) may have different values in the literature (see Table 4.4.1). Nevertheless, they are almost universal. The current study adopted the following values, which are found (by numerical experiment) the suitable constants for compound channel simulation.

$$c_\mu = 0.09, \quad c_{\epsilon 1} = 1.44, \quad c_{\epsilon 2} = 1.92, \quad \sigma_k = 1.225, \quad \sigma_\epsilon = 1.225$$

The k - ϵ model is robust, economic, easy to apply, and accurate enough for thin turbulent shear flow problems. However, the model cannot predict the secondary flow in non-circular conduits. Many authors (Patel et al, 1984, Lakshminarayana, 1986, Markatos, 1986, Speziale, 1987, Leschziner, 1990, Cokljat and Younis, 1995a) discussed the reasons of the incapability of the model as follows. The secondary circulation is induced mainly by the inequality between the normal stresses (Naot and Rodi, 1982). The k - ϵ model predicts that the normal Reynolds stresses are all equal -a result which is in substantial contradiction of experiments. Thus, the k - ϵ model yields unidirectional mean turbulent flows. Moreover, the model prediction of the low-Reynolds-number flow in the near wall vicinity is poor. There are low-Reynolds-

Table 4.4.1: k- ϵ model constants reported in the literature.

c_μ	$c_{\epsilon 1}$	$c_{\epsilon 2}$	σ_k	σ_ϵ	source
0.09	1.44	1.92	1.0	1.3	ASCE Committee (1987), Wilcox (1993), Pezzinga (1994)
0.09	1.45	1.90	1.0	1.3	Basara & Younis (1995)
0.09	1.44	1.92	1.225	1.225	Naot & Rodi (1982), Naot et al (1993), Lin & Shiono (1995)
0.09	1.43	1.92	1.0	1.3	Rastogi & Rodi (1978)
0.09	1.55	2.0	1.0	1.3	Jones & Launder (1972)

number versions of the model. However, the high near-wall resolution needed by these versions makes the computation expensive. The wall-function (Sec.4.6.2) is used to overcome the low-Reynolds-number problem. However, as shown in Sec. 4.6.2, the wall-function tends to mask the model's performance. Finally, the production term in the k- ϵ model must be modeled because $\overline{u_i u_j}$ are unknowns. This drawback disappears automatically in the ASM.

4.5 Algebraic Stress Model

4.5.1 Introduction

Algebraic Stress Models combine, at least to some extent, the economy of the isotropic eddy viscosity models with the universality of the stress/flux models (Rodi, 1980).

In the Reynolds stress equation (4.2.1), gradients of the dependent variables appear only in the rate of change, convection and diffusion terms. Hence, when these gradients can be eliminated by model approximations, the differential equations can be converted into algebraic expressions. The simplest model is to neglect the rate of

change and the transport terms, and this appears to be a sufficiently accurate approximation in many cases (e.g. Haque's model, Sec. 4.5.2). However, a more generally valid approximation is to assume that the transport of $\overline{u_i u_j}$ is proportional

to the transport of k , the proportionality factor being the ratio $\frac{\overline{u_i u_j}}{k}$, which is not a

constant (Rodi, 1980, ASCE Committee, 1988) (e.g. Naot's model, Sec. 4.5.3). Neglecting the rate of change and the transport terms gives rise to an inconsistency in the normal stresses when ϵ is not equal to Φ because then the resulting normal stresses do not sum up to $2k$ as they should. Rodi (1980) reported two possible solutions. The first is proposed by Hossain (1980). He solved for the normal stresses using the proportionality approximation for the transport terms, and solved for the shear stresses neglecting the transport terms. The second solution assumes local equilibrium, in which case ϵ can be replaced by Φ .

4.5.2 Haque's model

Haque (1994) adopted the second of the solutions reported by Rodi (1980) (see Sec. 4.5.1). Two more assumptions are adopted by Haque (1994). The first assumption is Launder's model (1975) for the pressure-strain term. The second assumption is that the dissipation is isotropic, with each normal stress dissipated at the same rate, $\frac{2}{3}\epsilon$ (Leschziner, 1990). Hence the model took the form (Haque, 1994)

$$\overline{u_i u_j} = \frac{k}{\epsilon} \frac{1 - c_2}{c_1} \left[-\overline{u_i u_k} \frac{\partial U_j}{\partial x_k} - \overline{u_j u_k} \frac{\partial U_i}{\partial x_k} \right] - \frac{2}{3} k \frac{1 - c_1 - c_2}{c_1} \delta_{ij} \quad (4.5.1)$$

where $c_1=2.2$ and $c_2=0.55$ are the constants of the pressure-strain model as reported by Haque (1994).

The ASM, seen as a redistribution of the eddy viscosity determined by the $k-\epsilon$ model, has overcome the first weakness of the $k-\epsilon$ model mentioned in section 4.4 (namely, the weakness that the $k-\epsilon$ model predicts that the normal stresses are equal, i.e., the turbulence is isotropic). However, the high-Reynolds-number ASM (Eq. 4.5.1) cannot solve the problem of the near-wall low-Reynolds-number flow. The law-of-the-wall (Sec. 4.6.2) is used to (partly) overcome this problem. Furthermore, the model fails when the transport of the turbulent stresses in the flow is too large to neglect.

4.5.3 Naot's model

On applying Haque's model to simulate the LIP2 experiment, the model showed limited applicability. First, the 3D form of the model (see Appendix B) needs the solution of a system of simultaneous equations with the consequent ill-conditioned problem (see Sec. 4.6.1). Haque (1994) tried to simplify the equations. However, the resulting expressions are still far from simple and could not solve the ill-conditioned problem. Second, as the model neglects the transport terms, it is not capable of adequately predicting the secondary circulation in compound channels which are characterized by strong turbulence level and transfer of momentum in the lateral shear layer. Naot et al (1993) used an ASM which was developed by Naot and Rodi (1981, 1982, 1983). The model will be referred to, hereafter, as Naot's model. The model is,

$$\overline{u'v'} = -v_{ty} \frac{\partial U}{\partial y} \quad \text{with} \quad v_{ty} = \frac{\left(c_4 + \frac{5}{2}c_3\right)}{\left(c_4 + 2c_3\right)} v_t \quad (4.5.2a)$$

$$\overline{u'w'} = -v_{tz} \frac{\partial U}{\partial z} \quad \text{with} \quad v_{tz} = \frac{c_4^2}{\left(c_4 + \frac{3}{2}c_3\right) \left(c_4 + 2c_3\right)} v_t \quad (4.5.2b)$$

$$\overline{v'w'} = \frac{\beta}{\left(c_4 + \frac{3}{2}c_3\right)} \frac{k}{\epsilon} \left(\overline{u'v'} \frac{\partial U}{\partial z} + \overline{u'w'} \frac{\partial U}{\partial y} \right) - v_t \left(\frac{\partial V}{\partial z} + \frac{\partial W}{\partial y} \right) \quad (4.5.2c)$$

$$\overline{w'w'} = \frac{k}{(c_4 + 2c_3)} \left[\frac{2}{3} \left(\alpha - \frac{1}{2}\beta + c_4 - 1 \right) + \frac{\beta}{\epsilon} \left(\overline{u'w'} \frac{\partial U}{\partial z} - \overline{u'v'} \frac{\partial U}{\partial y} \right) \right] - 2v_t \frac{\partial W}{\partial z} \quad (4.5.2d)$$

$$\overline{v'v'} = \frac{k}{c_4} \left[\frac{2}{3} \left(\alpha - \frac{1}{2}\beta + c_4 - 1 \right) + \frac{\beta}{\epsilon} \left(\overline{u'v'} \frac{\partial U}{\partial y} - \overline{u'w'} \frac{\partial U}{\partial z} \right) + c_3 \frac{\overline{w'w'}}{k} \right] - 2v_t \frac{\partial V}{\partial y} \quad (4.5.2e)$$

$$\overline{u'u'} = 2k - (\overline{v'v'} + \overline{w'w'}) \quad (4.5.2f)$$

where the model constants are

$$\alpha = 0.7636 - 0.06 f_1 \quad (4.5.3a)$$

$$\beta = 0.1091 + 0.06 f_1 \quad (4.5.3b)$$

$$c_4 = 1.5 - 0.5 f_1 \quad (4.5.3c)$$

$$c_3 = 0.1 f_2 \quad (4.5.3d)$$

f_1 and f_2 are functions accounting for the distance from solid walls and open surface, respectively. They are expressed as

$$f_1 = \left(\frac{l}{y_a} \right)^2 \quad (4.5.4a)$$

$$f_2 = \left(\frac{l}{h_a} \right)^2 \quad (4.5.4b)$$

where l is a dissipation length defined by

$$l = \left(\frac{c_\mu^{3/4}}{\kappa} \right) \frac{k^{3/2}}{\epsilon} \quad (4.5.4c)$$

y_a and h_a are the root mean squared reciprocal distances from the solid walls and open surface, respectively.

$$y_a = \left\langle \frac{1}{y^2} \right\rangle^{-1/2} \quad (4.5.4d)$$

$$h_a = \left\langle \frac{1}{(H-y)^2} \right\rangle^{-1/2} + 0.3162 l \quad (4.5.4e)$$

$\left\langle \frac{1}{y^2} \right\rangle$ is defined as

$$\left\langle \frac{1}{y^2} \right\rangle = \frac{1}{\pi} \int_{-\alpha}^{\phi} \frac{d\theta}{S^2} \quad (4.5.4f)$$

where S is the distance to the boundary segment that occupies the angle differential $d\theta$ (Fig. 4.5.1).

Naot et al (1993) explained that adjacent to the surfaces, both f_1 and f_2 become equal to one since l becomes equal to y near solid walls and l is finite near free surface. Away from the surfaces, both f_1 and f_2 vanish due to the quadratic formula (4.5.4a,b) and the numerical factor introduced into Eq. (4.5.4e) for h_w .

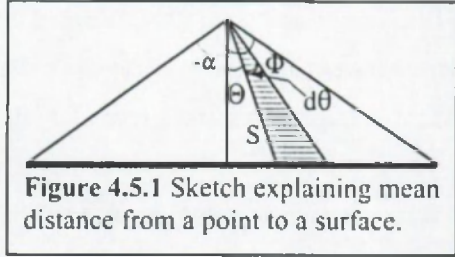


Figure 4.5.1 Sketch explaining mean distance from a point to a surface.

The model is simple and overcomes the ill-conditioned problem because the six equations (4.5.2) are mutually independent and all coefficients are functions of f_1 and f_2 whose values lie always in the range (0-1). Moreover, by introducing the functions f_1 and f_2 the model takes into account the wall effect everywhere within the compound-channel cross-section.

4.6 Numerical Model

4.6.1 Discretization and Solution Algorithm

1. *General:* To minimize the interpolation involved in evaluating the stress difference required for the Navier-Stokes equations, the stresses are divided into two groups (Fig. 4.6.1). The normal stress $u_i u_i$ group is located so that no interpolation is needed. The shear stress $u_i u_j$ group is located so that the interpolation is only between two grid points.

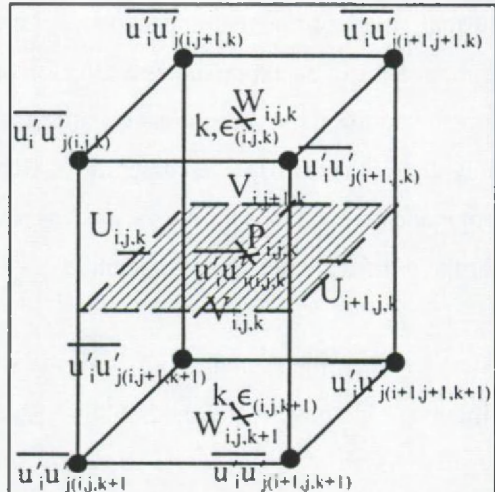


Figure 4.6.1 distribution of the variables on the finite difference mesh

Leschziner (1990), Naot et al

(1993) and Rocabado (1994) reported on the need to refine the mesh size in order to have a grid-size independent solution. Moreover, Naot et al (1993) recommended that $\frac{\Delta x}{\Delta y} < 1.25$ to avoid large errors in the secondary flow prediction.

Rocabado (1994) pointed out that negative or zero values of k or ϵ (which are due to mathematical operations and have no physical significance) cause solution divergence. He suggested that k and ϵ be limited to a certain minimum non-zero positive value. This limitation has effects only at the early stages of the solution iterations. Once the solution progresses towards a convergent stage, the approach becomes redundant. The approach is used by other modelers e.g. POM model, and is found useful in the current study.

It is found that the convergence to a steady solution is accelerated, when the initial conditions for the stream-wise velocity (U) are not zero. The initial cross sectional distribution of U is given the same distribution as the upstream boundary.

2. Haque's model: It can be seen that each normal stress equation contains one normal stress component and two shear stress components i.e. each normal stress component can be expressed as a function of the shear stress. If the normal stress is substituted for in the shear stress equations, one gets three shear equations containing only three (unknown) shear components. Hence, the ASM is reduced to solving three simultaneous equations for the shear stresses and three mutually independent equations for the normal stresses (see Appendix B).

When the system of equations is singular or ill-conditioned (very close to singular) the above-mentioned method (splitting method) fails to give satisfactory results. As an alternative, the so-called Singular Value Decomposition technique (Press, et al, 1986) can be used to diagnose the problem and give a useful numerical answer. The singular Value Decomposition technique could (partially) solve the ill-

conditioned problem. However, when the model is applied to the LIP2 experiment with a total of 700 computational grid points per cross section using an IBM-SP2 machine a reasonable time (up to one week) was too short to reach a steady solution. Haque's model is still computationally too expensive to be applied for LIP2 experiment using the current computer facilities.

3. *Naot's model*: Naot et al (1993) used the Patankar and Spalding (1972) algorithm. The algorithm is applied in the current study with a minor modification. In the boundary layer flow (defined in Sec. 3.4.1), the pressure term in the x-momentum equation can be expressed as a function of the total flow rate at any cross section, i.e., $\frac{\partial P}{\partial x}$ is assumed constant over the cross section and is replaced by $\frac{\partial \bar{P}}{\partial x}$

where \bar{P} is space-averaged pressure over a cross section. To maintain continuity, the mass flow rate at any cross section, \dot{m} at time step $n+1$ ($\sum \rho_0 U_p^{n+1} \Delta y \Delta z$) must be equal to the true mass flow rate applied at the open boundary (\dot{m}^*). Using Eq. 3.4.2:

$$U_p^{n+1} = U_p^* - \frac{\Delta t}{\rho_0} \left(\frac{\partial P}{\partial x} \right)^{n+1} \quad (3.4.2)$$

to substitute for U_p^{n+1} , one gets

$$\sum \rho_0 \left[U_p^* - \frac{\Delta t}{\rho_0} \left(\frac{\partial P}{\partial x} \right)^{n+1} \right] \Delta y \Delta z = \dot{m}^*$$

Hence $\left(\frac{\partial \bar{P}}{\partial x} \right)^{n+1}$ can be determined as

$$\left(\frac{\partial \bar{P}}{\partial x} \right)^{n+1} = \frac{\sum (\rho_0 U_p^* \Delta y \Delta z) - \dot{m}^*}{\Delta t \sum (\Delta y \Delta z)}$$

At each new time step, the upstream open boundary condition is updated by the velocity values at the section immediately downstream to it. Consequently, the algorithm does not take into account the actual flume length; instead, it takes into account only a small portion of the channel and moves it towards downstream as it marches in time.

The channel portion considered by Patankar and Spalding (1972) consists of two sections, Δx apart. To be able to apply the ULTIMATE QUICKEST (which uses at least five grid points) and Orlanski radiation open boundary conditions (discussed in chapter 3), the channel section should not be smaller than $10 \Delta x$. The true mass flow rate ($m \cdot$) is the flow rate applied as initial condition at the upstream section.

4.6.2 Boundary Conditions

The boundary conditions, especially near free and solid surfaces, have strong influence on the whole domain and may mask the real performance of the closure model (Markatos, 1986).

At inflow and outflow boundaries, Orlanski boundary conditions are applied for the differential equations of k and ϵ (see Sec. 3.5.2).

At the free surface, turbulent fluctuations normal to the plane and normal derivatives of other variables are set to zero except for the turbulence energy dissipation, ϵ . The fact that the free surface reduces (and re-distributes) the turbulence (Naot and Rodi, 1982, Haque, 1994) can be taken into account by the following modification for the energy dissipation (Lin and Shiono, 1995)

$$\epsilon = \frac{c_{\mu}^{\frac{3}{4}} k^{\frac{1}{2}}}{\kappa} \left(\frac{1}{y'} + \frac{1}{0.07 H} \right) \quad (4.6.1)$$

where y' is the distance from the solid wall, H is the total water depth, and κ is von Kármán's constant $= 0.41 \pm 0.015$ (Patel et al, 1984)

Near solid wall (viscous sub-layer), the viscous stress and the molecular diffusion are so important that the high Reynolds number models described above are not valid. Mean-flow equations and turbulence models are available that account for these effects, but since the gradients of most quantities are very steep in the viscous sub-layer, the numerical resolution of this region is very expensive and therefore not desirable. Although Launder (1992) criticized it and recommended looking for a better approach, the common practical approach (up till now) is to bridge the viscous sub-layer with semi-empirical wall functions which relate the values at the first numerical grid point placed outside the viscous sub-layer to conditions at the wall (Ferziger, 1987, ASCE Committee, 1988). The most common function is the logarithmic law-of-the-wall,

$$\frac{U_{res}}{U_*} = \frac{1}{\kappa} \ln(y' \cdot E) \quad (4.6.2)$$

where

U_{res} resultant velocity parallel to the wall

U_* shear velocity $= \sqrt{\frac{\tau_0}{\rho}}$

τ_0 wall shear stress

y^* non-dimensional wall distance $= \frac{y' U_*}{\nu}$

E roughness parameter ($= 9$ for hydraulically smooth walls)

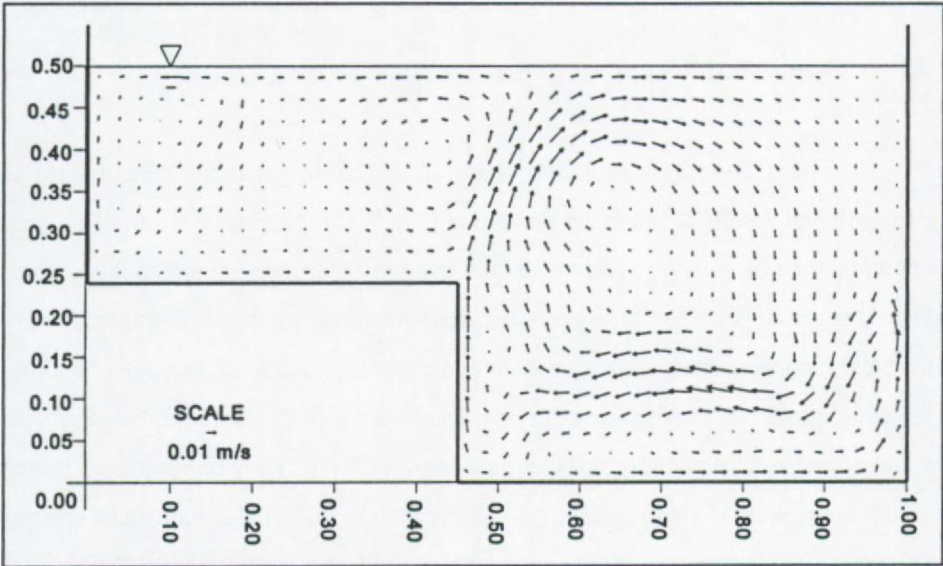
The domain of validity of Eq. 4.6.2 is a point of controversy. Rastogi and Rodi (1978), Rodi (1980) and the ASCE Committee (1988) recommended the range $30 < y^* < 100$. Patel et al (1984) recommended $30 < y^* < 200$. Haque (1994) reported the range $30 < y^* < 400$. Thomas and Williams (1995a) recommended a maximum value of $y^* = 600$. Rocabado (1994) stated that the distance of the first grid point from the wall represents a percentage of the domain that is eliminated out of the calculation. It has to be large enough to overcome the laminar sub-layer but as small as possible to avoid the introduction of errors originated by a too rough approximation. Naot et al (1993) suggested that the grid refinement should guarantee y^* value at the first grid point next to the wall in the range of 65-100. The value of $y^* = 100$ is adopted in the current study by numerical experiments.

In the logarithmic sub-layer, the shear stress is nearly constant and equal to the wall shear stress (ρU_*^2); and the local equilibrium assumption ($\epsilon = \Phi$) is valid. Hence, the boundary values of k and ϵ at the first grid point near the wall are (ASCE Committee, 1988)

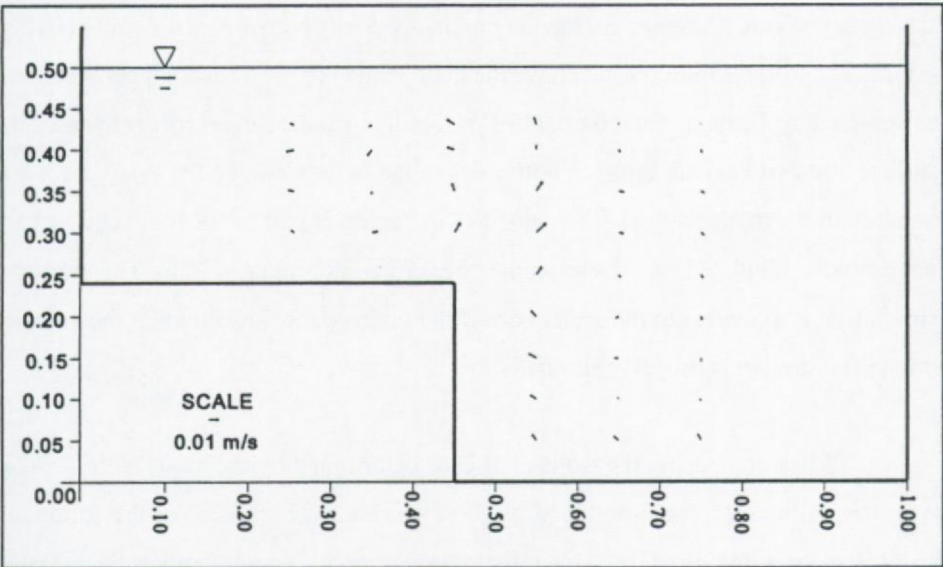
$$k = \frac{U_*^2}{\sqrt{c_\mu}} \quad \text{and} \quad \epsilon = \frac{U_*^3}{\kappa y^*}$$

It should be noted that the current grid structure (Fig. 4.6.1) provides the possibility of determining the shear and normal stresses using the ASM with the velocity gradients near the wall calculated from the law-of-the-wall (Cokljat and Younis, 1995a)

$$\frac{\partial U}{\partial y} = \frac{U_*}{\kappa y^*}$$



a) simulation by the numerical model



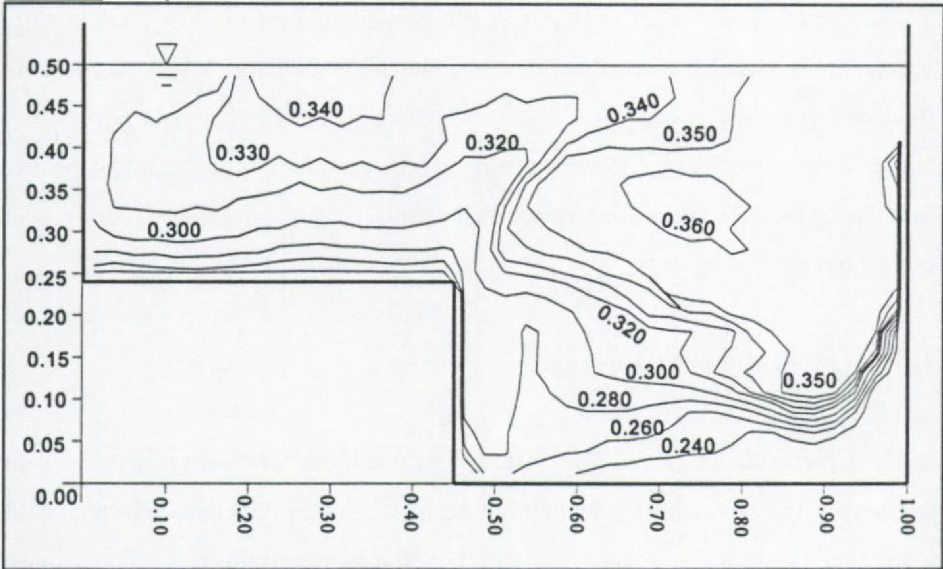
b) Experimental results

Figure 4.7.1 Secondary circulation (m/s)

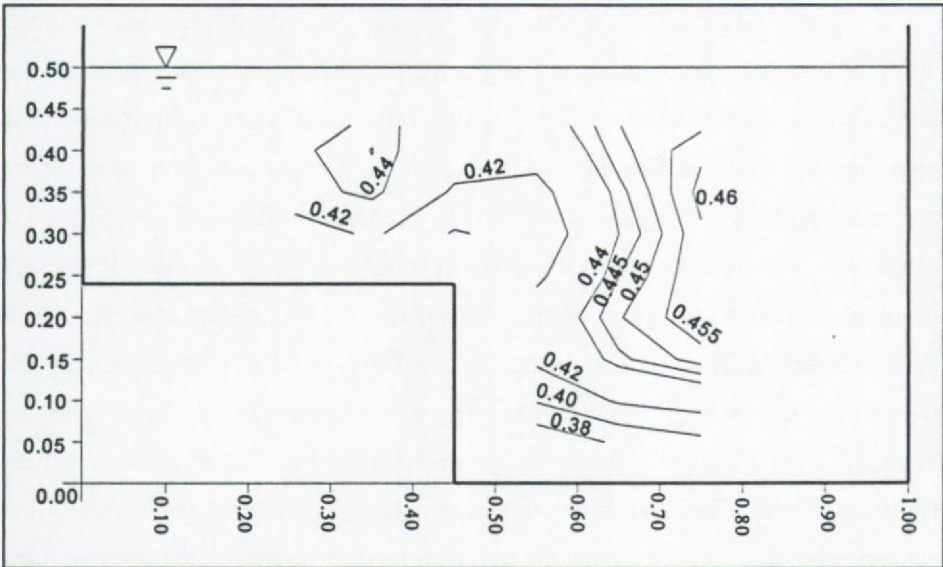
4.7 Numerical Results

The secondary circulation (Fig. 4.7.1a) is in good agreement with the experimental results at the salient corner (Fig. 4.7.1b). Near the bottom of the main channel, the secondary circulation is not properly simulated. Tominaga and Nezu (1991) reported that the main-channel vortex (the vortex on the main-channel side of the salient corner) spans a lateral distance of about 0.9 of the main channel depth and the flood plain vortex (the vortex on the flood plain side of the salient corner) spans a lateral distance of about 0.5 of the main channel depth. They reported on a bottom vortex in the main channel spanning a lateral distance ≤ 0.8 of the main channel depth. The three vortices are simulated by the current model as can be seen in Fig. 4.7.1. In Fig. 4.7.1, one more vortex is formed near the wall of the flood plain. It has no interaction with the flood plain vortex. The main channel vortex is stronger than the flood plain vortex. Contours for the longitudinal velocity component are shown in Fig. 4.7.2a. The isolines in Fig. 4.7.2a have the main features of flow in compound channel as depicted by Tominaga and Nezu (1991): A bulging at the salient corner towards the surface and two velocity dips (on both sides of the bulge), one on the flood plain and another on the main channel. The velocities in the lower part of the main channel are not properly simulated (see, for example, the 0.75 contour, Fig. 4.7.2a). The improper simulation is extended to the upper part of the main channel meanwhile the velocity on the flood plain is properly simulated.

When comparing the isolines of U as determined by the model (Fig. 4.7.2a) with the isolines of U as produced by the experiment (Fig. 4.7.2b), the following points can be noted. First, the general structure in both cases is similar. Second, the isolines of the experimental results are usually of higher values than those of the numerical model. The reason is attributed to the initial conditions at the upstream open boundary. The numerical grid points are much denser than the measuring points of



a) simulation by the numerical model



b) Experimental results

Figure 4.7.2 Isolines of U (m/s)

EMS. Therefore, it is needed to interpolate between the measured values. A linear interpolation is used. Consequently, the total numerical discharge is 124.5 l/s while the total experimental discharge is 150.0 l/s. Although the discharge is not properly simulated the velocity profile at the upstream open boundary is reasonably simulated. Simulating the velocity profile (rather than the discharge) is necessary to investigate the splitter plate effect.

4.8 Model Comparison

The code employed in this study is a result of a gradual refinement of the large-scale hydrodynamic model POM of the University of Princeton to be applicable to the small-scale example of LIP2. From the refinement procedure, it was possible to conduct the following comparison.

The POM model uses the boundary fitting (σ -) coordinates. The σ -coordinates are suitable to resolve complicated topographic features in large-scale shallow water bodies where large bathymetric irregularities often exist. The transformation to σ -coordinates introduces new terms in the governing equations, with some of the additional terms involving cross derivatives. Mellor and Blumberg (1985) tried to simplify the σ -transformed ASM. However, although the σ -transformation of the ASM is not impossible, it is far more complex than that of the Navier-Stokes equations and needs further investigation. For large bathymetric variations, Deleersnijder and Beckers (1992) and Stelling and van Kester (1994) proposed two different solutions. The sudden depth change of the LIP2 experiment can be modeled by any one of them. However, when the rigid lid assumption is used, the coefficients of the σ -transformed equations become 1 or 0 reducing the σ -transformed equations to the Cartesian form. Therefore, the σ -transformed equations are not needed for the current application and the current application cannot be used to check the applicability of the σ -transformed equations.

The large-scale models use some smoothing filters e.g. POM model uses Asselin's (1972) time smoothing filter and adds a correction to the vertical structure of the velocity to have its average equal to the (calculated) depth average velocity. Such filters cannot be used in small-scale modeling because the diffusive effect of the filters usually overrides the effects of the closure model.

The central difference discretization of the advective term is sufficient for the large-scale model because the diffusive effect due to the mesh size attenuates the oscillations produced by the central differencing. On the other hand, small-scale models need better interpolation methods which are neither diffusive nor oscillatory (e.g. ULTIMATE QUICKEST, Sec.3.3).

For large-scale shallow-water flows, the hydrostatic pressure assumption is adequate because the horizontal scale is much larger than the vertical one. In the current small-scale flow, the lateral and vertical scales are comparable. Therefore, a full vertical momentum equation is necessary (see Sec. 3.2)

In large-scale flows, the zero-gradient open-boundary condition is enough because the numerical waves are much smaller than the water surface fluctuations (due to e.g. tidal waves, wind waves...). In the unidirectional flume flow, the numerical wave should be disposed off out of the computational domain by e.g. Orlanski (1976) radiation open boundary conditions (see Sec. 3.5.2).

For large-scale flows, the turbulence terms in the momentum equations are unimportant so that the closure model has no influence anyway; and when the turbulence terms are important and determine the flow behavior, the model is mostly too coarse to describe this behavior correctly. Therefore, large-scale models apply an effective horizontal diffusivity which is due only in part to turbulence and in general also accounts for: numerical diffusion, convective sub-grid scale motion and (in the

case of depth averaged calculation) dispersion i.e. the horizontal diffusivity choice is a matter of numerical model calibration rather than a turbulence model problem. On the other hand, small-scale models need a full turbulence model which is able to reproduce the secondary currents effected by normal stresses difference (see Sec. 4.3).

The impact of the roundoff error on the final results is different in the case of large scale models from that of small scale models. The roundoff error is directly linked to the word length used by the computer. While roundoff errors produced by single precession word length is acceptable for large scale models, (at least) double precession is a must for small scale models.

4.9 Program Structure

The mathematical model, discussed in chapters 3 and 4, has been executed in a FORTRAN program (3DHYD). The program has a modular structure. The modular structure of POM was useful as a guide to have the 3DHYD structure. However, the two programs are completely different from each other and 3DHYD is a new independent code.

The input to the program consists of the following data elements.

1. Mesh size.
2. The structure of the canal cross-section; or, in general, the bathymetry of the domain.
3. Velocity distribution at the upstream boundary.
4. Time step and total simulation time (time is used, for steady flow, as an iterative variable).
5. Expected limits for the dependent variables.

After reading the input and initializing the variables, the iterative solution is

carried out as follows.

1. Transition values of the three velocity components are determined from the momentum equations taking into account only advection and diffusion (or Reynolds stress) terms (Eq. 3.4.1).
2. Open boundary conditions are applied to the transition values determined in step 1 above (Sec. 3.5.2).
3. The longitudinal velocity component U is determined in terms of the cross-sectional average pressure (Sec. 4.6.1, point no. 3).
4. The Poisson equation is solved, iteratively, to obtain the pressure field (Eq. 3.4.4)
5. The secondary velocity components (V and W) are determined from their momentum equations taking into account only the pressure term (Eq. 3.4.2).
6. Open boundary conditions are applied to the three velocity components (Sec. 3.5.2).
7. Transitional values for turbulence kinetic energy (k) and dissipation (ϵ) are determined from the k - ϵ model taking into account only advection and diffusion, i.e., the following two equations are solved.

$$\frac{\partial k}{\partial t} + U_i \frac{\partial k}{\partial x_i} = \frac{\partial}{\partial x_i} \left(\frac{v_i}{\sigma_k} \frac{\partial k}{\partial x_i} \right)$$

$$\frac{\partial \epsilon}{\partial t} + U_i \frac{\partial \epsilon}{\partial x_i} = \frac{\partial}{\partial x_i} \left(\frac{v_i}{\sigma_\epsilon} \frac{\partial \epsilon}{\partial x_i} \right)$$

8. Open boundary conditions are applied to k and ϵ (Sec. 4.6.2).
9. Turbulence kinetic energy (k) and dissipation (ϵ) are determined from the k - ϵ model taking into account only the production and dissipation terms, i.e., the following equations are solved.

$$\frac{\partial k}{\partial t} = \Phi - \epsilon$$

$$\frac{\partial \epsilon}{\partial t} = c_{\epsilon 1} \frac{\epsilon}{k} \Phi - c_{\epsilon 2} \frac{\epsilon^2}{k}$$

In this subroutine, the near surface conditions, discussed in Sec. 4.6.2 are taken into consideration.

10. Open boundary conditions are applied to k and ϵ (Sec. 4.6.2).

11. Eddy viscosity is determined as a function of k and ϵ (Eq. 4.4.1).

12. Naot's model is applied to determine the Reynolds stresses (Eqs. 4.5.2 to 4.5.4).

The output includes the dependent variables, i.e., the three velocity components, pressure, turbulence kinetic energy and dissipation and Reynolds (shear and normal) stresses.

4.10 Conclusion

The Reynolds stress equation (4.2.1) is the closure to the Navier-Stokes equations. It contains terms which must be modeled in order to have it solved for the Reynolds stresses. The different turbulence models are reviewed in Sec. 4.3. It is concluded that the turbulence transport models are the most appropriate models. The ASM is the model which combines the economy of the eddy viscosity model and the universality of the stress transport models. It redistributes the length and velocity scale parameters (k and ϵ) of turbulence which are calculated by the standard k - ϵ model. The full 3-D form of the ASM developed by Haque (1994) is discussed. Although the splitting method, discussed in Sec. 4.6.1, was not successful in determining the variables with the distribution of Fig. 4.6.1, it is believed that it can be improved to a workable level. However, it is replaced (for the time being) by the Singular Value Decomposition technique applied to the same distribution. Nevertheless, the model is still too expensive to be handled with the available hardware. It is replaced by Naot's model which is simple, economic and numerically robust. The model takes into

consideration the wall proximity. The numerical solution applied a modified form of the Patankar and Spalding algorithm. The initial and boundary conditions are discussed in Sec. 4.6.2. It is seen that when the initial conditions for U are identical with the open boundary conditions, the solution converges faster to the steady case and it provides better simulation of the secondary circulation.

The model results presented in Sec. 4.7 show the ability of the model to simulate the flow in compound channels.

The current model is compared with POM. It is concluded that the assumptions underlying large-scale models are so different from those underlying small-scale models that they cannot replace one another, even with any degree of approximation.

Chapter 5

CONCLUSIONS AND RECOMMENDATIONS

5.1 Summary

Within the framework of LIP2, the tidal flume of Delft Hydraulics has been used to study the secondary circulation in compound channels. The analysis is limited to the steady homogeneous case. The limitations and uncertainties of the experiment are discussed. However, the data are representative of typical turbulent flow in compound channels.

A numerical full 3D model is built to simulate the LIP2 experiment. The pressure is calculated by solving a Poisson equation obtained by substituting for the velocity from the momentum equation into the continuity equation. The advection term is discretized using the ULTIMATE QUICKEST scheme. The rate of change term is used as an iterative term to reach the steady solution.

The turbulence closure problem is addressed. The k - ϵ model is proven to be insufficient to reproduce the secondary circulation in a compound channel because of the assumption that the eddy viscosity is isotropic. The ASM provides a remedy to the isotropy problem by modelling the Reynolds stress equations into algebraic equations. The ASM combines the simplicity of the k - ϵ model and the anisotropy of the full Reynolds stress equations.

5.2 Conclusions

The following conclusions can be drawn out of the research.

5.2.1 The experiment

1. The measuring area is so limited that a full analysis of the flow characteristics in the cross section is hindered.
2. The laser instruments have to be warmed up for 24 hours before starting measurements and are not turned off up to the end of the experiment to avoid signal noise.
3. The vertical profile of the longitudinal velocity component, next to the upstream splitter plate, is not parabolic. Rather, the profile has two peaks, separated by a depression located at the plate (Fig. 2.3.2). The above-mentioned profile disappears at the upstream (measuring) section, but the flow is still developing. At the downstream (measuring) section, on the other hand, the flow is fully developed.
4. The alignment (orientation) error is the largest experimental error. It is corrected by applying the mass conservation law.
5. The lateral distribution of the depth-averaged longitudinal velocity is different from that obtained for a closed duct. Hence, the free surface in open channels does not correspond to the symmetry plane in closed ducts.
6. The distribution of the Reynolds stresses demarcate three zones in the compound channel: the deep main channel (below the flood plain bed), the shallow main channel and the flood plain.

5.2.2 The numerical model

1. In the LIP2 experiment, the horizontal (lateral) and vertical length scales are comparable. Hence, the hydrostatic pressure assumption is not applicable and a full

vertical momentum equation is needed.

2. The numerical model developed in this study is fully 3D. It can simulate flows that are governed by Eqs. 3.2.1. However, for typical 2D flows, where the vertical dimension is small compared to the horizontal dimensions, the model is not economic compared to the available models which apply the hydrostatic pressure assumption (e.g. shallow water flow in coastal areas). On the other hand, the model cannot be disposed of for flows which are 3D in nature (e.g. mixing behaviour in open channels and rivers especially when having over-bank flow, water and sewage treatment plants...).

3. The advective term is discretized using the ULTIMATE QUICKEST scheme. A new condition is applied (Eq. 3.3.6). The new condition provides the same result with less grid points.

4. The available upstream open boundary conditions unveil one of the limitations of the ULTIMATE QUICKEST. The ULTIMATE QUICKEST shares with other schemes the weakness of reverting to first order upwinding with the consequent inherent artificial diffusion. The ULTIMATE QUICKEST reverts to the first order upwinding when the monotonicity condition is violated.

5. The point-by-point approach is used to solve (iteratively) the Poisson equation for the pressure. It is better than the line-by-line approach because of two reasons. First, in 1D models, the point-by-point approach converges faster than the line-by-line approach because the solution seeks its own level rather than insisting on a definite value at a particular grid point. Second, in more than one dimension, the line-by-line approach converges to a solution with a fixed error of convergence while the point-by-point approach converges asymptotically to a solution with a zero error of convergence.

6. The relative nature of the pressure makes it possible to work with small pressure values avoiding that the pressure field acquires a large absolute value. Moreover, the next time step does not start with a cold start; rather, it starts from the previous pressure estimates, which are expected to be a good first guess because the

numerical method marches with small increments of the dependent variables.

6. The radiation boundary condition is the appropriate open boundary condition for parabolic differential equations in steady flow. The rigid lid assumption is used to avoid solving an extra equation for the water elevation. The assumption is good enough for steady flow.

5.2.3 The turbulence closure

1. The two-equation (k - ϵ) model is not able to predict the secondary circulation in a compound channel because it is based on the assumption that the eddy viscosity is isotropic.

2. The ASM is used to redistribute the stresses anisotropically.

3. The full 3D ASM developed by Haque (1994) is based on just neglecting the partial differential terms in the Reynolds stress equations and assuming local equilibrium. However, neglecting the transport terms is not suitable for the flow in compound channels.

4. Naot's model, as an alternative to Haque's model, is simple, economic and numerically robust. It is designed to take into account wall proximity and compound channel structure.

5. The numerical solution of the ASM of Haque (1994) using the splitting method has two advantages. First, the ASM is reduced to solving three simultaneous equations for the shear stress and three mutually independent equations for the normal stress. Second, it suits the variable distribution shown in Fig. 4.6.1. The proposed distribution minimizes the need for interpolation between Reynolds stress values and hence reduces the error arising from linear interpolation.

6. Haque's model is too expensive and cannot deal with the ill-conditioned problem. Naot's model, on the other hand, overcomes these two shortcomings. The results obtained showed that Naot's model could simulate flow in compound channels.

5.2.4 Model comparison

1. Comparing the current model with the large scale POM model, it is concluded that the assumptions underlying the large scale models are so different from those underlying the small scale models that they cannot replace one another with any degree of approximation.

5.2.5 New contributions by the current research

1. It is noticed that the shear layer extends inside the main channel more than on the flood plain. A new (qualitative, physical) interpretation is proposed (Sec. 2.4.2).

2. Leonard (1991) developed the ULTIMATE QUICKEST scheme using two adjacent control volumes. Therefore, he used four grid points to determine each (interpolated) face value. One condition (Eq. 3.3.6) is modified to allow for using only one control volume and hence only three grid points. Such a saving on the grid points, needed for interpolation, is very useful, especially at the downstream open boundaries.

3. The current research highlights one of the limitations of the ULTIMATE QUICKEST scheme. The scheme reverts to the diffusive first-order upwind scheme when the monotonicity condition is violated (Sec. 3.3.3).

4. The Patankar and Spalding algorithm is modified. First, Patankar and Spalding (1972) used only two consecutive cross sections. The current research uses few (~10) cross sections, which allows for applying sophisticated schemes, e.g., ULTIMATE QUICKEST (Sec. 4.6.1). Second, while Patankar and Spalding (1972) suggested the first guess in solving the Poisson equation for the pressure, the current research applied the pressure field estimated from the previous time step as a first guess. Such a guess accelerates convergence to the solution (see *Relative Nature of the Pressure* under Sec. 3.4.2).

5. The staggered distribution of the variables over the grid points (Fig. 4.6.1) reduces the need for interpolation.

6. Haque's turbulence closure model is solved using the Splitting Method explained in Appendix B. Both the model the Splitting method need further consideration.

5.3 Recommendations

1. The limited measuring area shown in Fig. 2.3.3 must be avoided by changing the carrying frame structure and using other instruments that can measure closer to the boundaries (than the ILDA's). This will help to perform detailed analysis and discussion of the flow behavior in the cross section.

2. Turbulence is not regarded today as a completely random process. It contains a certain sequence of events (Yalin, 1992). Studying turbulence behaviour at a single location lacks the general view point necessary to cope with the abovementioned concept of turbulence. To be able to study the coherent structure developed along the flume, it is necessary to study the turbulence development right from the inlet down to the outlet of the measuring reach. Hence new instruments are needed, e.g. high speed video camera, laser light sheet and laser induced fluorescence.

3. The main target of studying the flow dynamics is to study its effect on pollutant transport. It is recommended to run similar (LIP) experiments in compound channels with suspended sediments added to study sediment (or generally speaking, pollutant) interaction with the flow in both homogeneous and stratified flows.

4. The ULTIMATE QUICKEST scheme is diffusive under non-monotonic conditions (reverting to first order upwinding). It is recommended to find a suitable interpolation method to be used when the dependent-variable distribution is non-monotonic.

5. There must be a consistent check on the diffusivity of the scheme (especially the turbulence closure schemes). The numerical scheme must not redistribute the velocity (or momentum) deficit over the cross section.

6. The buoyancy term should be added to the current numerical model to be able

to predict stratified flow.

7. Faster numerical methods can enhance the performance of the code, e.g. using implicit methods, using parallel computation (either by partitioning the code or partitioning the domain), using over-relaxation methods.

8. The current logarithmic law of the wall applied at solid boundaries for the ASM has strong influence on the stresses in the interior of the domain. It is recommended to use more elaborate models, e.g. near wall low Reynolds number models to reduce the degree of empiricism involved in the law of the wall.

9. It is recommended to improve the splitting method for solving the ASM when the system of equation is ill-conditioned.

10. With the fast development in computer hardware, it is recommended to apply more accurate turbulence closure models (e.g. large eddy simulation, direct numerical simulation, Reynolds stress transport equation). It is recommended, also, to express the coherent structures in a mathematical form.

11. The effect of the hardware accuracy and the numerical method to be used may lead to erroneous interpretation of the numerical results as long as turbulence and secondary circulation is concerned. It is recommended to establish certain standards for the specifications of the hardware needed and the error arising from the discretization techniques (e.g. mesh size, truncation error, round off error).

References

1. **ASCE Task Committee on Turbulence Models in Hydraulic Computations** (1988) "Turbulence Modeling of Surface Water Flow and Transport", J. Hydr. Eng., ASCE, Vol.114, No.9, pp 970-991.
2. **Asselin, R.** (1972) "Frequency Filter for Time Integrations", Monthly Weather Review, Vol.100, No.6, pp 487-490.
3. **Basara, B. and B. A. Younis** (1995) "Prediction of Turbulent Flows in Dredged Trenches", J. Hydr. Research, Vol.33, No.6, pp 813-824.
4. **Cahyono** (1992) "Three-Dimensional Numerical Modelling of Sediment Transport Processes in non-Stratified Estuaine and Coastal Waters", Ph.D. thesis, Department of civil engineering, University of Bradford, U.K., 315pp.
5. **Chapman, D. C.** (1985) "Numerical Treatment of Cross-Shelf Open Boundaries in a Barotropic Coastal Ocean Model", J. Physical Oceanography, Vol.15, pp 1060-1075.
6. **Cokljat, D. and B. A. Younis** (1995a) "Second-Order Closure Study of Open-Channel Flows", J. Hydr. Eng., ASCE Vol.121, No.2, pp94-106.
7. **Cokljat, D. and B. A. Younis** (1995b) "Compound-Channel Flows: A Parametric Study Using a Reynolds-Stress Transport Closure", J. Hydr. Research, Vol.33, No.3, pp 307-320.
8. **Currie, G. I.** (1993) "Fundamental Mechanics of Fluids", McGraw-Hill, Inc., New York, 454 pp.
9. **Cushman-Roisin, B.** (1994) "Introduction to Geophysical Fluid Dynamics", Prentice-Hall, New Jersey, 320 pp.
10. **Deleersnijder, E. and J. Beckers** (1992) "On the Use of the σ -Coordinate System in Regions of Large Bathymetric Variations", J. Marine Systems, Vol.3, pp 381-390.

11. **Delft Hydraulics** (1986), Hydro-delft, Vol.74, 27 pp.
12. **Demuren, A. O. and W. Rodi** (1984) "Calculation of Turbulence-Driven Secondary Motion in Non-Circular Ducts", J. Fluid Mechanics, Vol.140, pp 189-222.
13. **Falconer, R. A. and Cahyono** (1993) "Water Quality Modelling in Well Mixed Estuaries Using Higher Order Accurate Difference Schemes", in *"Advances in Hydrosience and Engineering"*, S. S. Y. Wang, ed., Proc. 1st Int. Conf. Hydrosience and Engineering., Washington, June 7-11, Vol.1, pp 81-92.
14. **Ferziger, J. H.** (1987) "Simulation of Incompressible Turbulent Flows", J. Computational Physics, Vol.69, pp 1-48.
15. **Fletcher, C. A. J.** (1991) "Computational Techniques for Fluid Dynamics", Springer-Verlag, Berlin (*two volumes*).
16. **Guinot, V.** (1995) "A Monotonic Version of the Holly-Preissmann Scheme", in *"John F. Kennedy Student Competition"*, Proc. XXVth IAHR Congress (HYDRA 2000), London, Sept. 11-15, Vol.5, pp 49-54.
17. **Hageman, L. A. and D. M. Young** (1981) "Applied Iterative Methods", Academic Press, New York, 386 pp.
18. **Haque, M. A.** (1994) "Modelling Flow, Density and Turbulence Fields in a Stratified and in a Well-Mixed Tidal Medium", Ph.D.thesis, Hydraulic Laboratory, Katholiek Universiteit Leuven, Belgium, 238 pp.
19. **Hirsch, C.** (1991) "Numerical Computation of Internal and External Flows", John Wiley and Sons Ltd, Chichester, UK, (*two volumes*).
20. **Hossain, M. S.** (1980) "Mathematische Modellierung von Turbulenten Auftriebsströmungen", Ph.D. thesis, University of Karlsruhe, Germany.
21. **Israeli, M. and S. A. Orszag** (1981) "Approximation of Radiation Boundary Conditions", J. Computational Physics, Vol.41, pp 115-135.
22. **Jones, W. P. and B. E. Launder** (1972) "The Prediction of Laminarization with a Two-Equation Model of Turbulence", Int. J. Heat Mass Transfer, Vol.15, pp 301-314.
23. **Knight, D. W. and J. D. Demetriou** (1983) "Flood Plain and Main Channel

Flow Interaction", J. Hydr. Eng., ASCE, Vol.109, No.8, pp 1073-1092.

24. **Lakshminarayana, B.** (1986) "Turbulence Modeling for Complex Shear Flows", AIAA J., Vol.24, No.12, pp 1900-1917.

25. **Launder, B. E.** (1975) "On the Effects of a Gravitational Field on the Turbulent Transport of Heat and Momentum", J. Fluid Mechanics, Vol.67, part 3, pp 569-581.

26. **Launder, B. E.** (1992) "On the Modelling of Turbulent Industrial Flows", Computational Methods in Applied Sciences, Vol. , pp 91-102.

27. **Leonard, B. P.** (1980) "The QUICK Algorithm: A Uniformly Third-Order Finite-Difference Method for Highly Convective Flows" in "*Computer Methods in Fluids*" (K Morgan, C. Taylor, C.A. Brebbia, eds.), Pentech Pres, London, pp 159-195.

28. **Leonard, B. P.** (1988) "Elliptic Systems: Finite-Difference Method IV", in "*Handbook of Numerical Heat Transfer*" (W. J. Minkowycz, E. M. Sparrow, G. E. Schneider and R. H. Pletcher, eds.), John Wiley & Sons, Inc., pp 347-378.

29. **Leonard, B. P.** (1991) "The ULTIMATE Conservative Difference Scheme Applied to Unsteady One-Dimensional Advection", Computer Methods in Applied Mechanics and Engineering, Vol.88, pp 17-74.

30. **Leonard, B. P. and S. Mokhtari** (1990) "Beyond First-Order Upwinding: The Ultra-Sharp Alternative for Non-Oscillatory Steady-State Simulation of Convection", Int. J. Numerical Methods in Engineering, Vol.30, pp 729-766.

31. **Leschziner, M. A.** (1990) "Modelling Engineering Flows with Reynolds Stress Turbulence Closure", J. Wind Engineering and Industrial Aerodynamics, Vol.35, pp 21-47.

32. **Leschziner, M. A.** (1995) "Modelling Turbulence in Physically Complex Flows", in "*Industrial Hydraulics and Multi-Phase Flow*", M. A. Leschziner, ed., Proc. XXVIth IAHR Congress (HYDRA2000), London, Sept.11-15, Vol.2, pp 1-33.

33. **Lin, B. and K. Shiono** (1995) "Numerical Modelling of Solute Transport in Compound Channel Flows", J. Hydr. Research, Vol.33, No.6, pp 773-788.

34. **Lorenzetti, J. A. and J. D. Wang** (1986) "On the Use of Wave-Absorbing

Layers in the Treatment of Open Boundaries in Numerical Coastal Circulation Models", Appl. Math. Modeling, Vol.10, pp 339-345.

35. **Markatos, N. C.** (1986) "The Mathematical Modelling of Turbulent Flows", Applied Mathematical Modeling, Vol.10, pp 190-220.

36. **Mellor, G. L. and A. F. Blumberg** (1985) "Modeling Vertical and Horizontal Diffusivities with the Sigma Coordinate System", Monthly Weather Review, Vol.113, pp 1379-1383.

37. **Naot, D and W. Rodi** (1981) "Applicability of Algebraic Models Based on Unidirectional Flow to Duct Flow with Lateral Motion", Int. J. Numerical Methods in Fluids, Vol.1, pp 225-235.

38. **Naot, D. and W. Rodi** (1982) "Calculation of Secondary Currents in Channel Flow", J. Hydr. Division, ASCE, Vol.108, No. HY8, pp 949-968.

39. **Naot, D. and W. Rodi** (1983) "Interaction of the Turbulent Eddies with Free-Surface", in "*Liquid Metal Flow and Magnetohydrodynamics*" (H. Branover, P. S. Lykoudis and A. Yakhot, eds.), Progress in Astronautics and Aeronautics, 84, AIAA, New York, N.Y.

40. **Naot, D., I. Nezu and H. Nakagawa** (1993) "Hydrodynamic behaviour of Compound Rectangular Open Channels", J. Hydr. Eng., ASCE, Vol.119, No.3, pp 390-408.

41. **Nezu, I. and W. Rodi** (1986) "Open-Channel Flow Measurements with a Laser Doppler Anemometer", J. Hydr. Eng., ASCE, Vol.112, No.5, pp 335-355.

42. **Nezu, I. and H. Nakagawa** (1993) "Turbulence in Open-Channel Flows", IAHR monograph series, A. A. Balkema, Rotterdam, the Netherlands, 281 pp.

43. **Orlanski, I** (1976) "A Simple Boundary Condition for Unbounded Hyperbolic Flows", J. Computational Physics, Vol.21, pp 251-269.

44. **Patankar, S. V.** (1980) "Numerical Heat Transfer and Fluid Flow", Hemisphere Publishing Corporation, Washington, USA, 197 pp.

45. **Patankar, S. V. and D. B. Spalding** (1972) "A Calculation Procedure for Heat, Mass and Momentum Transfer in Three-Dimensional Parabolic Flows", Int. J.

Heat Mass Transfer, Vol.15, pp 1787-1806.

46. **Patel, V. C., W. Rodi and G. Scheuerer** (1984) "Turbulence Models for Near-Wall and Low Reynolds Number Flows: A Review", *AIAA J.*, Vol.23, No.9, pp 1308-1319.
47. **Peyret, R. and T. D. Taylor** (1983) "Computational Methods for Fluid Flow", Springer-Verlag, New York, USA, 358 pp.
48. **Pezzinga, G.** (1994) "Velocity Distribution in Compound Channel Flows by Numerical Modeling", *J. Hydr. Eng., ASCE*, Vol.120, No.10, pp 1176-1198.
49. **Press, W. H., B. P. Flannery, S. A. Teukolsky and W. T. Vetterling** (1986) "Numerical Recipes, the art of scientific computing", Cambridge University Press, 818 pp.
50. **Rastogi, A. K. and W. Rodi** (1978) "Predictions of Heat and Mass Transfer in Open Channels", *J. Hydr. Division, ASCE*, vol.104, No. HY3, pp 397-420.
51. **Rhodes, D. G. and D. W. Knight** (1994) "Velocity and Boundary Shear in a Wide Compound Duct", *J. Hydr. Research*, Vol.32, No.5, pp 743-764.
52. **Rocabado, O. I. H.** (1994) "Computation of Turbulent Flows with the k- ϵ Closure Model", Master thesis, Hydraulic Laboratory, Katholieke Universiteit Leuven, Belgium, 79pp.
53. **Rodi, W** (1980) "Turbulence Models and their Application in Hydraulics, state-of-the-art paper", *IAHR*, Delft The Netherlands, 104 pp.
54. **Roed, L. P. and O. M. Smedstad** (1984) "Open Boundary Conditions for Forced Waves in a Rotating Fluid", *SIAM J. Sci. Stat. Comput.*, Vol.5, No.2, pp 414-426.
55. **Shiono, K, R. A. Falconer, J. Berlamont and M. Karelse** (1994) "EC-LIP2 on Shearing Mechanisms and Mixing Processes in a Stratified Compound Estuary", draft report, Delft Hydraulics.
56. **Smith, G. D.** (1985) "Numerical Solution of Partial Differential Equations: Finite Difference Methods", Oxford University Press, New York, USA, 337 pp.
57. **Song, Z. W.** (1995) "Parallelization of Hydrodynamic Models for Distributed

Memory Computers", Ph.D. thesis, Katholieke Universiteit Leuven, Belgium, 148 pp.

58. **Speziale, C. G.** (1987) "On Non-Linear $k-l$ and $k-\epsilon$ Models of Turbulence", *J. Fluid Mechanics*, Vol.178, pp 459-475.

59. **Stelling, G. S. and J. A. Th. M. van Kester** (1994) "On the Approximation of Horizontal Gradients in Sigma Co-ordinates for Bathymetry with Steep Bottom Slopes", *Int. J. Numerical Methods in Fluids*, Vol.18, pp 915-935.

60. **Sweby, P. K.** (1984) "High Resolution Schemes Using Flux Limiters for Hyperbolic Conservation Laws", *SIAM J. Numerical Analysis*, Vol.21, No.5, pp 995-1011.

61. **Thomas, T. G. and J. J. R. Williams** (1995a) "Large Eddy Simulation of Turbulent Flow in an Asymmetric Compound Open Channel", *J. Hydr. Research*, Vol.33, No.1, pp 27-41.

62. **Thomas, T. G. and J. J. R. Williams** (1995b) "Large Eddy Simulation of a Symmetric Trapezoidal Channel at a Reynolds Number of 430,000" *J. Hydr. Research*, Vol.33, No.6, pp 825-842.

63. **Tominaga, A. and I. Nezu** (1991) "Turbulent Structure in Compound Open-Channel Flows", *J. Hydr. Eng., ASCE*, Vol.117, No.1, pp 21-41.

64. **Wilcox, D. C.** (1993) "Turbulence Modelling for CFD", DCW Industries, Inc., 5354 Palm Drive, La Canada, California 91011, 460 pp.

65. **Yalin, M. S.** (1992) "River Mechanics", Pergamon Press Limited, Heading Hill Hall, Oxford OX3 0BW, England, 220 pp.

appendix A

TENSOR NOTATION

Tensors are described in detail in books on linear algebra. However, for the sake of completeness, the most important features of tensor notation which are used in this work will be reviewed (see Wilcox, 1993).

The components of an n -dimensional vector \mathbf{x} are denoted as x_1, x_2, \dots, x_n . For example, in three-dimensional space, the coordinate vector $\mathbf{x} = (x, y, z)$ is rewritten as $\mathbf{x} = (x_1, x_2, x_3)$. Now consider an equation describing a plane in three-dimensional space, viz.,

$$a_1 x_1 + a_2 x_2 + a_3 x_3 = c \quad (\text{A.1})$$

where a_i and c are constants. This equation can be written as

$$\sum_{i=1}^3 a_i x_i = c \quad (\text{A.2})$$

In tensor notation, the Einstein summation convention is introduced and Eq. A.2 is rewritten in the shorthand form

$$a_i x_i = c \quad (\text{A.3})$$

Another example is introduced by Eq. 3.2.1b. It is repeated here for clarity.

The momentum equations in Cartesian coordinates are

$$\begin{aligned}
x: \quad \frac{\partial u}{\partial t} + \frac{\partial uu}{\partial x} + \frac{\partial uv}{\partial y} + \frac{\partial uw}{\partial z} &= \frac{1}{\rho_0} \left(-\frac{\partial p_d}{\partial x} + \frac{\partial \tau_{xx}}{\partial x} + \frac{\partial \tau_{xy}}{\partial y} + \frac{\partial \tau_{xz}}{\partial z} \right) \\
y: \quad \frac{\partial v}{\partial t} + \frac{\partial uv}{\partial x} + \frac{\partial vv}{\partial y} + \frac{\partial vw}{\partial z} &= \frac{1}{\rho_0} \left(-\frac{\partial p_d}{\partial y} + \frac{\partial \tau_{xy}}{\partial x} + \frac{\partial \tau_{yy}}{\partial y} + \frac{\partial \tau_{yz}}{\partial z} \right) \quad (A.4) \\
z: \quad \frac{\partial w}{\partial t} + \frac{\partial uw}{\partial x} + \frac{\partial vw}{\partial y} + \frac{\partial ww}{\partial z} &= \frac{1}{\rho_0} \left(-\frac{\partial p_d}{\partial z} - \rho' g + \frac{\partial \tau_{xz}}{\partial x} + \frac{\partial \tau_{yz}}{\partial y} + \frac{\partial \tau_{zz}}{\partial z} \right)
\end{aligned}$$

In tensor notation, Eqs. (A.4) are rewritten in short-hand form as

$$\frac{\partial u_i}{\partial t} + \frac{\partial u_i u_j}{\partial x_j} = \frac{1}{\rho_0} \left(-\frac{\partial p_d}{\partial x_i} + \rho' g_i + \frac{\partial \tau_{ij}}{\partial x_j} \right) \quad (A.5)$$

The Einstein summation convention is as follows.

Repetition of an index in a term denotes summation with respect to that index over its range.

The range of an index i is the set of n integer values 1 to n . An index that is summed over is called a *dummy index*, one that is not summed is called a *free index*.

Since a dummy index simply indicates summation, it is immaterial what symbol is used. Thus $a_i x_i$ may be replaced by $a_j x_j$, which is obvious if it is noticed that

$$\sum_{i=1}^3 a_i x_i = \sum_{j=1}^3 a_j x_j \quad (A.6)$$

A matrix is denoted by using two subscripts (indices). The first subscript (index) corresponds to row number while the second subscript corresponds to column number. For example, consider the 3x3 matrix $[A]$ defined by

$$[A] = \begin{bmatrix} A_{11} & A_{12} & A_{13} \\ A_{21} & A_{22} & A_{23} \\ A_{31} & A_{32} & A_{33} \end{bmatrix} \quad (A.7)$$

In tensor notation, the matrix $[A]$ is represented as A_{ij} .

The product of a square matrix and its inverse is the unit matrix, i.e.,

$$[A][A]^{-1} = \begin{bmatrix} 1 & 0 & 0 \\ 0 & 1 & 0 \\ 0 & 0 & 1 \end{bmatrix} \quad (\text{A.8})$$

Eq. (A.6) is rewritten in tensor notation as follows.

$$A_{ik}(A^{-1})_{kj} = \delta_{ij} \quad (\text{A.9})$$

where δ_{ij} is the Kronecker delta defined by

$$\delta_{ij} = \begin{cases} 1, & i=j \\ 0, & i \neq j \end{cases} \quad (\text{A.10})$$

Tensors are classified in terms of their rank. The number of the subscripts (indices) determine the rank of a tensor. The lowest rank tensor is rank zero which corresponds to a scalar, i.e., a quantity that has magnitude only. Thermodynamic properties such as pressure and density are scalar quantities. Vectors such as velocity, vorticity and pressure gradient are tensors of rank one. They have both magnitude and direction. Matrices are rank two tensors. The stress tensor is a good example for illustrating physical interpretation of a second rank tensor. It defines a force per unit area that has a magnitude and two associated directions, the direction of the force and the direction of the normal to the plane on which the force acts. For a normal stress, these two directions are the same; for a shear stress, they are (by convention) normal to each other.

The physical interpretation of tensors of rank three and beyond is difficult to ascertain. This is rarely an issue of great concern since virtually all physically relevant tensors are of rank two or less.

A tensor a_{ij} is *symmetric* if $a_{ij} = a_{ji}$. Many important tensors in mathematical

physics are symmetric, e.g., stress, strain and strain-rate tensors.

The trace of a second rank tensor a_{ij} is defined by

$$\text{tra} = a_{ii} = a_{11} + a_{22} + \dots + a_{nn} \quad (\text{A.11})$$

The trace of the direct product is defined by

$$\text{tr} \mathbf{u} \mathbf{v} = \mathbf{u} \cdot \mathbf{v} \quad (\text{A.12})$$

The trace function seems to be genuinely more algebraic than geometric.

Possible References:

- 1- **Dodson, C.T.J. and T. Poston** (1977) "Tensor Geometry", Pitman, London, 598pp.
- 2- **Simmonds, J.G.** (1982) "A Brief on Tensor Analysis", Springer Verlag, New York, 92pp.
- 3- **Wilcox, D.C.** (1993) "Turbulence Modeling for CFD", DCW Industries, Inc., USA, 460pp.
- 4- **Wylie, C.R.** (1975) "Advanced Engineering Mathematics", 4th edition, MacGraw-Hill, New York, 937pp.

Appendix B

SPLITTING METHOD FOR THE ASM

The splitting method used in section 4.6.1 to discretize the ASM developed by Haque (1994) is described in detail in this appendix. However, it should be noticed that the method still needs refinement to take into account ill-conditioned system of equations.

For simplicity, the stresses will be expressed in lower case letters (omitting over-bars and primes)

Assume that

$$A_k = \frac{k}{\epsilon} \frac{1-c_2}{c_1} \quad \text{and} \quad F = \frac{2}{3} k \frac{1-c_1-c_2}{c_1}$$

The ASM (Eq. 4.5.1) can be written in Cartesian coordinates as

$$uu = 2A_k \left(-uu \frac{\partial U}{\partial x} - uv \frac{\partial U}{\partial y} - uw \frac{\partial U}{\partial z} \right) - F \quad (\text{B.1})$$

$$vv = 2A_k \left(-uv \frac{\partial V}{\partial x} - vv \frac{\partial V}{\partial y} - vw \frac{\partial V}{\partial z} \right) - F \quad (\text{B.2})$$

$$ww = 2A_k \left(-uw \frac{\partial W}{\partial x} - uv \frac{\partial W}{\partial y} - uw \frac{\partial W}{\partial z} \right) - F \quad (\text{B.3})$$

$$uv = A_k \left(-uu \frac{\partial V}{\partial x} - uv \left(\frac{\partial V}{\partial y} + \frac{\partial U}{\partial x} \right) - uw \frac{\partial V}{\partial z} - vv \frac{\partial U}{\partial y} - vw \frac{\partial U}{\partial z} \right) \quad (\text{B.4})$$

$$uw = A_k \left(-uu \frac{\partial W}{\partial x} - uv \frac{\partial W}{\partial y} - uw \left(\frac{\partial W}{\partial z} + \frac{\partial U}{\partial x} \right) - vw \frac{\partial U}{\partial y} - ww \frac{\partial U}{\partial z} \right) \quad (\text{B.5})$$

$$vw = A_k \left(-uv \frac{\partial W}{\partial x} - vv \frac{\partial W}{\partial y} - vw \left(\frac{\partial W}{\partial z} + \frac{\partial V}{\partial y} \right) - uw \frac{\partial V}{\partial x} - ww \frac{\partial V}{\partial z} \right) \quad (\text{B.6})$$

The augmented matrix for this set of equations can be written as

	uu	vv	ww	uv	uw	vw	absolute term
row 1	Q	0	0	R	S	0	$-Z_1$
row 2	0	T	0	U	0	V	$-Z_2$
row 3	0	0	W	0	X	Y	$-Z_3$
row 4	A	B	0	C	D	E	$-Z_4$
row 5	F	0	G	H	I	J	$-Z_5$
row 6	0	K	L	M	N	P	$-Z_6$

(B.7)

where

$$Q = 1 + 2A_k \frac{\partial U}{\partial x}, \quad R = 2A_k \frac{\partial U}{\partial y}, \quad S = 2A_k \frac{\partial U}{\partial z}, \quad Z_1 = F,$$

$$T = 1 + 2A_k \frac{\partial V}{\partial y}, \quad U = 2A_k \frac{\partial V}{\partial x}, \quad V = 2A_k \frac{\partial V}{\partial z}, \quad Z_2 = F,$$

$$W = 1 + 2A_k \frac{\partial W}{\partial z}, \quad X = 2A_k \frac{\partial W}{\partial x}, \quad Y = 2A_k \frac{\partial W}{\partial y}, \quad Z_3 = F,$$

$$A = A_k \frac{\partial V}{\partial x}, \quad B = A_k \frac{\partial U}{\partial y}, \quad C = 1 + A_k \left(\frac{\partial V}{\partial y} + \frac{\partial U}{\partial x} \right),$$

$$D = A_k \frac{\partial V}{\partial z}, \quad E = A_k \frac{\partial U}{\partial z}, \quad Z_4 = 0,$$

$$F = A_k \frac{\partial W}{\partial x}, \quad G = A_k \frac{\partial U}{\partial z}, \quad H = A_k \frac{\partial W}{\partial y},$$

$$I = 1 + A_k \left(\frac{\partial W}{\partial z} + \frac{\partial U}{\partial x} \right), \quad J = A_k \frac{\partial U}{\partial y}, \quad Z_5 = 0,$$

$$K = A_k \frac{\partial W}{\partial y}, \quad L = A_k \frac{\partial V}{\partial z}, \quad M = A_k \frac{\partial W}{\partial x},$$

$$N = A_k \frac{\partial V}{\partial x}, \quad P = 1 + A_k \left(\frac{\partial W}{\partial z} + \frac{\partial V}{\partial y} \right), \quad Z_6 = 0,$$

It is clear from Eq. (B.7) that the first three rows of the matrix represent a diagonal matrix if the shear stresses are known. Also, it can be noticed that each row of the last three rows (4 to 6) contains coefficients for two of the normal stresses.

The idea of the splitting method is to substitute from rows 1-3 into rows 4-6

for the normal stresses. For example, substitute from rows 1 and 2 into row 4 for the normal stresses uu and vv , respectively. The result is the following matrix for the shear stress

uv	uw	vw	absolute term	
$C - \frac{A}{Q}R - \frac{B}{T}U$	$D - \frac{A}{Q}S$	$E - \frac{B}{T}V$	$-Z_4 + \frac{A}{Q}Z_1 + \frac{B}{T}Z_2$	
$H - \frac{F}{Q}R$	$I - \frac{F}{Q}S - \frac{G}{W}X$	$J - \frac{G}{W}Y$	$-Z_5 + \frac{F}{Q}Z_1 + \frac{G}{W}Z_2$	(B.8)
$M - \frac{K}{T}U$	$N - \frac{L}{W}X$	$P - \frac{K}{T}V - \frac{L}{W}Y$	$-Z_6 + \frac{K}{T}Z_2 + \frac{L}{W}Z_2$	

Eq. (B.8) is solved for the shear stresses, uv , uw , vw . By back substitution into the normal stress equations one gets the normal stresses

$$uu = \frac{-1}{Q}[Z_1 + R.uv + S.uw] \quad (B.9)$$

$$vv = \frac{-1}{T}[Z_2 + U.uv + V.vw] \quad (B.10)$$

$$ww = \frac{-1}{W}[Z_3 + X.uw + Y.vw] \quad (B.11)$$

Curriculum vitae

Mohamed ELZEIR was born on the 23rd of July, 1963 in Belkas, Egypt. In 1986, he graduated from the Department of Civil Engineering, El-Mansoura University, Egypt, with a B.Sc. in Civil Engineering degree. Then, he worked in El-Behera company for land reclamation as an engineer within the framework of El-Salam canal project. In 1987, he joined the Civil Engineering Department, Faculty of Engineering and Technology, El-Minia University, El-Minia, Egypt as an assistant lecturer. In 1989, he was granted a scholarship from the Belgian government to pursue a Master in Irrigation Engineering. In 1991, he completed the master degree with an overall appreciation of Greatest Distinction ranking the first position in his batch. Therefore, the Belgian government offered him an extension for his scholarship to pursue his Ph.D.. Since October, 1991, he has been working in his Ph.D.. In 1994, he participated in the E.C. project LIP2.

List of Relevant Publications

Elzeir, M. and J. Berlamont (1996) "A First Step in Building a Genralized Hydrodynamic Model", in 6th Inter. Conf. HYDROSOFT 96, Penang, Malaysia, 11-13 September.

Shiono, K., R. A. Falconer, J. Berlamont, M. Elzeir and M. Karelse (1995) "A Note of Stratified Flow in a Compound Channel", in XXVIth IAHR Congress, London, U.K., V.3, p.134.